Report No. 93D-03-0423
Revised

P. 86

Smart Skin Technology Development for Measuring Ice Accretion, Stall, and High AOA Aircraft Performance

Final Technical Report

Part 1

Capacitive Ice Detector Development

SBIR 1988 Phase II

Sponsored by:

National Aeronautics and Space Administration
Small Business Innovation Research Program
Contract No. NAS3-25966
SBIR - 03.01-0633
NASA Lewis Research Center
Cleveland, Ohio 44135
RELEASED: 5-B-92

Contractor:

Innovative Dynamics, Inc.
Cornell Research Park
Langmuir Labs, M/S 243
95 Brown Road
Ithaca, New York 14850-1252

Daniel A. Pruzan, Ph.D
Ateen A. Khatkhate
Joseph J. Gerardi
Gail A. Hickman

April 23, 1993

SBIR Rights Notice

Table of Contents

Introduction

A reliable way to detect and measure ice accretion during flight is required to reduce the hazards of icing currently threatening present day aircraft. Many of the sensors used for this purpose are invasive (probe) sensors which must be placed in areas of the airframe where ice does not naturally form. Due to the difference in capture efficiency of the exposed surface, difficulties result in correlating the ice accretion on the probe to what is happening on a number of vastly different airfoil sections. Most flush mounted sensors in use must be integrated into the aircraft surface by cutting or drilling the aircraft surface. An alternate type of ice detector which is based on a NASA patent is currently being investigated at Innovative Dynamics, Inc. (IDI).

As described in patent #4,766,369, the ice detector consists of two capacitance sensors, namely, a Type 1 and a Type 2 sensor and a temperature sensor. The Type 1 sensor is sensitive only to very thin layers of ice and it's capacitance reaches a constant maximum for the minimum ice thickness desired to be detected, while, the Type 2 sensor response is linear with ice thickness over the desired operating range. Both these sensors also respond to temperature and ice composition. However, the ratio of the outputs of the two sensors is only a function of ice thickness, and is independent of ice properties. The temperature sensor ensures that ice rather than water on the sensor is being detected.

The driving criteria behind the usefulness of this detector is to integrate the sensor with a neoprene pneumatic de-icer manufactured by BFGoodrich. Since de-icers must be routinely replaced, the new de-icers could be configured with the ice detector to enable an autonomous ice protection capability. Additionally, the sensor can be retrofitted to existing de-icers or embedded in new ones.

The NASA patented ice detector when configured as a thin sensor array promises to provide indication of leading edge, top wing and runback refreeze ice accretion without costly through the surface installation procedures. This market driven design is especially suitable for nondestructive installation on fuel tanks and other surfaces which should not be penetrated.

Results of the investigation into the performance of different capacitive type sensor designs, both rigid as well as elastic, are presented. Initially, sensor evaluation was performed using the ESTAR electro-magnetic analysis module of the finite element analysis program COSMOS/M. Sensor designs were based on integration with a functional standard pneumatic de-icer supplied by BFGoodrich. Static icing tests on some of the promising sensor designs were simulated in the lab at IDI by using paper which has a dielectric constant close to that of dry rime ice. In addition, dynamic tests were performed in the Icing Research Tunnel (IRT) at NASA Lewis on two separate occasions and at the BFGoodrich Icing Wind Tunnel (IWT) on three occasions. Key results from some of these tests are outlined in **Table 1** below and discussed in greater detail later in the report. Knowledge gained from these tests was utilized in sensor optimization. Designing sensors which have optimum sensitivity to ice with minimal effect on the de-icing efficiency of the de-icer, sensor integration techniques, and manufacturing simplicity were emphasized during this iterative design process. One such optimized sensor design was installed

on the NASA DHC-6 Twin Otter Icing Research Aircraft and flight tested in real-world icing conditions.

The test matrix in **Table 1** highlights the tests performed at BFGoodrich Icing Wind Tunnel, NASA Lewis Icing Research Tunnel and the flight test on the NASA Twin Otter and some of the key issues addressed during these tests.

BFG I	April 1991	• sensor geometry proportional to leading edge curvature. • a capacitance circuit measuring in real-time required.
BFG II	Sept. 1991	• data acquisition system tested successfuly. • sensor responds to ice thickness.
NASA I	April 1992	• improved sensor configuration developed. • phase change based capacitance meter designed. • sensor response depends on types of ice. • Type 2/Type 1 sensor ratio independent of ice type. • sensor output repeatable under similar icing conditions. • output independent of angles-of-attack in -1.5^{o} to $+1.5^{o}$ envelope.
NASA II	July 1992	• elastic wire sensor developed. • rigid underboot sensor developed. • temperature compensation of sensors necessary.
BFG III	Oct. 1992	• elastic fabric sensor developed. • guard circuit designed.
OTTER	Nov. 1992	• sensors successfully detected onset of icing and boot de-icing. • sensors immune to noise from communications or navigation equipment • sensors performed boot diagnostics.

Table 1. Test matrix of capacitance ice detector development program.

Patent Sensor Design

The ice detector design described in the NASA Langley patent[1] consists of three sensors as shown in **Figure 1**, a Type 1 and a Type 2 capacitance sensor and a temperature sensor. The geometry of the two capacitance sensors is such that the voltage output is proportional to the thickness of ice, regardless of ice temperature or composition. The temperature sensor ensures that ice rather than water on the sensor is being detected.

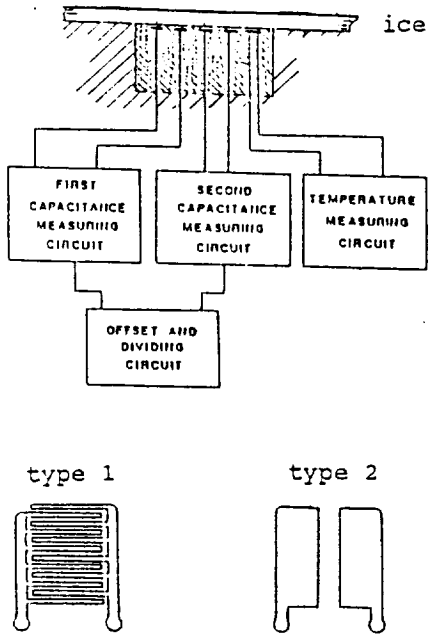

Figure 1. Capacitance ice detector configuration described in the NASA patent.

The capacitance sensor is based on the electromagnetic relationship of a two flat plate capacitor separated by a dielectric, given by the following equation,

$$C = \frac{\varepsilon A}{t}$$

where,

- C = system capacitance
- ε = permittivity of the dielectric material
- A = surface area of the electrodes
- t = separation distance (gap) between the two electrodes

However, instead of the parallel plate configuration, the patent suggests placing the electrodes next to each other in the same plane and separated by a gap. It is evident that the capacitance of the sensor is directly proportional to the dielectric constant of the medium above the electrodes. The dielectric constant of ice is different from that of water, both of which are different from the

dielectric of air. Thus as ice and/or water accumulates over the sensor the capacitance increases relative to the average thickness of the accumulating layer.

The Type 1 capacitance sensor has a comb-like grid with small conductors separated by a small gap and is therefore sensitive only to very thin layers of ice. Above a threshold value, the sensor response does not vary with ice thickness. The sensor is designed such that the sensor capacitance reaches a constant maximum for the minimum ice thickness desired to be detected. In general, the ice thickness at which the capacitance levels off is directly related to the electrode gap. Its output is also a function of temperature and ice composition.

The Type 2 capacitance sensor has two electrodes separated by a relatively large gap. Its response is linear with ice thickness over the desired operating range. Its output is a function of ice thickness as well as ice temperature and impurities. This sensor is designed such that the capacitance reaches a constant maximum at the maximum ice thickness desired to be measured.

The effect of temperature and ice composition is a common scaling factor for both the sensors. The patent therefore suggests that the ratio of the outputs of the two sensors is only a function of ice thickness, and is independent of ice properties.

The temperature sensor is used to determine whether the increase in the capacitance sensor signal is due to ice or water on the sensors.

References

[1] Weinstein, Leonard M., *Ice Detector*, United States Patent, # 4,766,369, August 23, 1988.

Analytical Model of Sensor

Initial evaluation of capacitance sensor designs was accomplished by using the finite element analysis software COSMOS/M[1], a powerful structural analysis program designed to run on PC-based computers. The ESTAR electromagnetic analysis module of this software can be used to model a broad spectrum of electric and magnetic field problems. It has the capability for solving two and three dimensional magnetostatic, electromagnetic and electrostatic problems.

The capacitance sensor was modeled as a two dimensional electrostatic problem. This two dimensional analysis is sufficient because: 1) sensor has a uniform cross-section 2) sensor is much longer than it is wide and 3) end effects are negligible.
A typical finite element model of the capacitance sensor is shown in **Figure 2**. A 10 cm x 5 cm rectangular x-y plane was defined to model the capacitance sensor cross-section consisting of sensor electrodes, insulator separating the electrodes, sensor backing and cover material, and layers of ice and air above this sensor cross-section. This plane was modeled using 5000 nodes, defined in right handed Cartesian coordinates. A meshing routine was used to create the finite element mesh, consisting of 5000 MAG2D elements, 0.1 cm square, to describe the plane. MAG2D is a four node quadrilateral element defined in the x-y plane for use with two dimensional and axisymmetric electromagnetic analyses.

Each of the sensor materials was specified by assigning a unique material property set. For electrostatic analysis, the only material property required to completely define the material is the permittivity value. The region above the sensor cross-section with or without ice, was always defined as air, as shown in **Figure 2**. The air extended at least 4.5 cm above the sensor surface and this enabled us to examine the electric field above the sensor. No electric field lines of any significance were observed beyond 3 cm from the sensor surface. The following permittivity values were specified for some of the materials used in the finite element model:

Air:	8.85×10^{-14} F/cm	Rime Ice:	28.32×10^{-14} F/cm
Neoprene:	61.065×10^{-14} F/cm	Glaze Ice:	159.3×10^{-14} F/cm
Silicon:	26.55×10^{-14} F/cm		

The voltage at the boundary of the positive and ground electrode was prescribed to be 1 and 0 volt respectively, while, all the nodes on the plane boundary had 0 volt boundary conditions to prevent electric field leakage. An electrostatic analysis was performed. The electric field of the capacitance sensor and the energy stored in the electric field were output by the program.

From theory, the energy stored in the electric field of a capacitor is given by:

$$W = \frac{1}{2} C V^2$$

where,

W = energy stored in the electric field
C = capacitance
V = potential difference between the capacitor electrodes

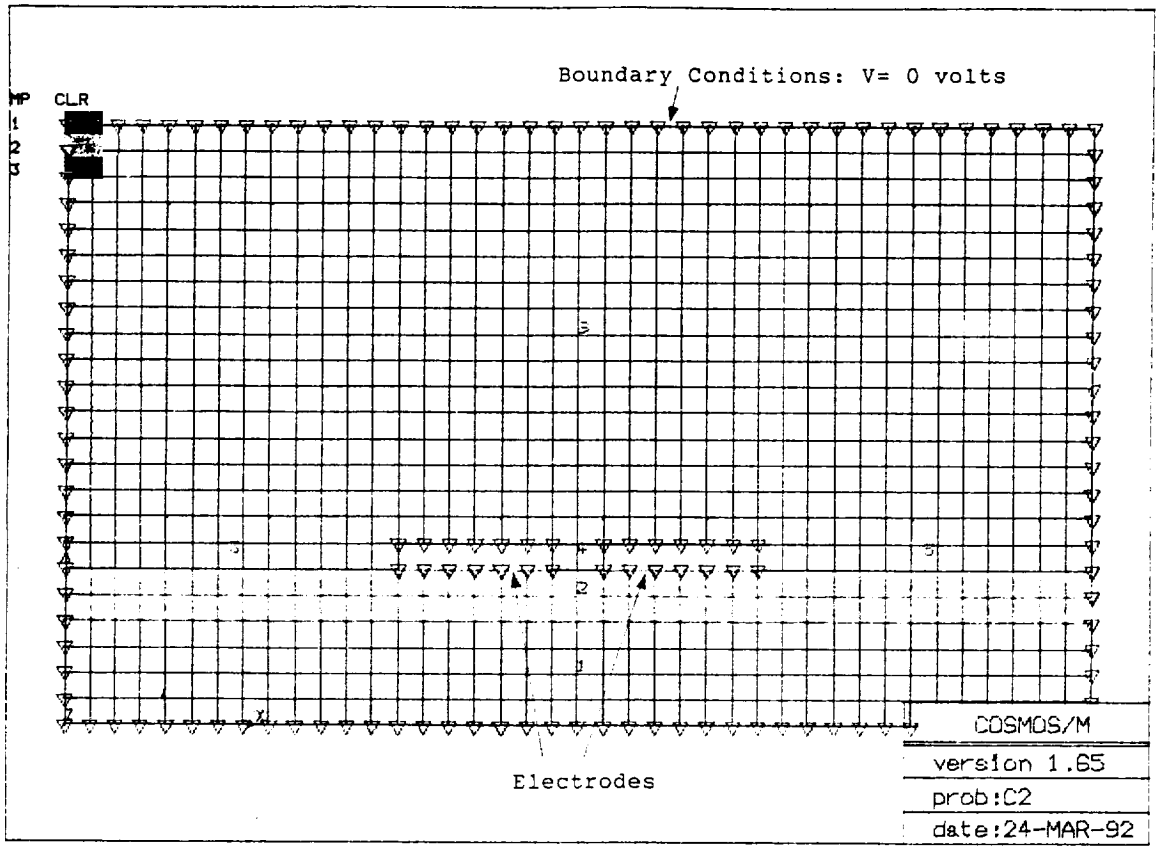

Figure 2. Typical finite element model of a capacitance sensor created using Estar.

Since the potential difference V between the positive and ground electrode is 1 in the finite element model, the capacitance of the sensor per unit length is twice the energy calculated by the finite element method.

Evaluation of Sensor Configuration

A finite element model of a Type 2 sensor with two 1.6 cm electrodes separated by a 0.6 cm gap between them was created. The electrodes were placed on a 0.2 cm thick neoprene insulating layer and had no covering layer. The analysis was repeated several times as the ice thickness over the sensor was increased from 0 cm to 2.5 cm in 0.1 cm increments. Each time, a 0.1 cm layer of air at the ice-air interface above the sensor was replaced by a 0.1 cm layer of rime ice (dielectric constant= 3.2). The capacitance per unit length was calculated for each of these cases. The change in capacitance per unit length is shown in **Figure 3**. From icing tests at BFG on an identical sensor with a 0.04 cm neoprene cover, the sensor seemed to flatten out with ice accumulations of 1.5 cm. However, from the FEM model, the change in capacitance with increasing ice thickness is noticeable even with 2.5 cm of ice over the sensor. This is because: 1) the lack of a cover over the sensor increases its sensitivity to ice and 2) after about 1.5 cm of ice, the slope is very small indicative of a very small change in capacitance (about 1.5 pF for a 24" long sensor) which may be hard to detect in a practical application.

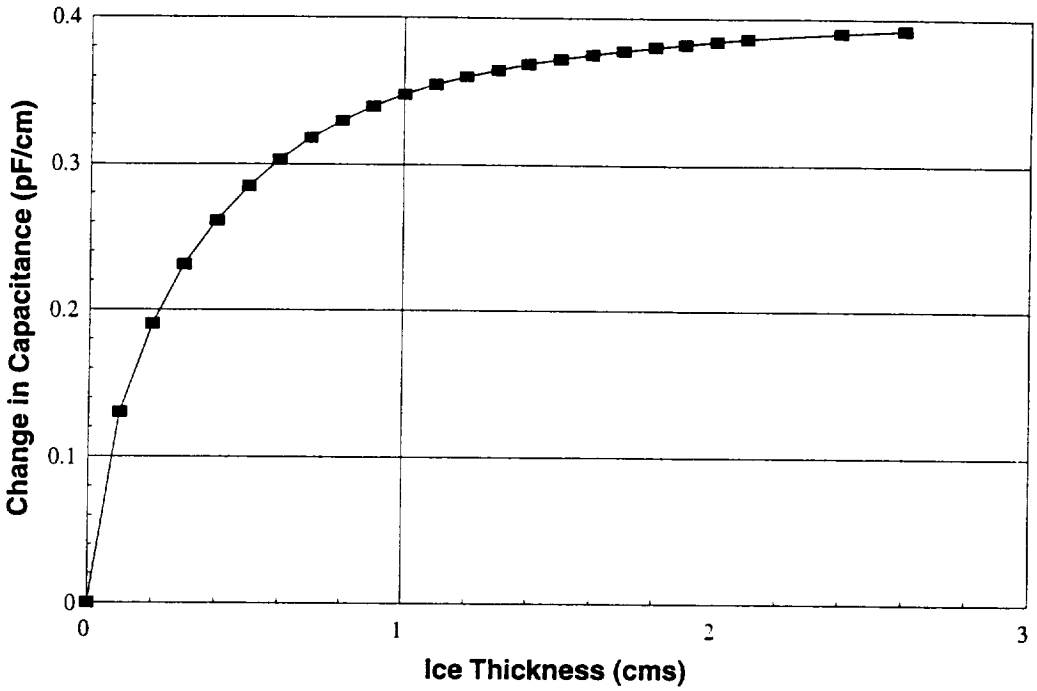

Figure 3. Response of sensor with two 1.6 cm electrodes separated by a 0.6 cm gap from Estar results. Both electrodes were positioned on a 0.2 cm neoprene insulating layer and had no covering layer.

The electric field due to this capacitance sensor is examined. The positive and negative electrode are modeled side-by-side in the same plane which is close to the lower boundary of the rectangular plane. With 0 volt boundary constraints, this boundary acts like a ground plane, simulating sensor installation on a grounded wing. **Figure 4** shows the electric field lines around the sensor plotted for one of the ice cases. The electric field lines originate from the positive electrode and travel towards the lower ground plane. The field is symmetric about the center of the positive electrode with no significant field lines going from the positive electrode to the negative electrode. Thus, the capacitive field between the positive electrode and the ground plane is a lot more dominant than the field between the positive and negative electrode. This is because the gap between the positive electrode and the ground plane below is 0.2 cm, much smaller than the 0.6 cm gap between the positive and negative electrode.

Tests were performed in the lab at IDI to verify this phenomena using a Type 2 sensor tested previously at BFG. The sensor was attached to the outer surface of a pneumatic de-icer mounted on a grounded graphite leading edge. At first, sheets of paper were used to cover just the positive electrode of the sensor. This was repeated with the paper just over the negative electrode. It was observed that the sensor capacitance increased significantly when the paper was over the positive electrode but did not change when the paper was over the negative electrode. This is because the

electric field was due to the capacitance between the positive electrode and the grounded leading edge. When the paper was over the positive electrode, the field lines passed through this paper with a higher dielectric ($Dielectric_{paper}$=3, $Dielectric_{air}$=1) resulting in increased capacitance. However, when the paper was over the negative electrode it did not disturb the field lines and hence had little influence on the capacitance reading.

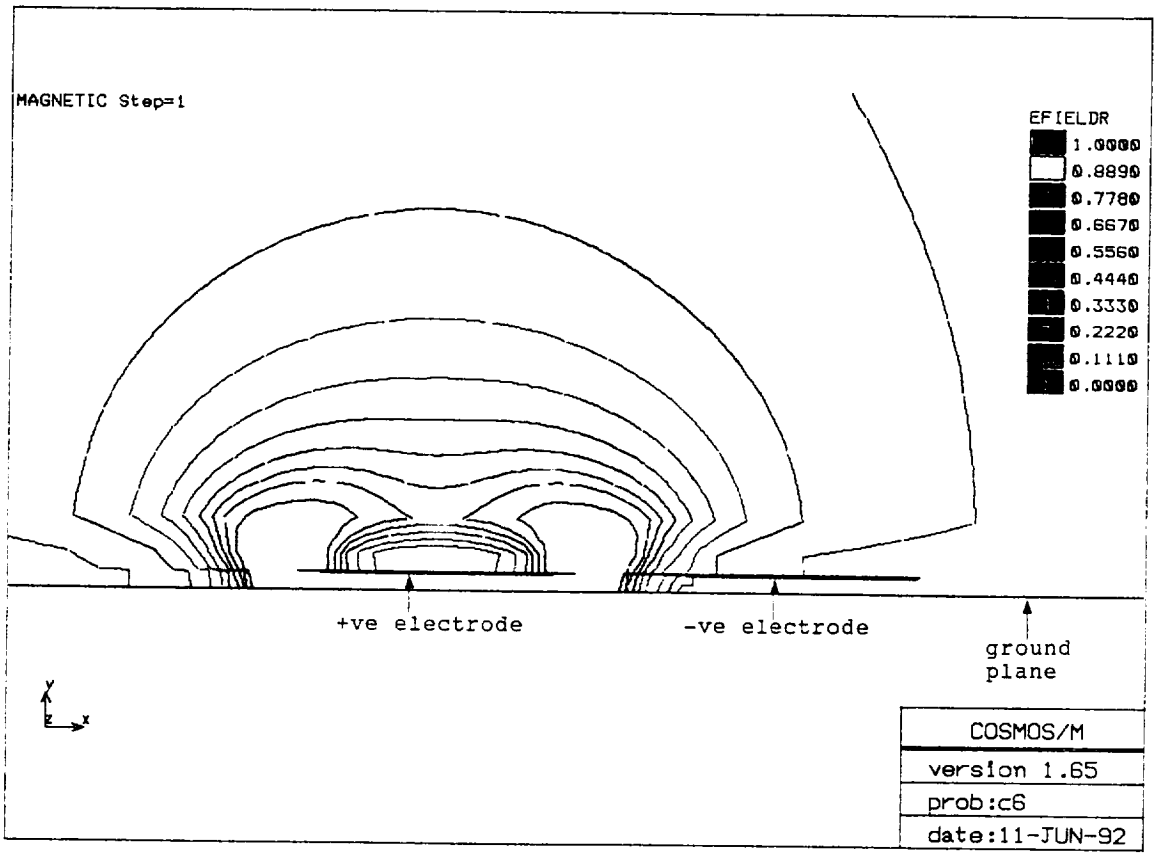

Figure 4. Electric field contours near a capacitance sensor output by Estar. Sensor had two 1.6 cm electrodes with a 0.6 cm gap, a 0.2 cm neoprene insulator and no cover.

This phenomenon does not, however, seem to adversely affect the operational range of the sensor in terms of ice thickness or the sensitivity to ice. Also, this design has an advantage because the width of the sensor is reduced by more than 50%. Thus, as the ice accretion grows simultaneously outward from the stagnation line, it covers the entire sensor quickly, thereby reducing the probability of uneven ice distribution over the sensor.

Before any further conclusions were made based on the finite element analyses of the capacitance sensor, the model predictions were verified by comparing to results from lab tests on the sensor.

Verification of Analytical Model

A lab test was performed on the embedded Type 2 sensor tested previously at BFG. The initial capacitance of the sensor was noted. Sheets of paper were placed over the sensor and the capacitance was recorded. The paper thickness was increased from 0 cm to 3 cm in 0.2 cm and 0.4 cm increments. The change in capacitance was adjusted for the dielectric of ice by multiplying it by 1.067 ($Dielectric_{ice}/Dielectric_{paper}$ = 3.2/3). The text book value of dielectric constant for paper is between 2.5 and 4. The dielectric of the paper used in our test was calculated in the lab. Sheets of paper were clamped between two similar flat metal plates and the capacitance noted. From the definition of a parallel plate capacitor, the dielectric of the paper was calculated. The change in capacitance per unit length is shown in **Figure 5**.

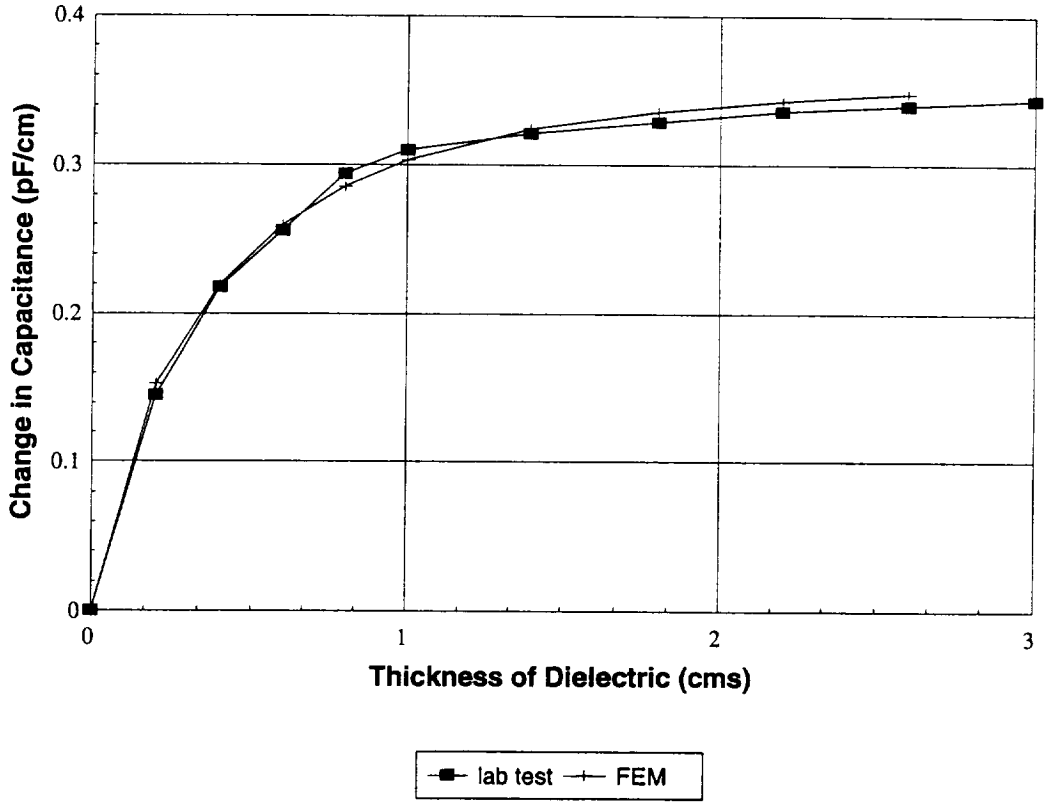

Figure 5. Comparison of Type 2 sensor responses from i)lab tests and ii) FEM. Sensor had a 0.65" electrode, neoprene insulating layer and neoprene cover.

A finite element model of this Type 2 capacitance sensor was created. Several analyses were performed as the rime ice (Dielectric = 3.2) thickness over the sensor was increased from 0 cm to 2.5 cm in 0.2 cm and 0.4 cm increments. The capacitance per unit length calculated from the output of Estar is shown in **Figure 5**.

The finite element calculations of the change in capacitance with ice thickness are in good agreement with lab results. Thus, we have a model that is representative of an actual capacitance sensor and can be used to reasonably predict sensor performance.

Parametric Study

This finite element modeling technique was used to evaluate the effect of various design parameters on the sensitivity of the sensor to ice and also on the operational range in terms of ice thickness. The influence of the different sensor construction materials on sensor performance was also investigated. Additionally, the effect of types of ice and the sensor compensation scheme were evaluated. Sensor designs were based on integration with a functional de-icing boot.

Type 1 and Type 2 sensor designs followed the new configuration where the positive electrode is placed on top of the ground electrode and the two electrodes are separated by an insulating layer. In this case, the gap between the two electrodes is determined by the thickness of the insulating layer. Unlike previous designs, where the Type 1 sensor had a series of closely spaced interleaved electrodes, the new Type 1 is similar to a Type 2 sensor but with a much smaller electrode width.

Effect of Positive Electrode Width

The effect of positive electrode width on the operational range of the sensor with respect to ice thickness was investigated. Sensors with 0.1, 0.6, 1.1, 1.6, 2.6, and 3.6 cm wide positive electrodes were modeled. In each instance, this electrode was separated from a 10 cm wide ground plane beneath it by a 0.025 cm silicon insulating layer and covered with a 0.03 cm neoprene layer. The sensor response as ice thickness over the sensor was increased from 0 cm to 2.6 cm is shown in **Figure 6**. The sensors with smaller electrode widths tend to level out quicker and therefore have smaller operating ranges. In the region before the sensor begins to flatten, the sensor sensitivity is the same for all. However, in the region after the sensor flattens, for an electrode width above 2.6 cm, the change in sensitivity is small and it diminishes further as the electrode is made wider.

This explains the primary difference in the Type 1 and Type 2 sensors. The small electrode width sensors fail to project vertical electric field lines such as are generated by the wider electrodes, resulting in decreased ability to detect thicker ice.

Effect of Ground Electrode Width

Figure 7 shows the influence of ground plane width on sensor response to ice. The sensor had a 1.6 cm positive electrode separated from the ground plane beneath it by a 0.025 cm silicon insulating layer. The sensor had a 0.03 cm neoprene covering layer. The sensor was modeled with 1.6 and 10 cm wide ground planes. Ice thickness over the sensor was increased from 0 to 2.6 cm. The sensitivity of the sensor increases slightly with the increase in the width of the ground plane. However, not much effect on the operational range of the sensor is observed.

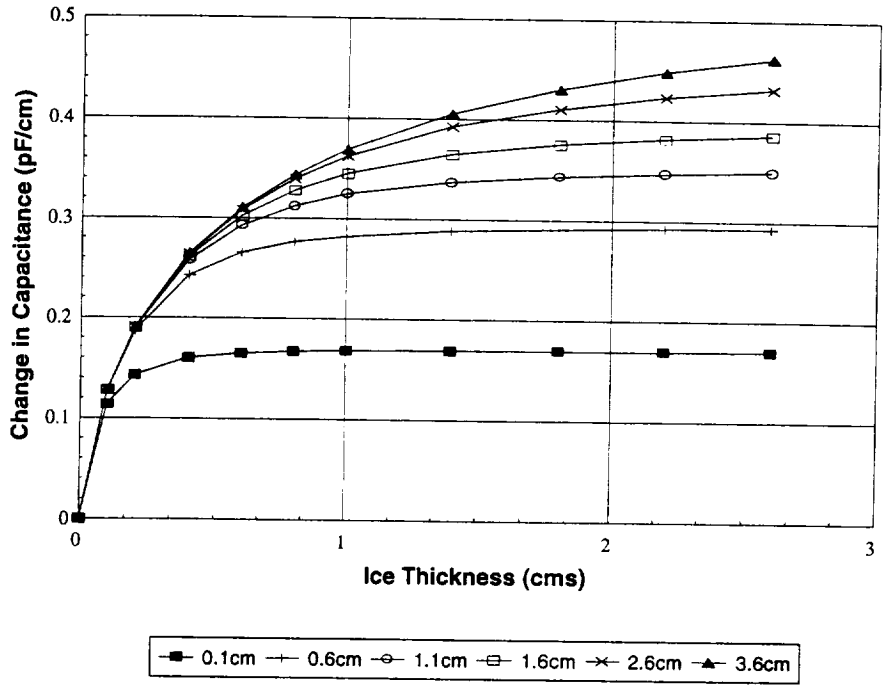

Figure 6. Effect of positive electrode width on sensor with a 10 cm wide ground plane, a 0.025" silicon insulating layer and 0.03 cm neoprene cover; from Estar results.

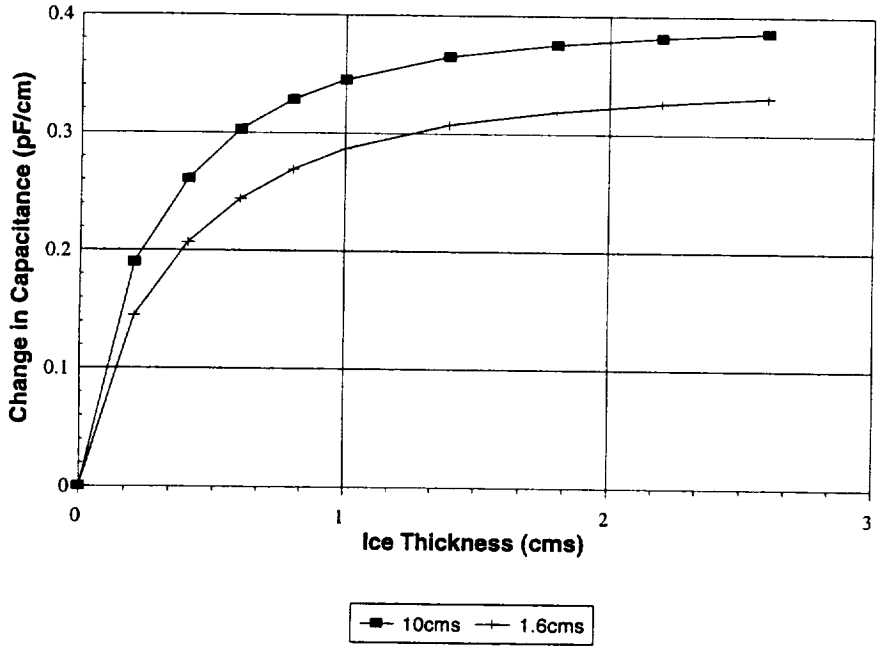

Figure 7. Effect of ground electrode width on sensor with a 1.6 cm positive electrode, a 0.025 cm silicon insulating layer and a 0.03 cm cover; based on Estar results.

Effect of Neoprene Thickness

The influence of thickness of neoprene covering the sensor was investigated. To study this effect, sensor models were created with 0, 0.03, and 0.06 cm of neoprene covering the sensor. The sensor had a 1.6 cm electrode separated from the ground plane beneath it by a 0.025 cm silicon insulating layer. The change in capacitance as ice thickness was varied from 0 cm to 2.5 cm is shown in **Figure 8**. As expected, the neoprene thickness tends to reduce the sensor's sensitivity to ice but appears to have little effect on it's operational range.

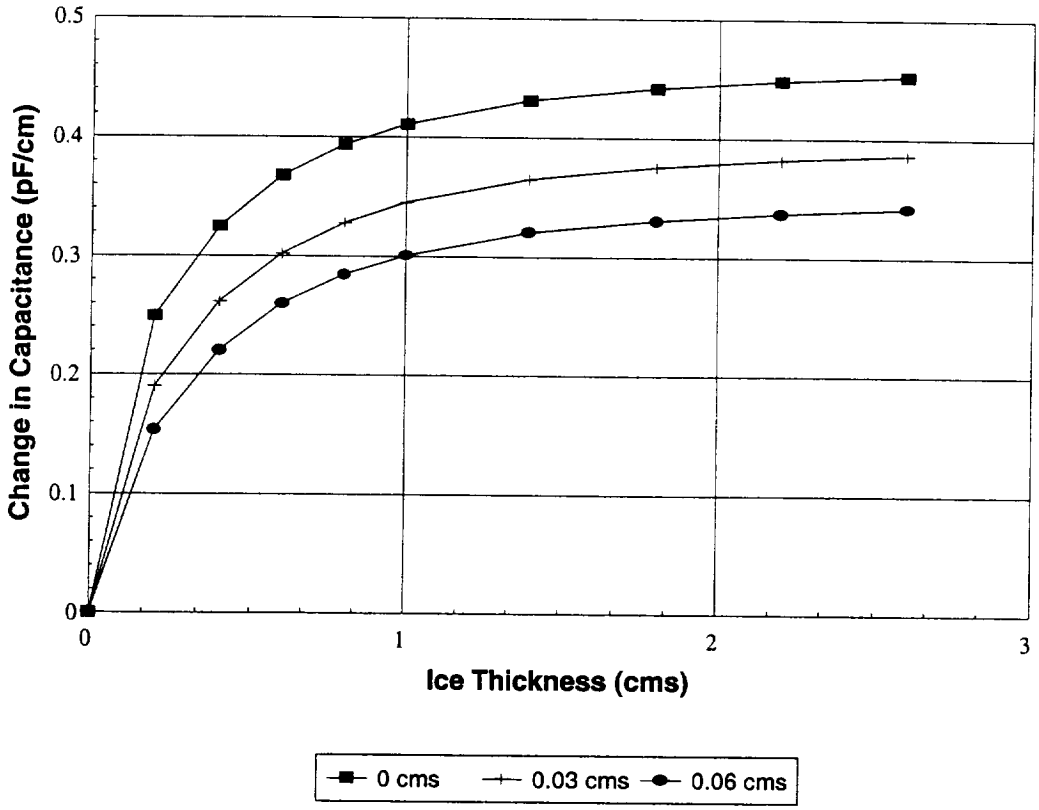

Figure 8. Effect of neoprene cover thickness on sensor with a 1.6 cm positive electrode, a 10 cm ground plane and a 0.025 cm silicon insulating layer; from Estar results.

Effect of Types of Ice

The response of a Type 1 sensor to ice types ranging from rime to glaze is evaluated. A Type 1 sensor with a 0.1 cm positive electrode, a 10 cm ground electrode, a 0.025 cm silicon insulating layer, a 0.03 cm neoprene cover layer, and 2.6 cm of ice covering the entire sensor was modeled. The dielectric constant of this ice was varied from 1 to 26 to simulate different ice types. From icing tests performed in the past under many different icing conditions, it is believed that the dielectric of rime ice varies from 3 to 10 while that of glaze ice can be as high as 35. **Figure 9** shows the influence of the dielectric constant of ice on the Type 1 sensor capacitance. The response of the Type 1 sensor does not vary linearly with the dielectric constant of ice.

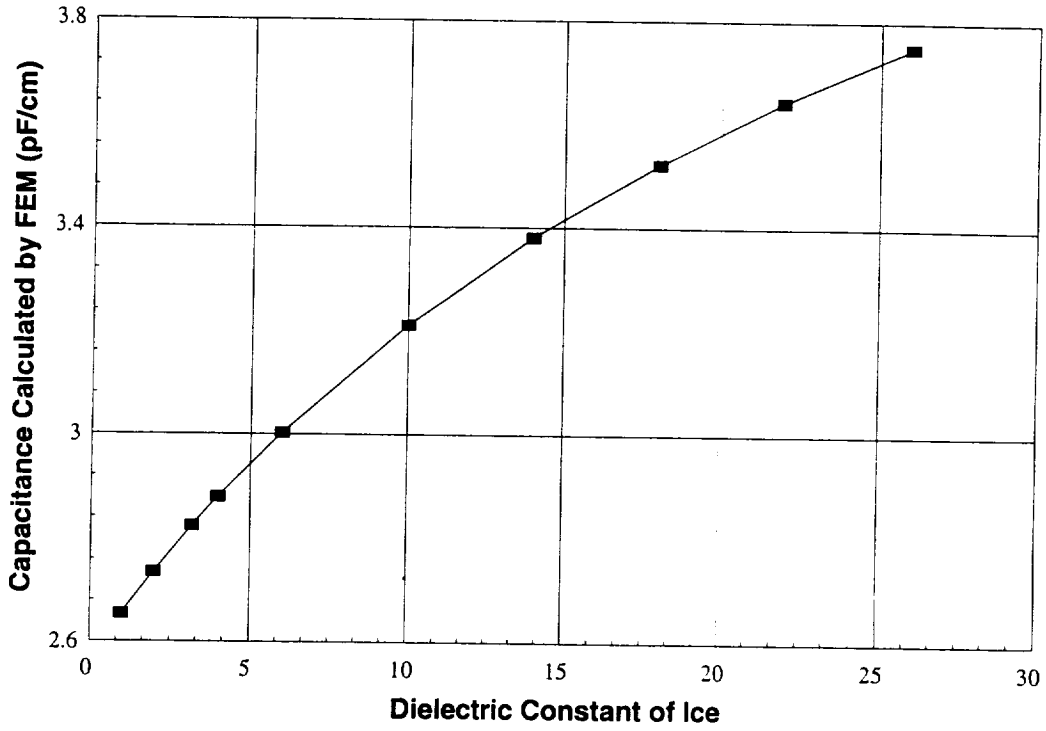

Figure 9. Influence of types of ice on Type 1 sensor based on Estar. Sensor had a 0.1 cm positive electrode, a 10 cm ground electrode, a 0.025 cm silicon insulating layer, a 0.03 cm neoprene cover and a 2.6 cm of ice covering the entire sensor.

Evaluation of Sensor Compensation Scheme

According to the patent, the Type 1 and Type 2 sensors can be designed such that the ratio of the outputs of the two sensors is only a function of ice thickness, and is independent of temperature or composition. Models of the Type 1 and Type 2 sensor were created to evaluate this compensation scheme.

The Type 1 sensor had a 0.1 cm positive electrode while the Type 2 sensor had a 1.6 cm electrode. Both electrodes were separated from a 10 cm wide ground electrode by a 0.025 cm silicon insulating layer and they had a 0.03 cm neoprene layer covering them. For the Type 2 sensor the capacitance was calculated at 1, 1.4, 1.8 and 2.2 cm of ice over the sensors. The properties of the ice were changed to represent types of ice, namely, rime (dielectric=3.2), mixed (dielectric=10) and glaze (dielectric=22). Since the Type 1 sensor had leveled off before 1 cm of ice (refer **Figure 6**), the analysis was performed for 2.6 cm of rime, mixed and glaze ice types covering the sensor.

Figure 10 shows the ratio of the change in capacitance of the sensors (Type2/Type1) for the different types of ice. This capacitance sensor ratio varies with ice composition. Contrary to

patent predictions, this ratio is highest for glaze ice and lowest for rime ice, indicating that the influence of dielectric on the Type 1 sensor is different than the influence on the Type 2 sensor and cannot be factored out. This results in a best case deviation of roughly +/-8% between curves of capacitance rates versus ice thickness.

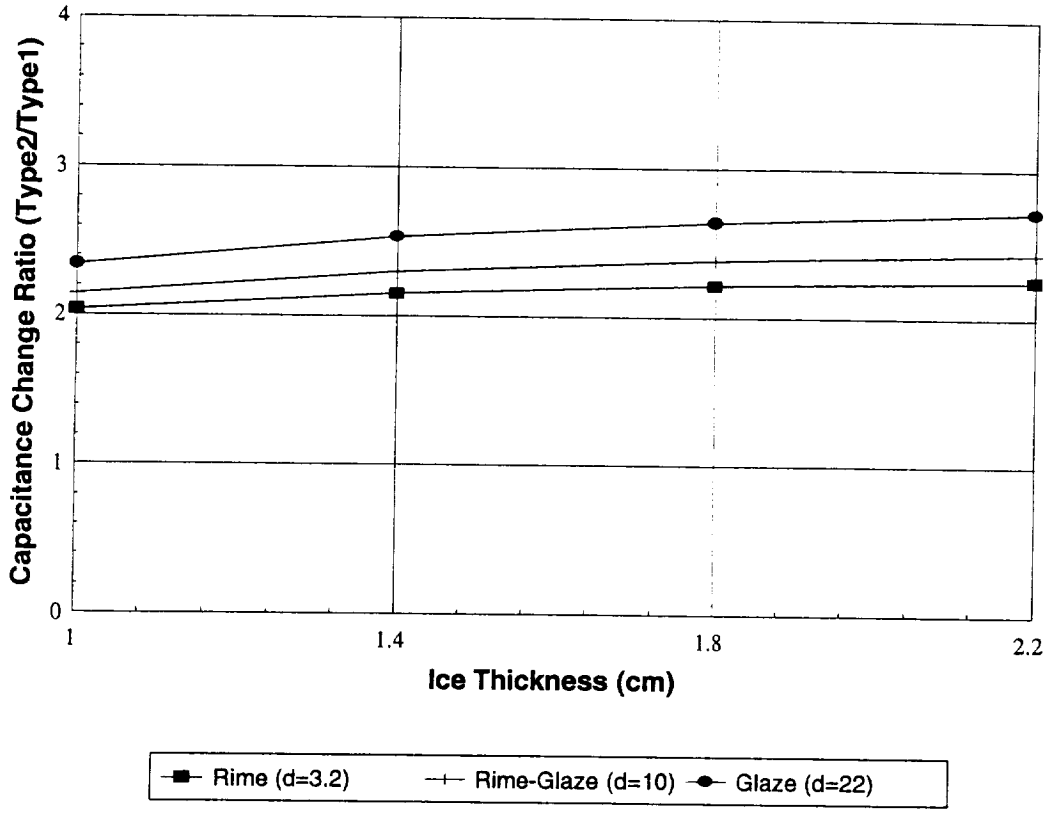

Figure 10. Type2/Type1 sensor ratio for different ice types based on Estar. Both 0.1 cm Type 1 electrode and 1.6 cm Type 2 electrode sensors had a 10 cm ground plane, a 0.025 cm silicon insulating layer and a 0.03 cm neoprene cover.

Results from Analytical Study

The analytical study helped us make improvements in the configuration of the sensor electrodes. It also helped us understand the influence of various design parameters on sensor performance and to study the effects of types of ice. The results from this study are discussed below.

1) For some sensor configurations, when a positive and a ground electrode separated by a gap are above an underlying ground plane, electric field lines originate from the positive electrode and travel towards the lower ground plane instead of the ground electrode. This is because the insulator between the positive electrode and the ground plane is much thinner than the gap between the positive and ground electrode. This phenomenon does not affect the operational range of the sensor in terms of ice thickness or sensitivity to ice. Also, this sensor has an advantage because it's width is reduced by more than 50% which reduces the probability of uneven ice distribution over the sensor.

2) Sensors with smaller electrode widths tend to level out quicker and therefore have smaller operating ranges. In the region before the sensor begins to flatten, the sensor sensitivity is the same for all. However, in the region after the sensor flattens, for an electrode width above 2.6 cm, the change in sensitivity is small and it diminishes further as the electrode is made wider. This explains the primary difference in the Type 1 and Type 2 sensors. The small electrode width sensors fail to project vertical electric field lines such as are generated by the wider electrodes, resulting in decreased sensitivity to thicker ice.
3) The sensitivity of the sensor increases slightly with the increase in the width of the ground plane. However, not much effect on the operational range of the sensor is observed.
4) The thickness of the neoprene covering layer tends to reduce the sensor's sensitivity to ice but does not affect it's operational range.
5) The response of the Type 1 sensor does not vary linearly with the dielectric constant of ice.
6) The ratio of capacitance varies with ice composition. Contrary to patent predictions, this ratio is highest for glaze ice and lowest for rime ice, indicating that the influence of dielectric on the Type 1 sensor is different than the influence on the Type 2 sensor and cannot be completely factored out. This results in a best case deviation of roughly +/-8% between curves of capacitance rates versus ice thickness.

References

[1]COSMOS/M User Guide, Version 1.65, Structural Research and Analysis Corporation, Santa Monica, CA, 1991.

First Icing Tunnel Test at NASA Lewis

An icing tunnel test was performed at the NASA Icing Research Tunnel, IRT, from April 22 through April 24 1992. The objectives of this test were to 1) evaluate a rigid and an elastic sensor attached to the outer surface of a de-icing boot, 2) examine the effect of types of ice on ice thickness measurements made by the rigid sensor, 3) examine the influence of angle-of-attack on ice thickness measurements, 4) test repeatability of measurements under similar icing conditions, 5) test the capacitance measuring circuit, and 6) study the influence of both rigid and elastic sensors on the de-icing capability of the boot. During the tests data collection proceeded very smoothly. As the data was post-processed at IDI, most of the stated objectives were achieved. The following sections detail the development work at IDI to manufacture the sensors used in these tests, the hardware used, and the results obtained.

Sensor Development

Type 1 and Type 2 sensor designs were based on Estar analyses. The rigid sensors were fabricated and tested in the lab at IDI to ensure that the sensor performance was in agreement with Estar predicted results. During this period we also investigated making elastic sensors which could stretch in both chordwise and spanwise directions. These elastic sensors could possible be in de-icer tubes without adversely affecting tube inflation and de-icing efficiency. In addition to sensor development we also designed and built a signal conditioning module and a new capacitance measuring circuit with better signal resolution and less sensitivity to the conductivity of fluids.

Rigid Sensor Development

The sensors were manufactured using a sandwich construction as shown in **Figure 11**. The Type 1 and Type 2 sensors were 24" long with a 0.2" gap separating them. The Type 1 sensor had a 0.050" wide electrode while the Type 2 sensor had a 0.65" electrode. These electrodes were constructed using BEND/Flex printed circuit board laminate manufactured by Rogers. This 0.004" thick laminate, with 1 oz copper on one side, is formable and can be used in a curved mode application. The electrodes were marked on the board using indelible ink and the sensor pattern was etched using ferric chloride etching solution. A common ground plane, 0.95" wide and 24" long, was made by cutting another strip of BEND/Flex. The positive electrodes of these sensors were separated from the ground plane by a 0.010" thick silicon insulating layer, which is very flexible. The sensor was sealed between two 0.015" thick flexible neoprene sheets which were slightly bigger than the sensor size. This ensured that the sensor was completely encapsulated and also provided resistance to delamination of the sensor during de-icing boot inflation cycles. The different sensor layers were glued using RTV silicone adhesive which is flexible when dry. A second identical sensor pair was manufactured as a back-up sensor. These flexible but non-elastic sensors were wired with short RG-62 coaxial cables.

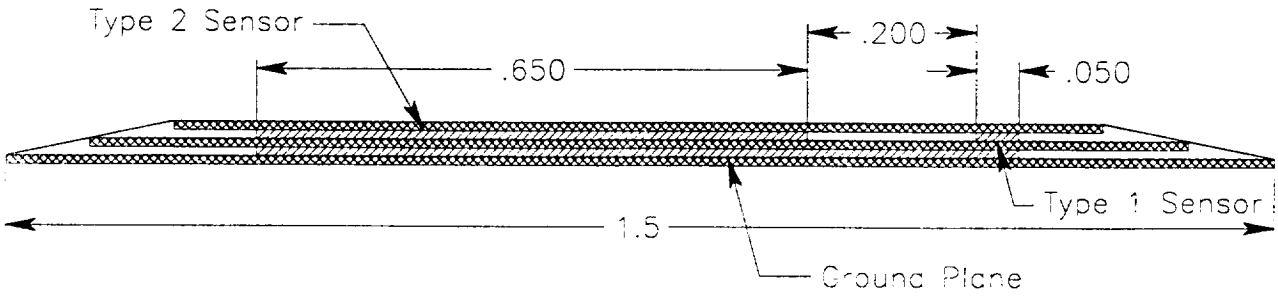

Figure 11. Cross-sectional view of the rigid sensor showing the Type 1 and Type 2 electrodes.

Both sensor pairs were tested in the lab at IDI. Paper, which has a dielectric constant similar to that of rime ice, was used to simulate ice growth over the sensors instead of performing time consuming icing tests in the freezer. The capacitance of the sensors was noted each time a few sheets of paper were placed over the sensors. Initially, the thickness of paper was increased in smaller increments to get better resolution for small thicknesses. The change in capacitance per unit length of sensor was calculated. This value was scaled by 1.067 to adjust it for the dielectric of rime ice ($Dielectric_{ice}/Dielectric_{paper} = 3.2/3 = 1.067$). As mentioned previously, the dielectric of the paper was measured experimentally in the lab and found to be 3. This change in capacitance per unit length shown in **Figure 12**, is indicative of the sensor response to rime ice. The response for both the Type 1 and Type 2 sensors is in line with our expectations. The Type 1 sensor responds to thin ice after which it flattens out while the Type 2 sensor has field lines going out a lot farther and hence is able to detect thicker ice. The tests were repeated for the backup sensor pair. Both the sensor pairs had an identical response, indicating that the manufacturing process was repeatable.

Elastic Sensor Development

The elastic sensor was made 12" long and 0.9" wide. The sandwich construction used to manufacture this sensor was similar to that of the rigid sensor. The Bend/Flex was replaced with conductive silicon with a low durometer. This sensor strip was both flexible and elastic. Laboratory tests indicated that the baseline capacitance of the sensor was constantly changing and varying as a function of time. Also, this sensor did not respond repeatably to step increases in capacitance. This anomalous behavior is probably due to the changing manner in which metal particles embedded in the non-conductive elastomer matrix make contact with each other. However, a non-functional sensor was installed to compare the performance of such a sensor to that of a rigid sensor in de-icing different types of ice.

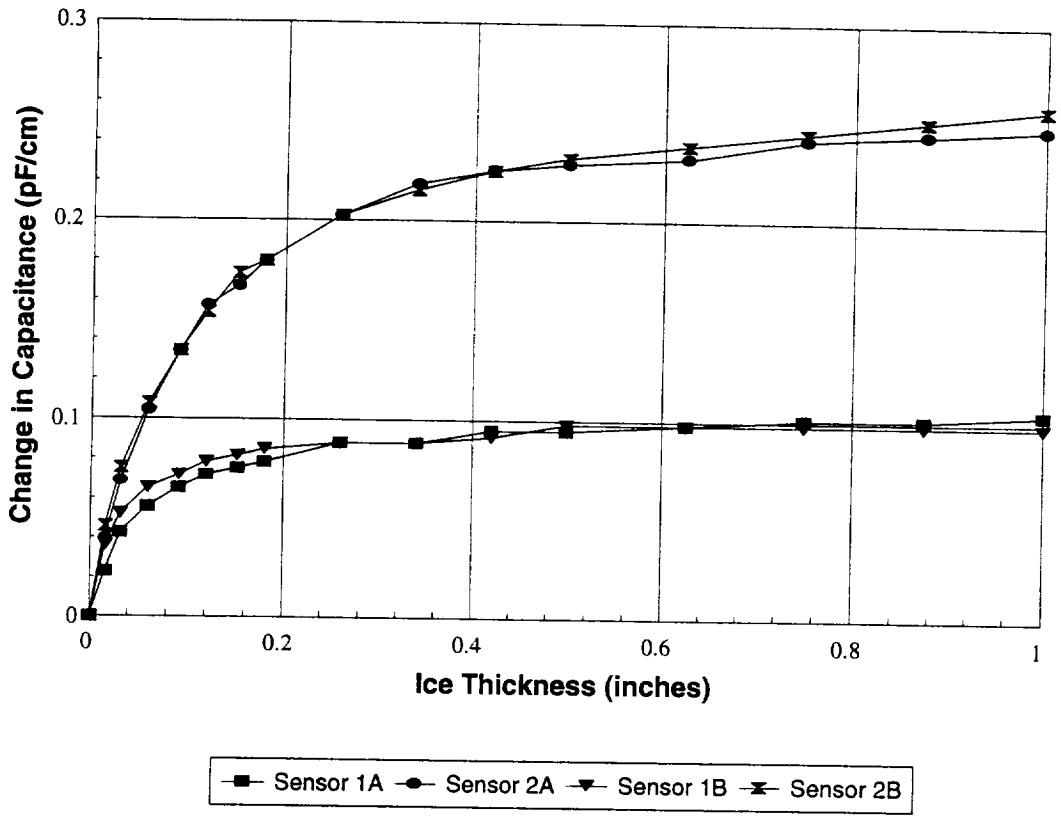

Figure 12. Lab test response of the Type 1 and Type 2 sensors to be tested in the NASA IRT.

Wind Tunnel Experimental Apparatus

Hardware

Capacitance Meter

A new capacitance measuring circuit, based on phase change, was manufactured. This custom meter had suitable measurement ranges and other useful features. A block diagram of the TBE 214 capacitance meter is shown in **Figure 13**. This meter could measure capacitors in a broad range from 1fF (1 femtofarad = 10^{-15} farads) to 1μF in six ranges. The meter had a nulling potentiometer to zero out stray capacitances. Since the change in the capacitance due to ice build up was sometimes small as compared to the initial dry sensor and cable capacitance, a 100% offset circuit was added to cancel out the voltage due to the initial capacitance. Offset adjustment was done using a 10 turn precision potentiometer with a dial. Depending on the change in capacitance during the icing test, the difference in voltage resulting from this change could be amplified by an adjustable gain of 1 to 10. The display could be switched between an output of x1 and an output of x10. The meter had an anti-aliasing filter and its analog output was between 0 and 1 Volt.

From a previous test at BFG, when two sensors were hooked up to two capacitance meters, the sensor signals seemed to pick up some noise as a result of the clock frequencies of the two capacitance meters not being synchronized. To get rid of this noise, the clock frequency of one of the meters was increased to 14 kHz while the other meter was kept at 10 kHz.

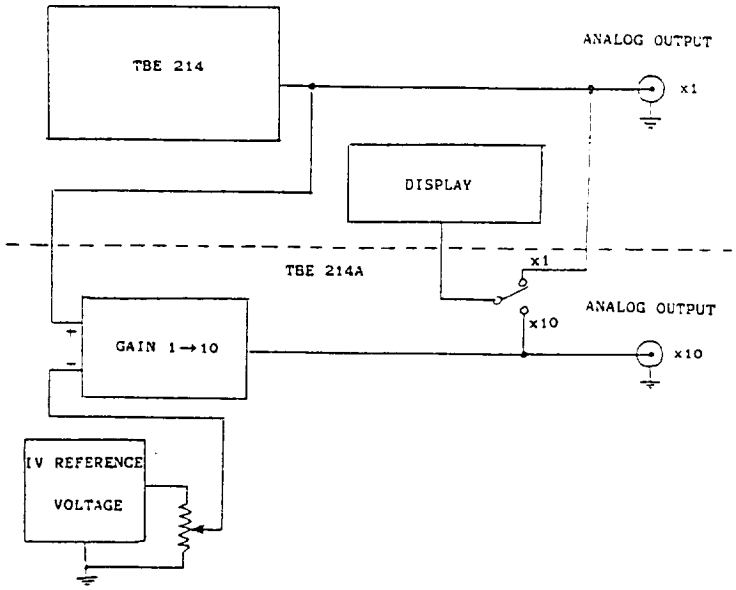

Figure 13. Block diagram of a TBE 214 capacitance measuring circuit.

Conditioning Module

The conditioning module consisted of four capacitance channels and a +/- 12 Volt power supply. It served as a break out box by bringing the individual capacitance sensor signals into a Metrabyte DAS-20 data acquisition card. In this module, the capacitance sensor signal could be further amplified with an optional x1/x10 gain amplifier.

Test Setup

The rigid and elastic sensors were tested in the NASA Icing Research Tunnel (IRT) near the leading edge of a 50" span wing cuff. This cuff had previously (in 1990) been tested in the IRT during IDI's Ice Sensing and Ice Protection Systems (ISIPS) NASA Phase II program. The cuff, with a well rounded leading edge, ensured total and uniform ice coverage over a wide area near the leading edge.

A functional non-conductive de-icer manufactured by BFGoodrich was attached to the wing cuff such that the de-icer centerline was against the leading edge of the cuff. This de-icer was 8" wide, 48" long and had 6 spanwise inflatable tubes. The two tubes near the leading edge were 1.25" wide while the other tubes were 1" wide. The rigid and elastic sensors were attached to the outer face of the de-icer. They were centered between stitch lines of one of the wide tubes near the leading edge such that the electrodes had a spanwise orientation.

The co-location of the Type 1 and Type 2 sensors, with a 0.2" chordwise gap, ensures that they witness identical ice accumulation. Thus, as ice accretion grows outward from the stagnation line, it covers both the sensors quickly, thereby providing ice thickness information rather than chordwise ice distribution rate. Also, if the de-icing boot does not cleanly de-ice the leading edge then chunks of ice over the sensor would influence both Type 1 and Type 2 sensors and the ratio would indicate this presence of ice. However, if the sensors are not co-located, ice over the Type 1 or Type 2 sensor may not be completely de-iced, leading to conservative or inflated predictions of ice thickness respectively.

The cuff was mounted on a Twin Otter wing test section. As shown in **Figure 14**, this wing section was bolted to the icing tunnel floor such that the cuff was vertical. Thirty foot long RG-62 low capacitance (12pF/foot) coaxial cable extensions were used to bring the rigid sensor signals out of the tunnel and into two capacitance meters. This cable is insensitive to temperature variations, change in position, as well as the proximity of different dielectric materials such as ice/water near the cable. A pneumatic hose was hooked up to the de-icer. The other end of the hose was attached to a control/regulator panel used to maintain vacuum in the de-icer tubes and to inflate them when necessary. A typical test setup is shown in **Figure 15**. Note that in this test we did not use any thermocouples.

Figure 14. Photograph of the wing cuff mounted on a Twin Otter wing section during the NASA IRT test.

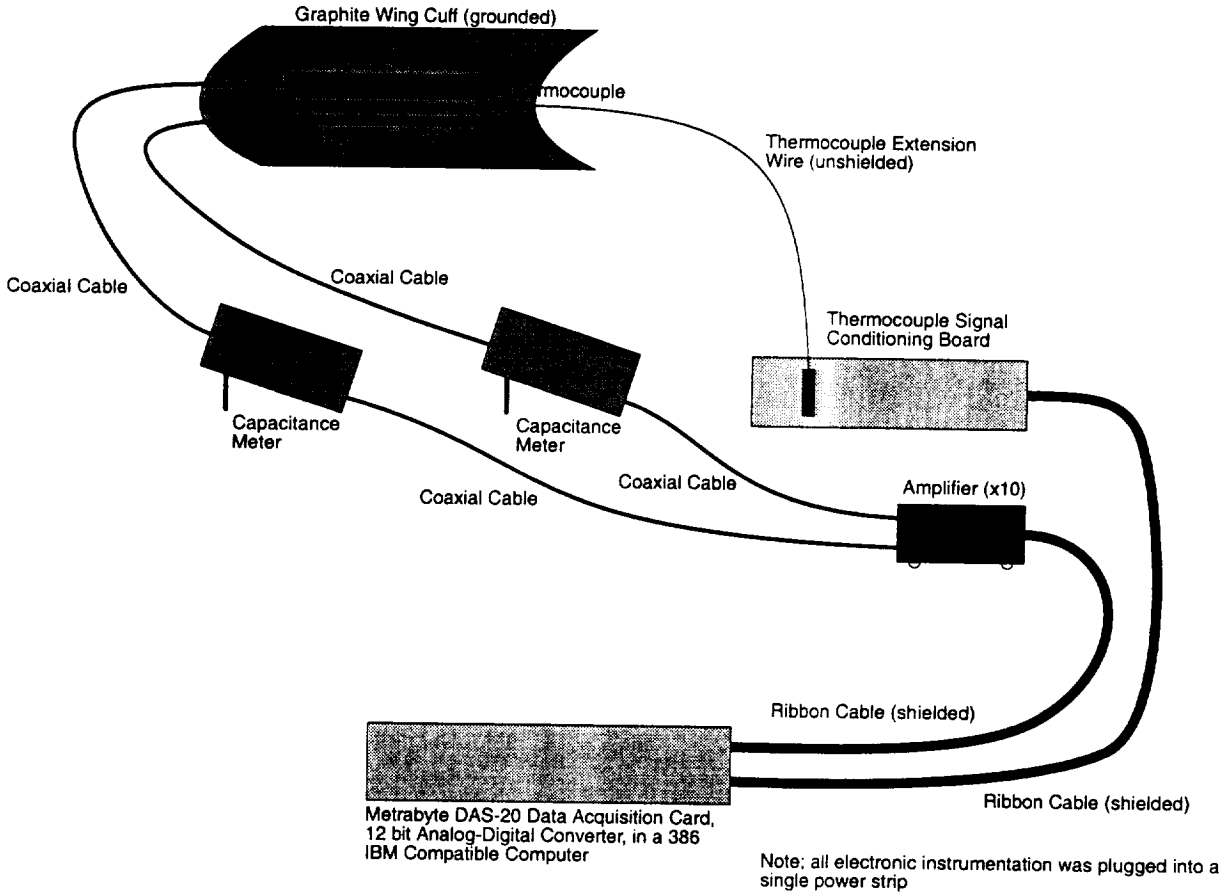

Figure 15. Block diagram of the data acquisition hardware used at the NASA IRT test.

Data Acquisition

A Metrabyte DAS-20 card installed in a 286 IBM compatible computer was used for data acquisition. The Labtech Notebook software was used to acquire and store this data in usable form. The number of channels, sampling rate, input range, number of averages, etc. of data could be determined. Math operations transformed this raw data to engineering units. A plot of the change in voltage (y-axis) with time (x-axis) was displayed on the screen in real time and stored for future reference. This data could be retrieved and plotted using standard graphics software like Lotus 1-2-3 or Quattro.

Test Procedure

Initially, the sensors were calibrated versus temperature as the tunnel temperature was lowered. Then, preliminary icing tests were performed to determine the angle-of-attack at which the stagnation line coincides with the center of the sensor strip. This is referred to as the 0^{o} angle-of-attack position with respect to the sensor. All future angles-of-attack are with reference to this position.

The rigid sensors were tested in glaze, mixed, and rime icing conditions, as outlined in **Table 2.**

Ice Type	Liquid Water Content (g/m^3)	Droplet Size (microns)	Airspeed (MPH)	Temperature (deg F)
Rime	1.5	20	100	-5
Mixed	1.5	20	100	12
Glaze	1.5	20	100	26

Table 2. Summary of test conditions used at the NASA IRT test.

Tests were also run to measure ice accretion rates for rime, mixed and glaze ice in the tunnel. Ice was allowed to build up continuously on the sensors for 3, 6, 9, 12 and 15 minutes. At the end of each interval the capacitance readings were recorded, ice thickness was measured with a pair of calipers and then the sensor was de-iced manually. For the rime ice case, thickness readings were only taken after a 15 minute interval as ice thickness appeared to increase linearly with spray time. From **Figure 16**, it appears that ice accretes linearly for glaze and mixed ice cases as well. The ice accretion rate is 0.054 in/min, 0.040 in/min and 0.030 in/min for rime, mixed and glaze ice cases respectively.

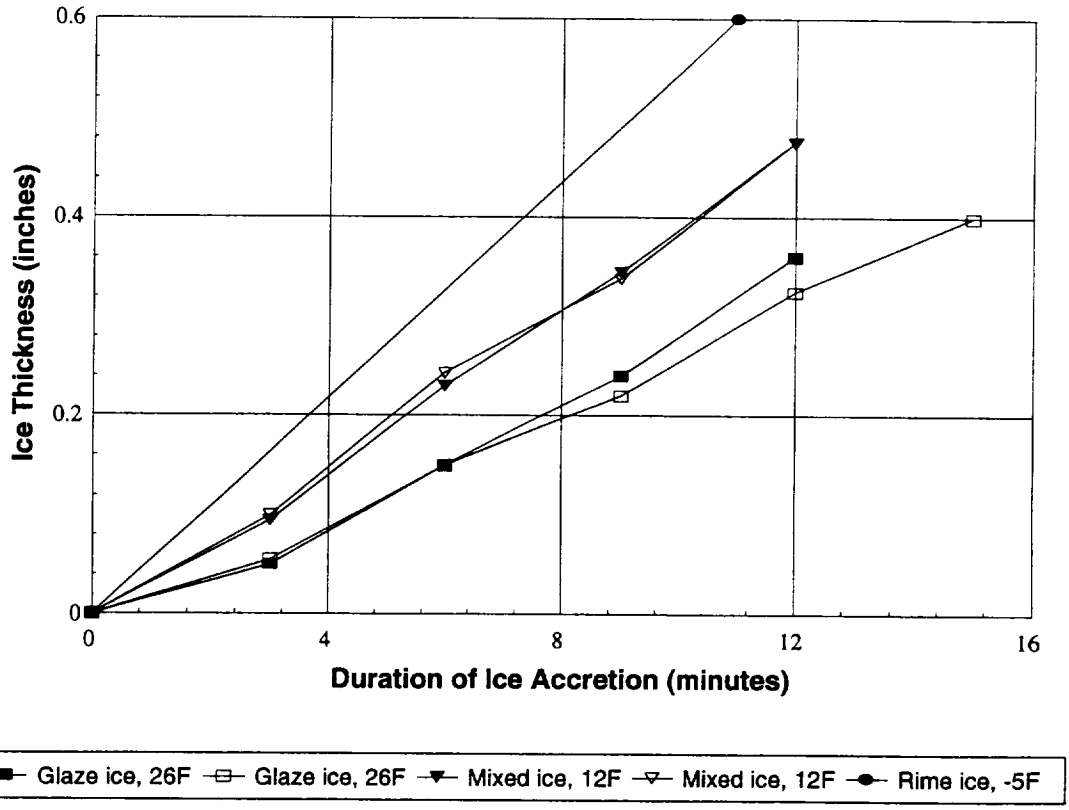

Figure 16. Ice accretion rates at NASA IRT for rime, mixed and glaze ice.

For the icing tests, the 1 nF range on the meter was selected so that the expected change in the capacitance sensor signal was less than one-tenth of the maximum reading in that range. The

signal was then multiplied by using a gain of 5 for the mixed (12°F) and glaze (26°F) ice cases and a gain of 10 for the rime (-5°F) ice case. The frequency of measurement for the 1 nF range is 10 KHz. This range was used for all icing tunnel tests as the expected change in capacitance is less than 200 pF. The meter offset was adjusted so that the signal for both capacitance sensors appears at the bottom of the voltage scale. The Labtech Notebook software acquired baseline data just before the start of icing. Dynamic measurements were taken as a function of time as icing was continued for about 12 to 15 minutes. The sensor data was acquired at a sampling rate of 10 Hz. An average of 10 readings was stored in the data file and plotted on the screen. Averaging tends to attenuate the noise in the signal.

Experimental Results

The rigid and elastic (non-functional) sensors were tested in rime, mixed, and glaze icing conditions. Overall, results for the rigid sensor under rime and glaze icing conditions looked good. However, certain anomalies were noticed in the capacitance readings for mixed icing conditions. A possible explanation for this anomaly and some key results are discussed.

For all icing cases, the Type 1 sensor seems to jump for ice thicknesses up to 0.15" after which it reaches a maximum threshold value and flattens out. The Type 2 sensor, however, increases with ice thickness up to at least 0.45" of ice after which it starts to asymptote to its threshold value. Typical Type 1 and Type 2 sensor responses at -5°F (powdery rime), 12°F (mixed) and 26°F (glaze) are shown in **Figure 17**. The change in Type 1 sensor signal is 0.7 V, 1.5 V and 2.2 V for rime, mixed and glaze ice respectively while the change in Type 2 sensor signal is 4.25 V, 12 V and 16 V respectively for the same ice cases. Thus, both Type 1 and Type 2 sensors respond to density of ice.

The Type 2/Type 1 sensor ratio in different icing conditions is shown in **Figure 18**. Contrary to patent projections, this ratio is not unique for all ice cases. Thus, while both Type 1 and Type 2 sensors do respond to changes in ice properties, this effect cannot be factored out completely. Also, the ratio does not increase linearly in the 0.15" to 0.4" ice thickness range.

From **Figure 18**, the sensor ratio for 12°F icing case is higher than that for the 26°F case. Since dielectric constant of mixed ice is between that of rime and glaze ice, the ratio for 12°F case should fall between that for the 26°F and -5°F cases. But, the 12°F icing cases were performed in the second half of the third day of testing. During these tests it was observed that ice did not form uniformly over the sensors, but, was tapered towards the top end of the cuff resulting in thinner ice over the Type 1 sensor and hence a higher sensor ratio. Also, in **Figure 19**, the ratio for a -5°F icing test performed on the third day is compared to a similar test performed on the first day of testing. The ratio on the last day was a lot higher than that for first day. This suggests some abnormality in tunnel behavior on the last day of testing. Thus, the 12°F runs may not be accurate.

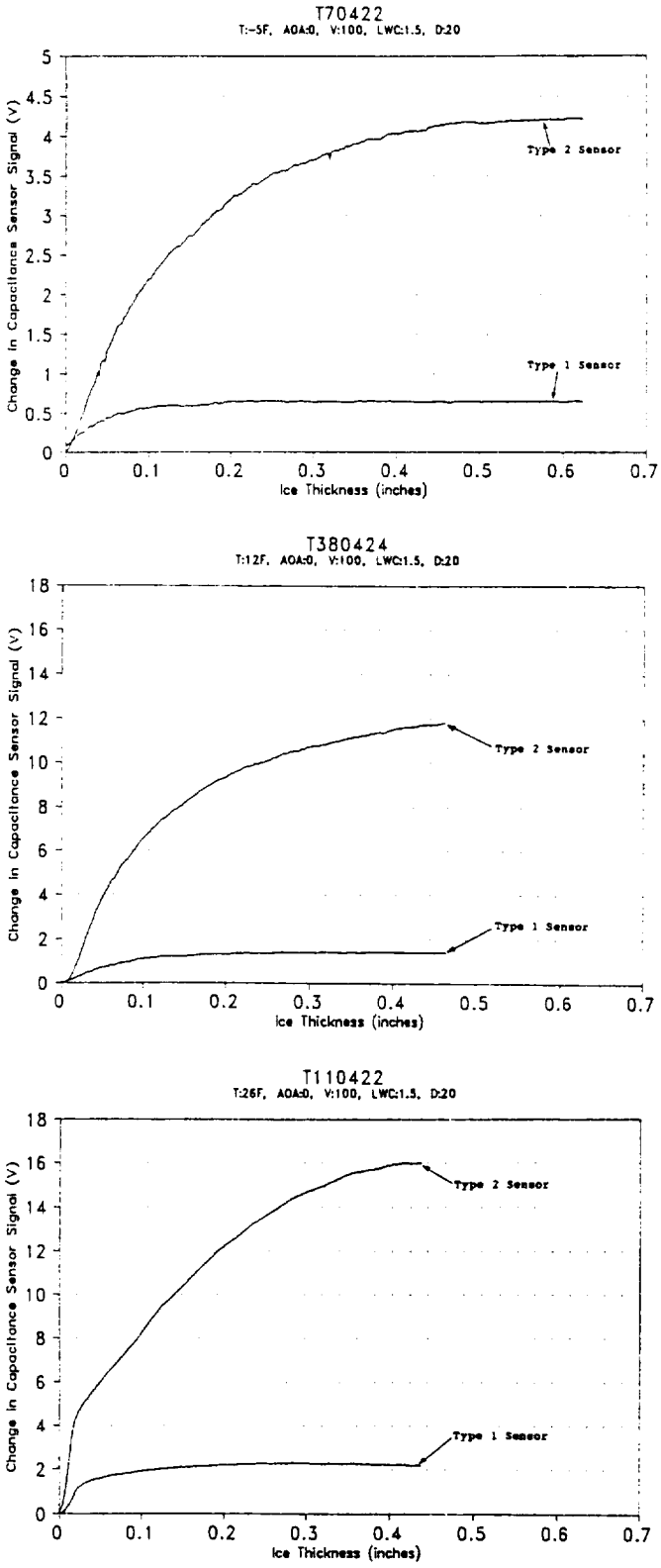

Figure 17. Typical Type 1 and Type 2 capacitance sensor response in a) rime, b) mixed and c) glaze icing conditions at the NASA IRT test.

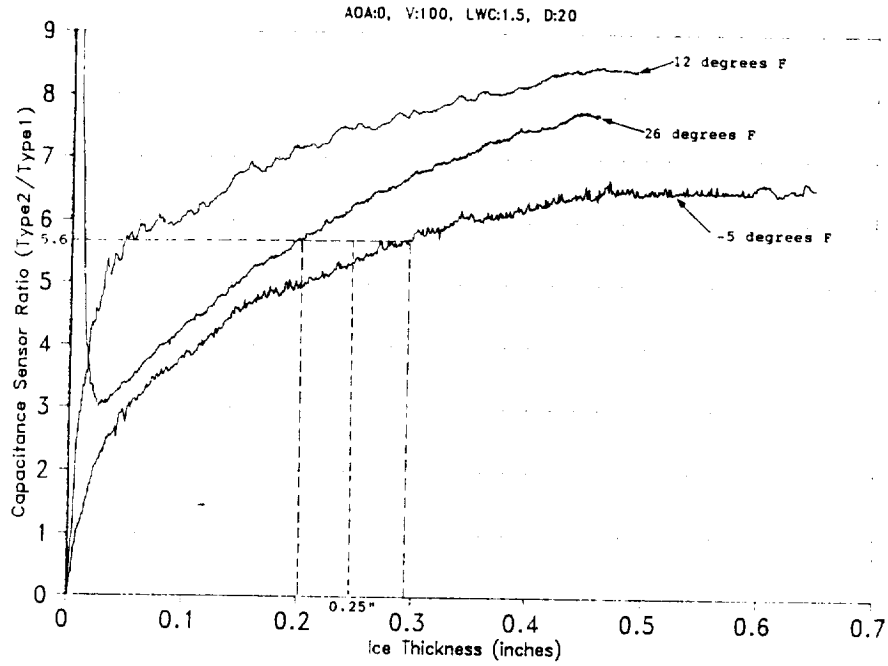

Figure 18. Capacitance sensor ratio (Type2/Type1) under different icing conditions at IRT.

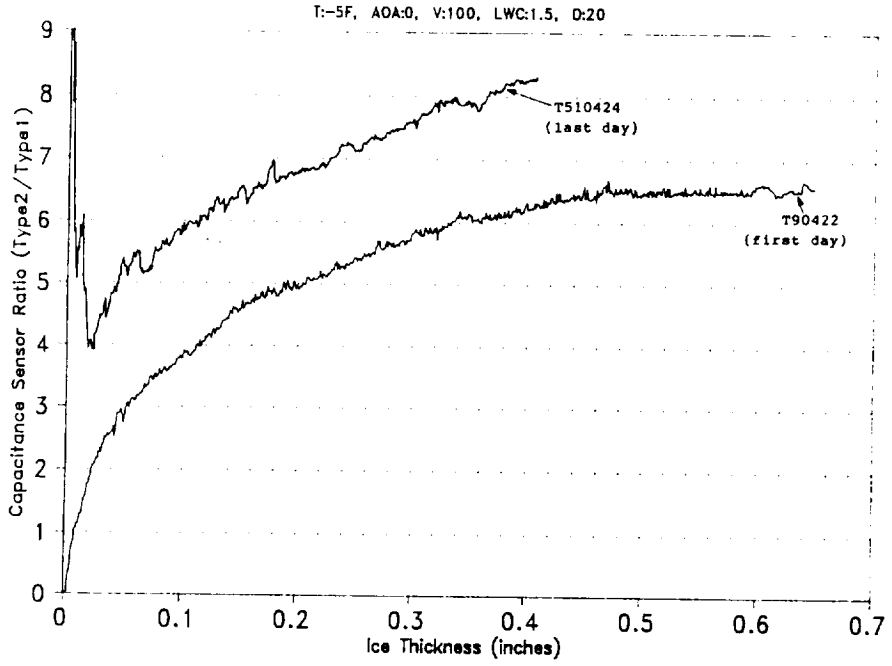

Figure 19. Comparison of sensor ratio for rime ice on first and third day of testing at IRT.

From **Figure 18**, if the automatic de-icing system is instructed to de-ice the plane when the capacitance sensor ratio is 5.6, from the -5°F ratio curve the predicted ice thickness is 0.29" and from the 26°F ratio curve the predicted ice thickness is 0.2". Thus, the error in the ice thickness measurement is +/- 0.045" for a target ice thickness of 0.25". It is important to remember that if the target ice thickness is lowered this error will be smaller, but if the target is made higher, their is a potential danger that the de-icer will never be activated. Note that the 12°F icing case has not been taken into consideration because of it's anomalous behavior.

The repeatability of test results was examined over a spectrum of angles-of-attack for rime, mixed and glaze ice cases. Many tests were performed back-to-back for each case under identical icing conditions. The Type 2/Type 1 sensor ratios for the different cases are included in **Appendix A**. In almost all cases, the sensor ratio curve is very repeatable. This is true even for tests performed on different days (not back-to-back) with the exception of repeatability data collected on the latter half of the last day.

Tests were performed to investigate the capacitance sensor response when an airplane goes in and out of icing clouds. To simulate this, ice was allowed to build up on the sensors for 6 minutes, after which it was turned off for three minutes, then re-started for another 6 minutes. The sensor response is shown in **Figure 20**. This response was compared to the response for 12 minutes of continuous icing. After the icing is turned off which represents the sensor coming out of an icing cloud, the signal drops as some of the water in the ice freezes resulting in a drop in the dielectric constant. Even with this drop, the sensor ratio after the two 6 minute interval icing case is the same as the ratio after 12 minutes of continuous icing.

The effect of angle-of-attack on sensor response is shown in **Figure 21** for the rime (-5°F) and glaze (26°F) ice case. For glaze ice, at small ice thicknesses, the Type 2/Type 1 sensor ratio has similar slopes at 0°, +/-1.5° and -3° angles-of-attack. This ratio is 6 with an error of +/-0.3 for 0.25" of ice. The error increases for thicker ice. The ratio curve is higher for +3° aoa case because the thickness of ice over the Type 2 sensor is a lot higher than that over the Type 1 sensor. However, this effect is not confirmed from the rime ice tests at 0° and +3° aoa.

After about 0.5" of ice accumulation at 26°F, when the de-icer was inflated several times, the ice removal was complete even over the sensors. But this was not true for the -5°F icing case when de-icing over the sensors was partial and required more inflation cycles. This may be because: i) rough neoprene over the sensors increases adhesive strength of ice and ii) the sensor may slightly inhibit inflation of the de-icer tubes at the leading edge. After complete sensor de-icing, the Type 1 and Type 2 sensor signals returned to their pre-test values.

Over most conditions, the rigid and elastic sensors did de-ice. For some rime ice cases when the non-elastic sensor did not de-ice the elastic did.

As temperature varies from 60°F to -5°F, the capacitance of Type 1 and Type 2 sensors change 1 pF and 20 pF respectively. However, the measured capacitance change was 6 pF and 40 pF for Type 1 and Type 2 sensors respectively, with rime ice; and 17 pF and 130 pF for Type 1 and Type 2 sensors respectively, with glaze ice. Thus, the influence of temperature on the Type 2 sensors though significant is not the dominant effect as compared to the influence of ice.

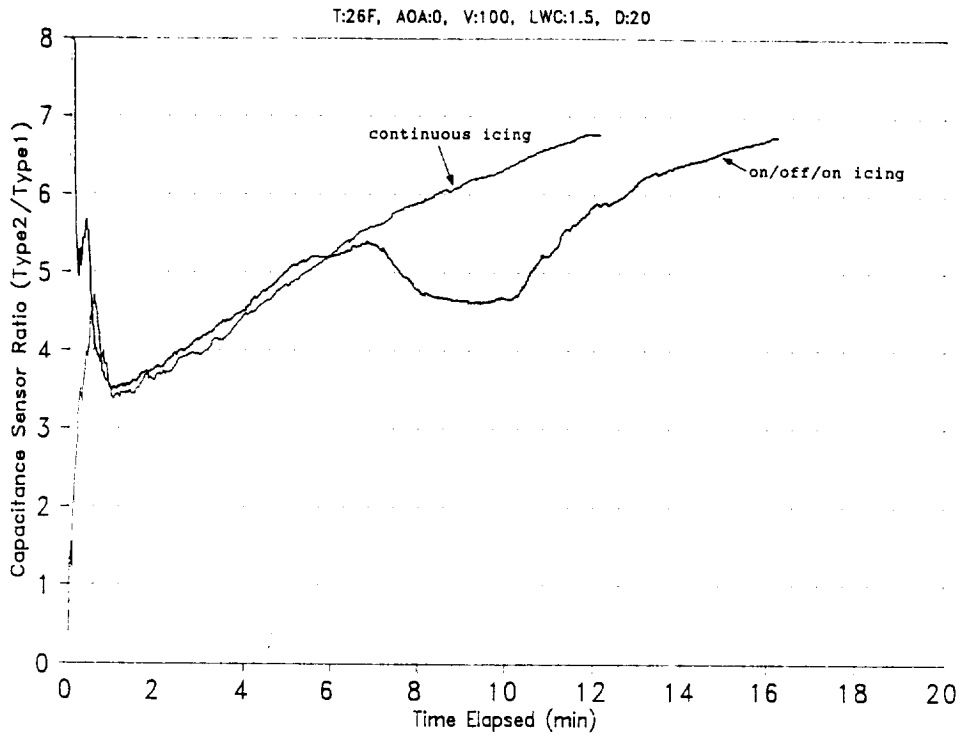

Figure 20. Comparison of sensor ratio for on/off versus continuous icing at IRT.

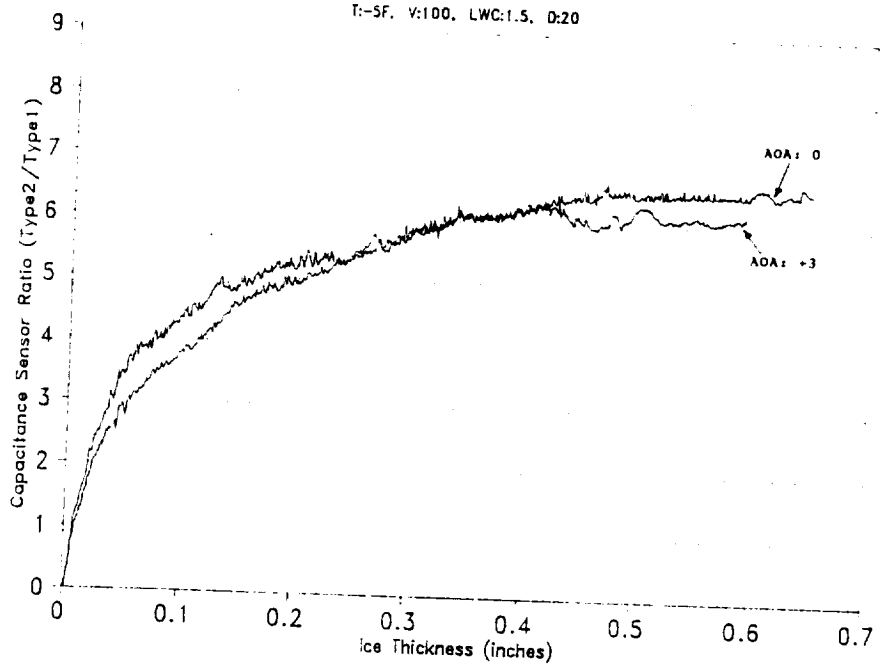

a)

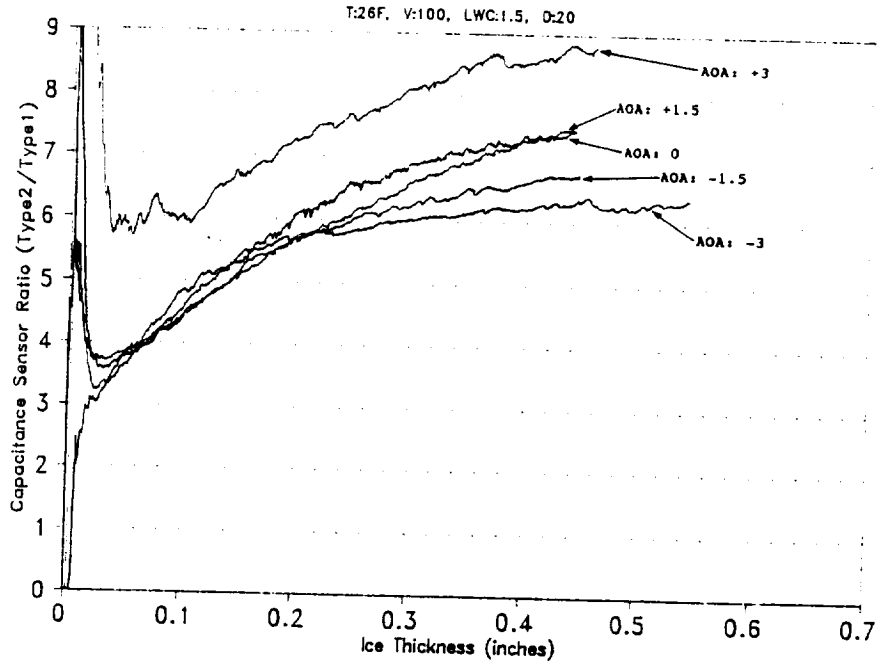

b)

Figure 21. Effect of angle-of-attack on sensor response for a) rime and b) glaze ice at IRT.

APPENDIX A

This appendix contains the Type 2/Type 1 capacitance sensor ratio for repeatability icing tests performed at different temperatures and angles-of-attack on the functional standard de-icer mounted on a wing cuff.

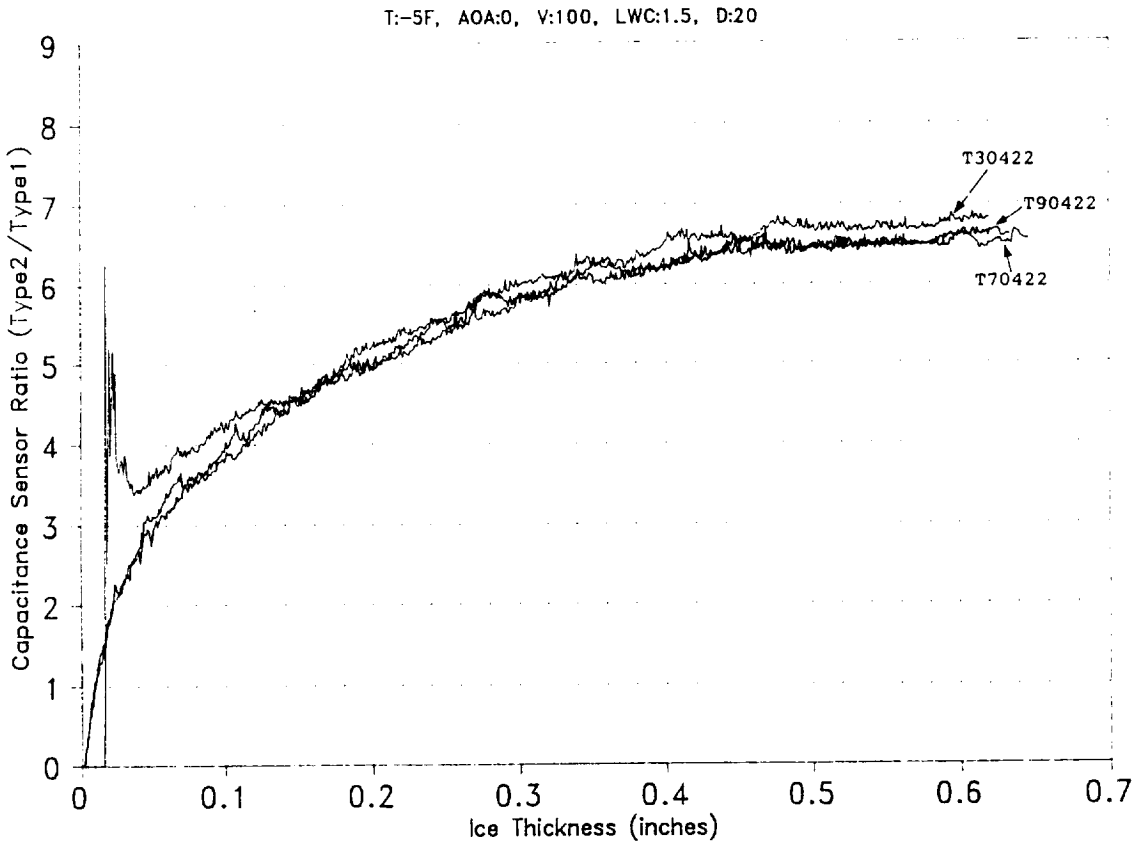

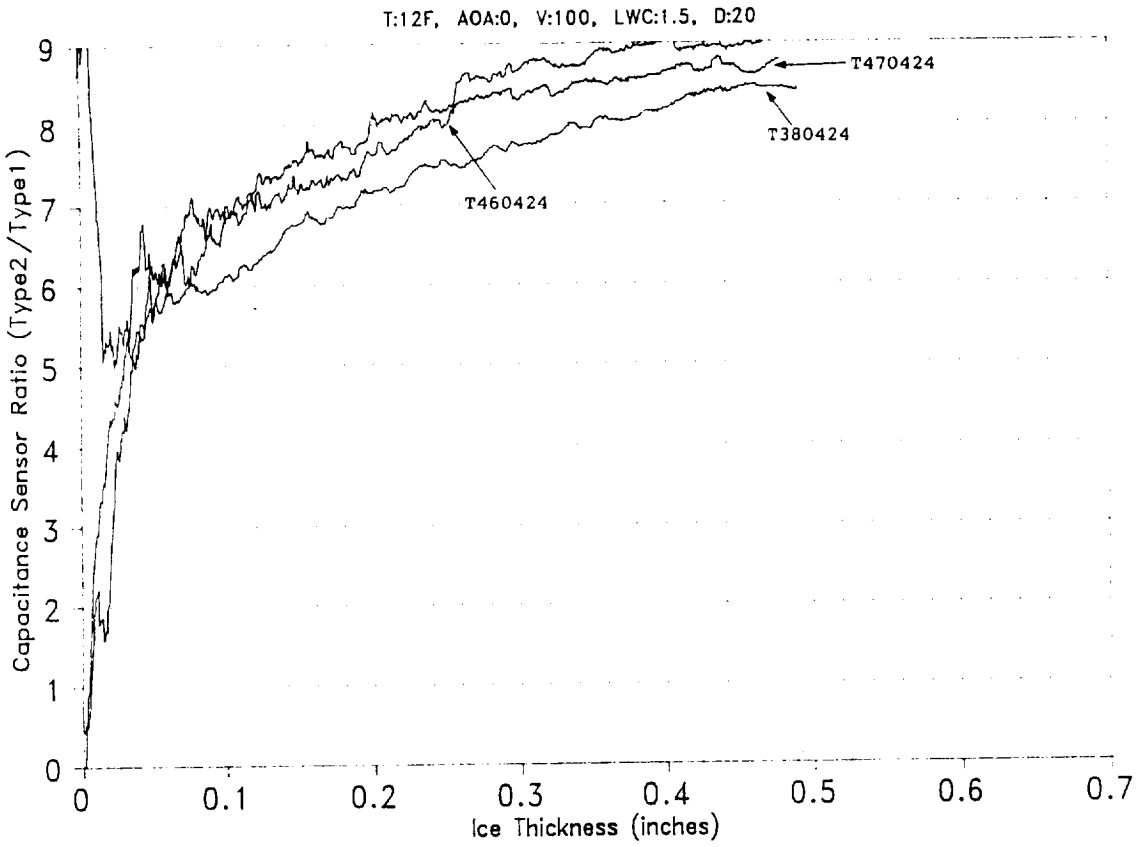
T:12F, AOA:0, V:100, LWC:1.5, D:20
T470424
T380424
T460424
Capacitance Sensor Ratio (Type2/Type1)
Ice Thickness (inches)
0
1
2
3
4
5
6
7
8
9
0
0.1
0.2
0.3
0.4
0.5
0.6
0.7

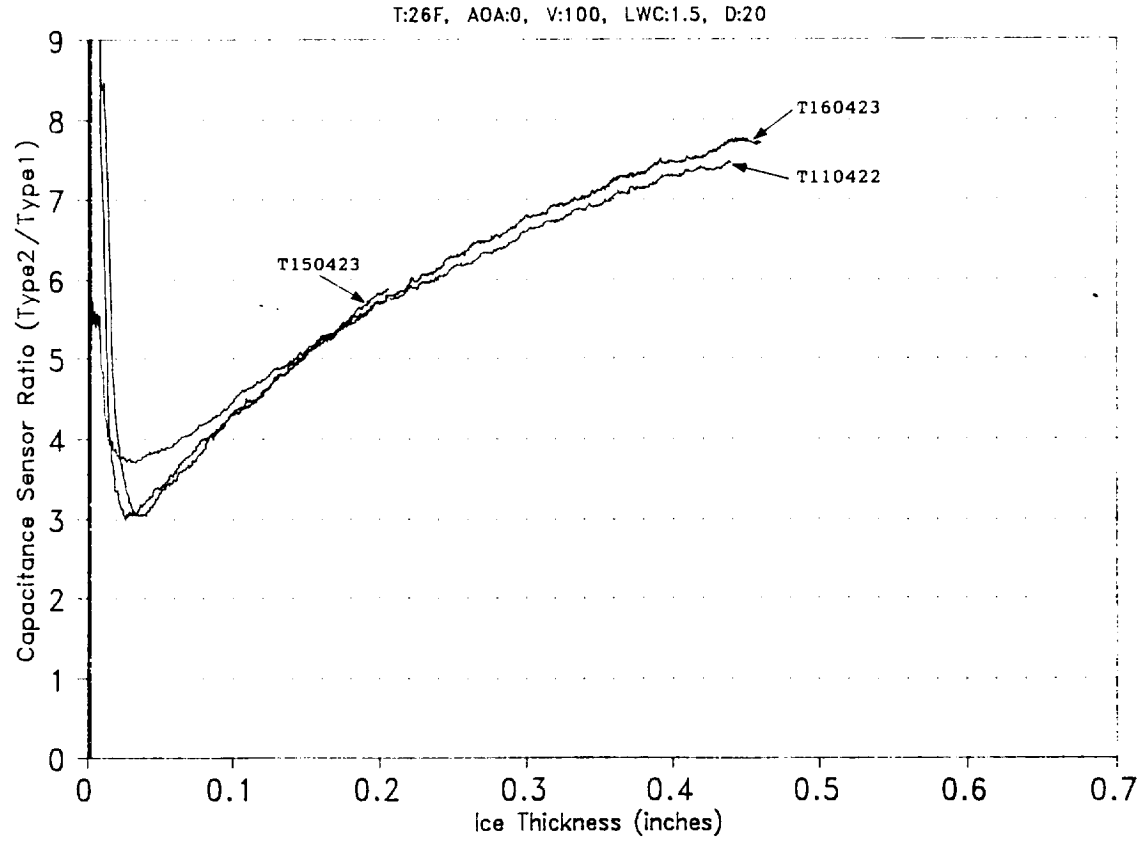
T:26F, AOA:0, V:100, LWC:1.5, D:20
T160423
T110422
T150423
Capacitance Sensor Ratio (Type2/Type1)
Ice Thickness (inches)
0
1
2
3
4
5
6
7
8
9
0
0.1
0.2
0.3
0.4
0.5
0.6
0.7

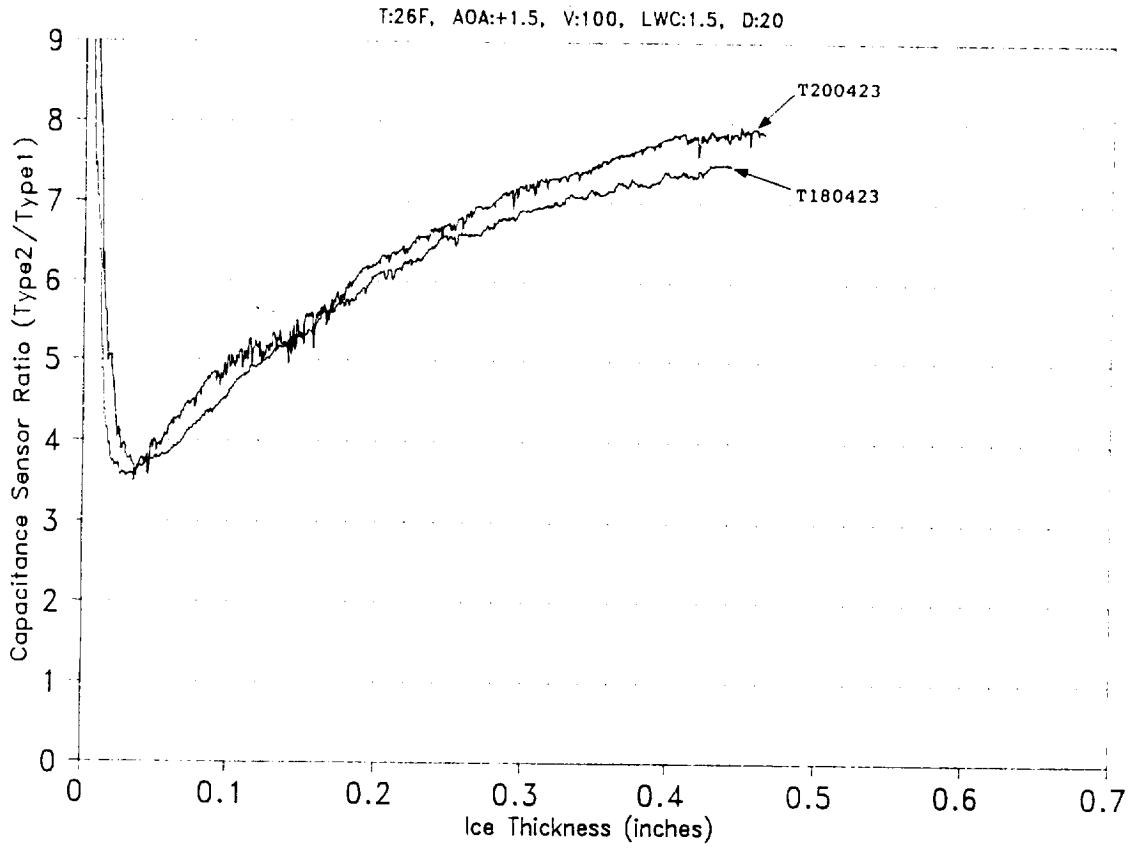
T:26F, AOA:+1.5, V:100, LWC:1.5, D:20
T200423
T180423
Capacitance Sensor Ratio (Type2/Type1)
Ice Thickness (inches)
0
1
2
3
4
5
6
7
8
9
0
0.1
0.2
0.3
0.4
0.5
0.6
0.7

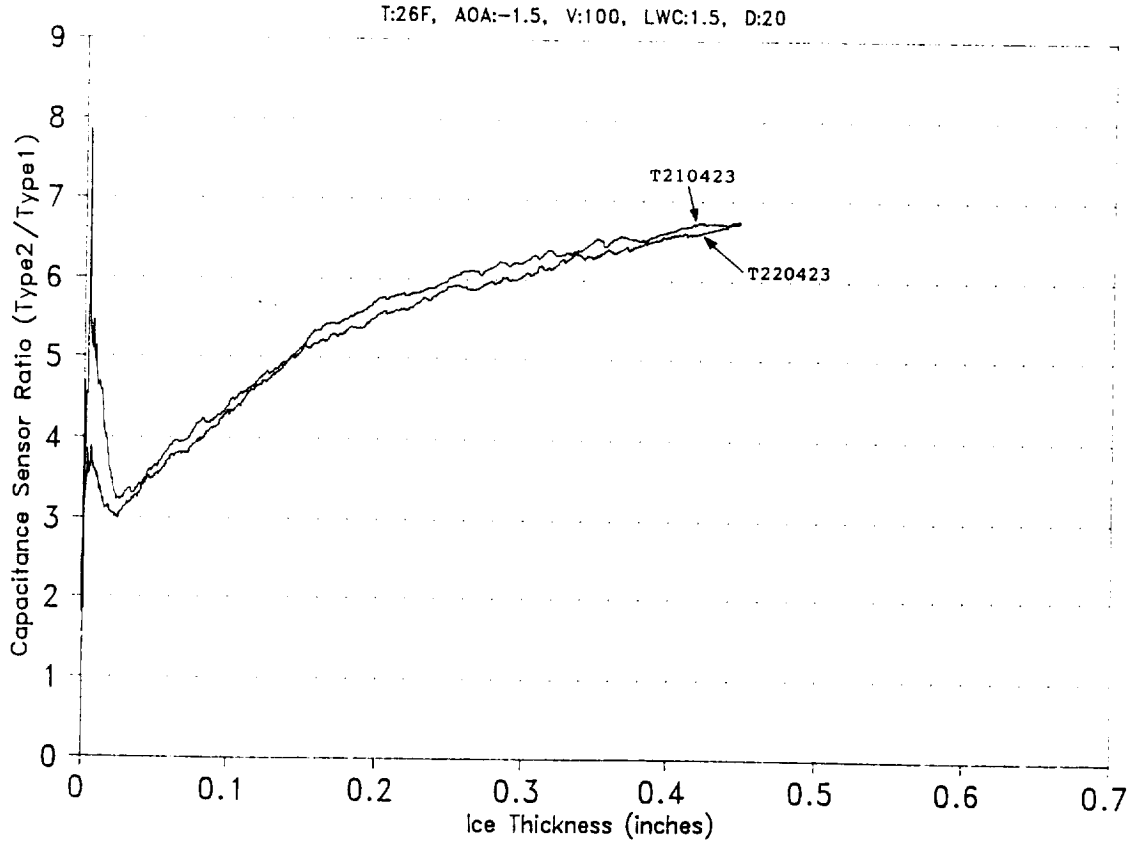
T:26F, AOA:-1.5, V:100, LWC:1.5, D:20
T210423
T220423
Capacitance Sensor Ratio (Type2/Type1)
Ice Thickness (inches)
0
1
2
3
4
5
6
7
8
9
0
0.1
0.2
0.3
0.4
0.5
0.6
0.7

Second Icing Tunnel Test at NASA

A second icing tunnel test was performed at the NASA IRT, from July 28 through July 31, 1992. The objectives of this test were to 1) evaluate the performance of a rigid sensor installed under the de-icing boot, 2) evaluate the performance of an elastic wire sensor attached to the outer de-icer surface, and 3) examine the effect of types of ice on ice thickness measurements made by the sensors. During the tests data collection proceeded smoothly. After post-processing the data at IDI, the underboot Type 1 sensor appeared to be unable to differentiate between ice types. Thus the third objective was not accomplished for the underboot sensor. The following sections detail the development work at IDI to manufacture and optimize the sensors used in these tests, a description of the tests, and the results obtained.

Sensor Development

We continued refining the rigid sensors that were tested in the first NASA IRT test. However, this time they were to be installed under the de-icing boot. Tests were conducted to determine the range of operation of these underboot sensors. Since conductive fabric was not readily available to manufacture elastic sensors, a wire sensor was developed which could also possibly be integrated within the de-icer. This sensor had the ability to stretch in one direction. For the wire sensor the influence of wire to wire spacing, wire diameter, insulating layer material, and adhesive on sensor performance was investigated.

Rigid Sensor Development

The Type 1 sensor was made wider to enable it to detect ice even when installed under the de-icer. Tests were conducted to determine the operational range of the Type 1 and Type 2 underboot sensors. Paper, which has a dielectric constant similar to that of rime ice, was used to simulate ice growth in these tests.

A simpler sandwich construction than that described in the first IRT test was used in making the sensor. As before, the Type 1 and Type 2 sensor electrodes were etched on a 0.0085" thick BEND/Flex laminate and a common ground plane was cut from another BEND/Flex strip. But in this case, the positive electrode strip was glued directly on top of the ground strip using spray adhesive, without an additional insulating layer. Thus, the composite backing of the positive electrodes separates them from the ground electrode and acts as the insulating layer. Also, since this sensor was to be installed under the de-icer it was not necessary to encapsulate it in neoprene.

The Type 1 and Type 2 sensors were made 18" long with a 0.100" wide electrode representing the Type 1 sensor and a 0.65" wide electrode representing the Type 2 sensor. The sensors had a 0.95" wide common ground plane. The sensor pair was installed under a functional de-icer on an aluminum plate which simulates the aircraft wing surface. Spray adhesive was used for the installation. Vacuum was drawn in the de-icer tubes and the sensors were tested with paper. **Figure 22** shows a typical sensor response. The Type 1 sensor responds to thin paper and

flattens out after a paper thickness of 0.15" while the Type 2 sensor has field lines going out a lot farther and hence is able to detect up to 0.45" of paper.

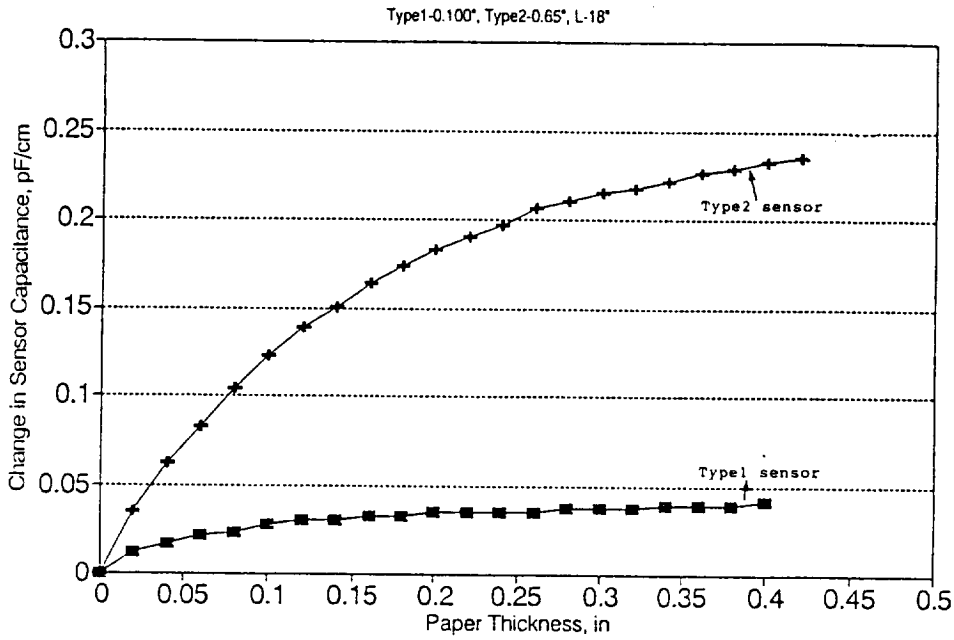

Figure 22. Lab test response of rigid sensors installed under a de-icing boot. This sensor design was later evaluated at the NASA IRT.

Wire Sensor Development

Since conductive fabric was not readily available to manufacture the elastic sensor a wire sensor was developed. This sensor had the ability to stretch in one direction and could possibly be integrated within a de-icer without inhibiting the inflation of tubes and adversely affecting de-icing efficiency. The effect of some of the design parameters such as spacing between the wires, wire diameter, material of insulating layer and different adhesives was investigated. The goal of this investigation was to improve sensor performance in the 0" to 0.5" ice thickness operating range. The sensor width was not varied during this study.

The electrodes for these elastic sensors were made using many thin wires. For each electrode, the wires were oriented lengthwise and separated by small uniform gaps. The positive and negative electrodes were separated by a thin flexible and elastic insulating layer and aligned in such a manner that each wire in the positive electrode has a corresponding wire in the ground electrode directly beneath it. The wires on both sides were attached to this insulating layer and held together by embedding them in a thin layer of adhesive with elastic properties. This adhesive layer was not much thicker than the diameter of the wires. Near the end of the sensor the wires in each of the electrodes were twisted together so that they are electrically connected. The sensor was wired by soldering co-axial cable to this twisted pair. Both the Type 1 and Type 2 sensors were manufactured using this method. A jig was fabricated to standardize the manufacturing technique for these sensors.

Tests were conducted with the sensor attached to the nose of a graphite MD-91 tail section (identical to that used in the BFG IWT tests) to include the effects of sensor curvature. The tail section was electrically grounded to simulate an aircraft wing while flying. Paper, which has a dielectric constant similar to that of rime ice, was used to simulate ice growth in all of the tests. The test sensors were all 0.65" wide and were fabricated with 0.010" Monel wire, 0.010" neoprene insulator, and RTV silicone adhesive, unless, the influence of one of the above parameters on sensor performance was being investigated.

A series of tests were conducted to investigate the influence of wire diameter on sensors employing the latest fabrication materials and techniques. 0.004" and 0.010" diameter wires were used to construct the sensors. While no significant advantage in terms of performance was observed of one wire size over the other, the 0.004" wires were difficult to work with and tended to break during the manufacturing process. Note that the maximum diameter of wire in this investigation was limited to 0.010" so that final thickness of the sensor could be kept under 0.035". For all subsequent wire sensors the wire diameter was fixed at 0.010".

The influence of wire gap size was investigated next. Three sensors with 0.030", 0.040" and 0.050" wire gap sizes were manufactured. The results, shown in **Figure 23**, indicate that using a wire to wire gap of 0.040" was the optimal choice. For gap widths both 0.010" larger and smaller the output sensitivity drops off noticeably for smaller ice thicknesses and to a lesser extent for greater ice thicknesses. For all subsequent wire sensors the wire to wire gap was fixed at 0.040".

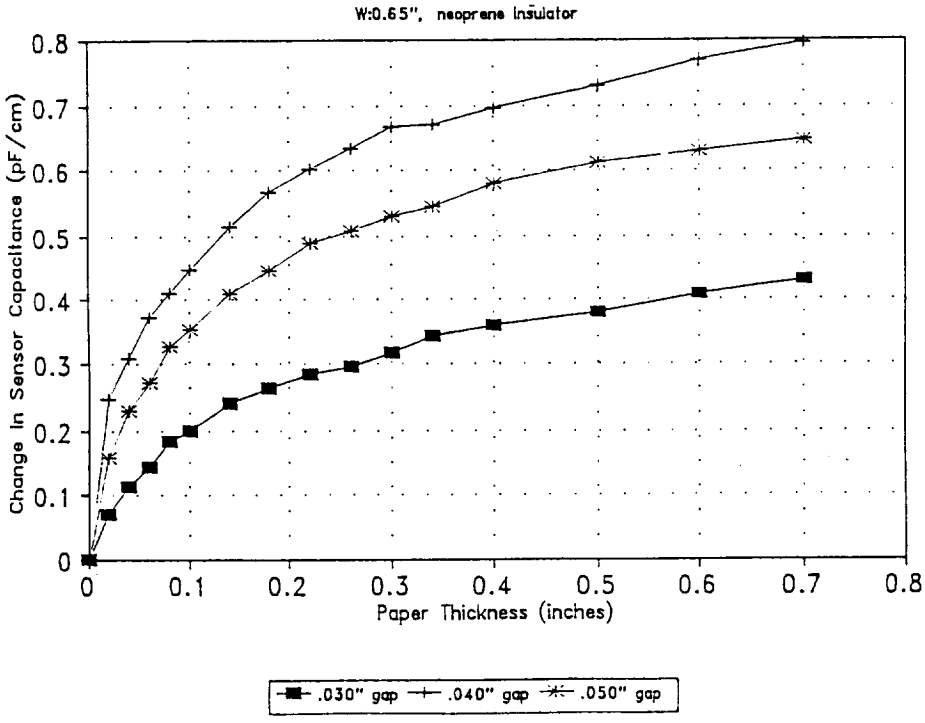

Figure 23. The influence of wire to wire gap size on a 0.65" wide Type 2 wire sensor using 0.010" Monel wire, a 0.010" neoprene insulating layer, and RTV silicone adhesive.

The influence of the insulating layer material is investigated next. Sensors with 0.010" thick silicone, latex and neoprene insulators separating the positive and ground electrodes were manufactured. The sensitivity of sensor with neoprene as insulator is higher than the sensitivity of the silicone and latex sensors and seems to be proportional to the dielectric constant of the insulating layer. The dielectric constant of neoprene and silicone is about 6.9 and 3 respectively and that for latex is between neoprene and silicone, from tests in the lab.

RTV silicone gel, latex caulk, and liquid neoprene were investigated as adhesives to glue the wires to either side of the insulator. The sensors were 0.85" wide. As in **Figure 24**, the change in capacitance for the silicone sensor is 0.38 pF/cm while that for the latex sensor is 0.42 pF/cm, in the 0.1" to 0.7" paper thickness range. Thus, the sensitivities for both sensors are fairly similar in this range of interest. However, silicone adhesive is preferred over latex because it provides a slightly longer working life and is easier to work with. The liquid neoprene adhesive uses a petroleum based solvent which caused the neoprene insulating layer to wrinkle making it very difficult to work with. As a result, this neoprene adhesive was not investigated further.

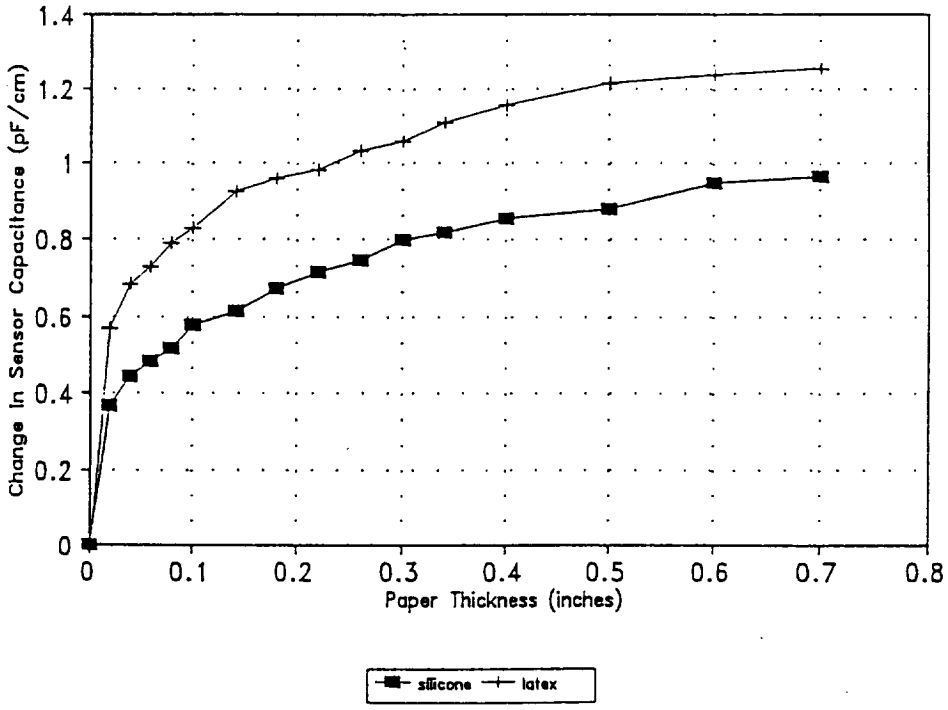

Figure 24. The influence of type of adhesive on a 0.65" wide Type 2 wire sensor using 0.010" Monel wire with a 0.040" wire to wire gap, and a 0.010" neoprene insulating layer.

Influence of electrode width on Type 1 sensor performance was investigated. Using two wires for Type 1 sensor electrodes results in sensor response flattening out at higher ice thicknesses, as the field lines go out much farther than desired. Hence, the Type 1 electrode was made by gluing just one wire to either side of the insulating layer. A typical Type 1 response is shown in **Figure 25**. The sensor flattens out after 0.15" of ice. The design parameters discussed above did not influence the performance of this Type 1 sensor.

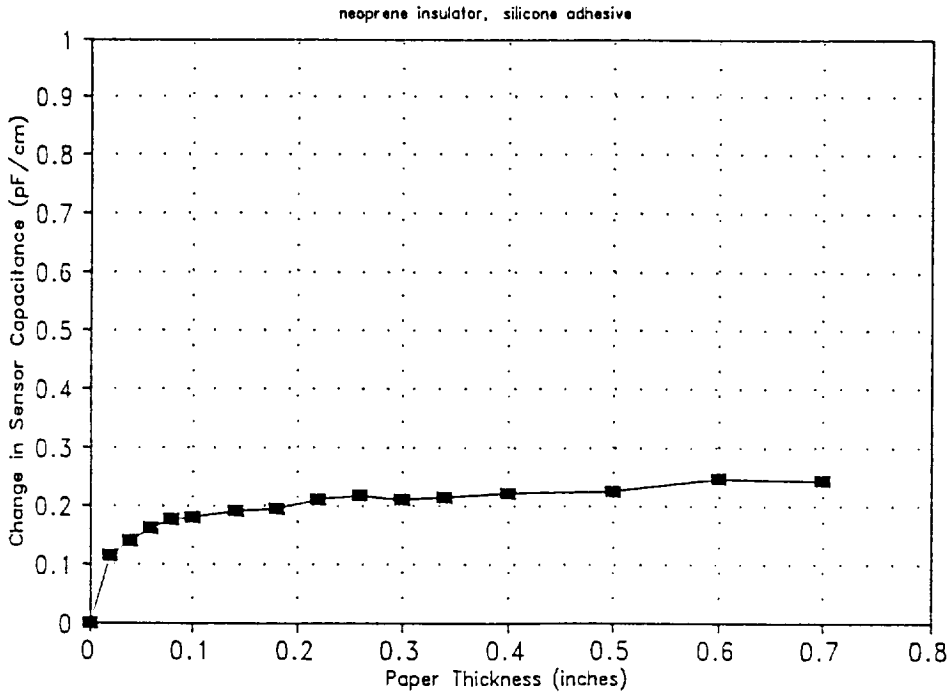

Figure 25. Typical response of a Type 1 sensor made using a single 0.010" diameter wire.

Wind Tunnel Experimental Apparatus

Test Setup

The overall test setup was similar to that at the first IRT test. One variation was that the rigid sensor was installed underneath the de-icing boot instead of being attached to the outer de-icer surface as in the first IRT test. Also, the non-functional fabric sensor from the previous test was replaced by a functional wire sensor at the same location on the outer surface of the boot. As a result of the spanwise orientation of the sensor electrodes, the elastic sensor is able to stretch in the chordwise direction. The rigid and elastic sensors were made 18" long and 0.95" wide.

Data Acquisition

The data acquisition hardware used for the second IRT test was the same as that used for the first test and will not be described here.

Test Procedure

After calibrating the sensors versus temperature and determining the 0^{o} angle-of-attack position with respect to the sensor, the sensors were tested in glaze, mixed, and rime icing conditions, as outlined in **Table 3**.

Ice Type	Liquid Water Content (g/m^3)	Droplet Size (microns)	Airspeed (MPH)	Temperature (deg F)
Rime	0.9	20	125	5
Mixed	1.1	20	125	15
Glaze	0.6	20	125	25

Table 3. Summary of test conditions used at the NASA IRT test.

Experimental Results

Rigid Sensor Data

Typical Type 1 and Type 2 sensor responses at 5°F, 15°F and 25°F are shown in **Figure 26**. For all ice types, the Type 1 sensor seems to reach a constant maximum threshold value when ice thickness is above 0.15". The Type 2 sensor, however, increases with ice thickness up to at least 0.45" of ice after which it starts to asymptote to its maximum threshold value. The change in Type 1 sensor capacitance is about 10 pF for all ice cases while the change in Type 2 sensor signal is 35 pF, 55 pF and 67 pF respectively for rime, mixed and glaze ice cases. Thus, while the Type 2 sensor responses are proportional to density of ice the Type 1 sensor is unable to differentiate between ice types. This could be attributed to the field lines of the Type 1 sensor not extending much above the de-icer surface, making it insensitive to variations in density of ice.

Figure 27 indicates that the Type2/Type1 sensor ratio is not identical for different ice types. Because of the undiscriminating nature of the Type 1 sensor to ice properties, the effect of ice types on sensor response cannot be factored out. The ratio increases with ice thickness in the 0.050" to 0.4" but not linearly.

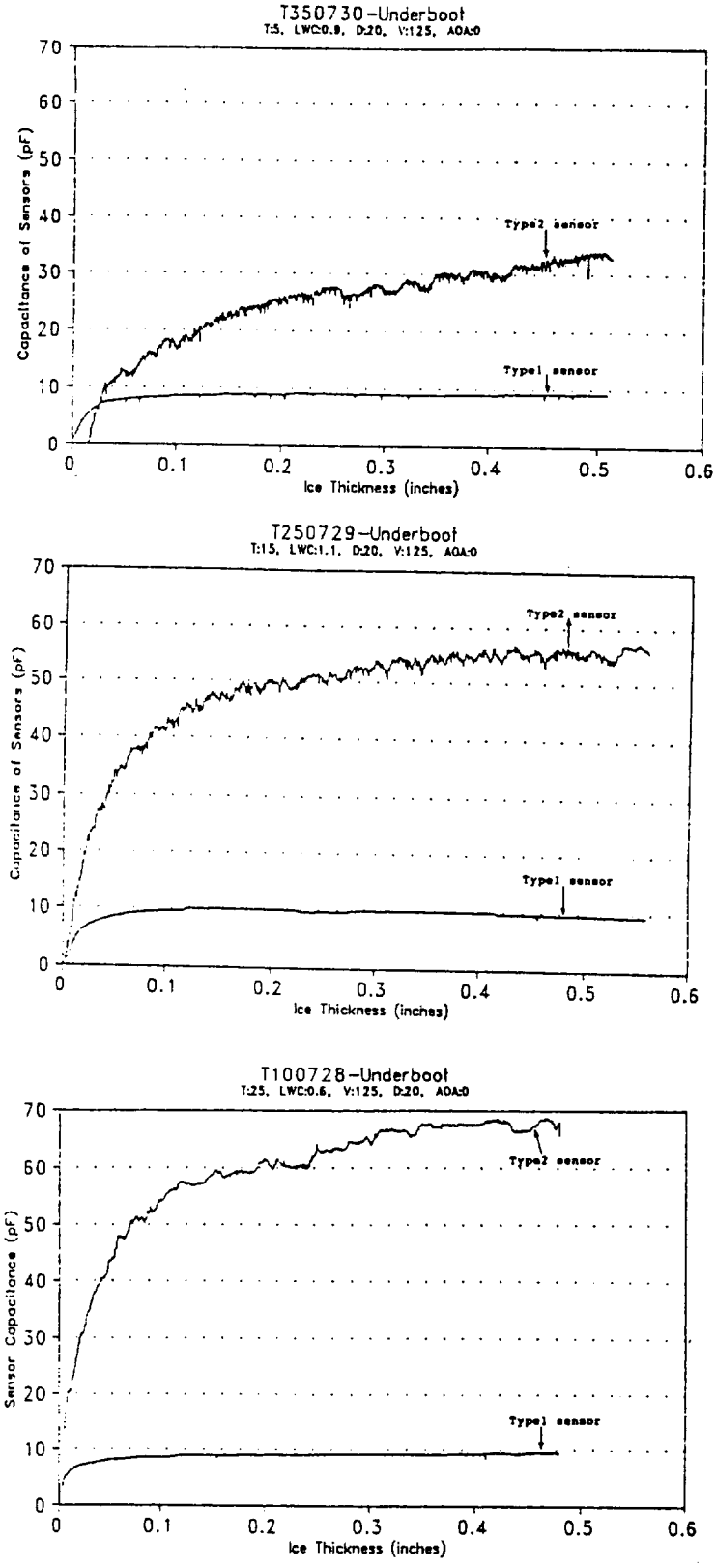

Figure 26. Rigid underboot Type 1 and Type 2 capacitance sensor response in a) rime, b) mixed and c) glaze icing conditions at IRT.

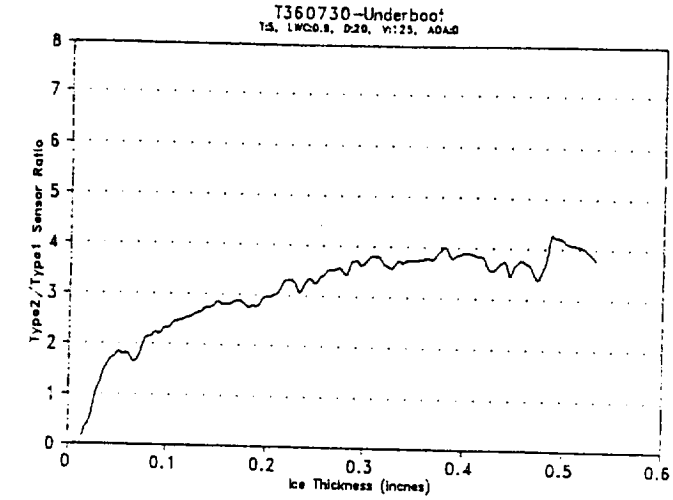

(a)

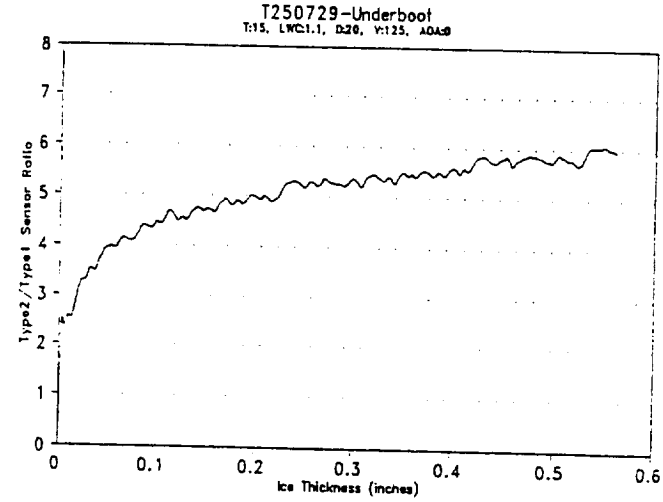

(b)

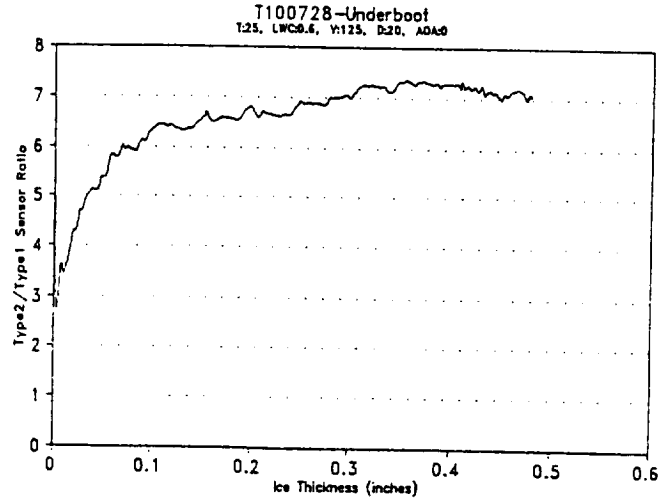

(c)

Figure 27. Capacitance sensor ratio (Type2/Type1) under different icing conditions at IRT.

Elastic Sensor Data

Figure 28 shows the sensor response to rime, mixed and glaze ice cases. The Type 1 sensor reached a constant maximum threshold value after 0.15" of ice. The Type 2 sensor, however, increased with ice thickness up to at least 0.45" of ice, for the 15°F and 25°F cases. Surprisingly, for the 5°F case, the Type 2 sensor seemed to jump for small ice thicknesses after which it started flattening out, almost like a Type 1 sensor. The change in Type 1 sensor was 12 pF, 16 pF and 20 pF for rime, mixed and glaze ice respectively while the change in Type 2 sensor signal was 50 pF, 67 pF and 85 pF respectively for the same ice cases. Thus, both Type 1 and Type 2 sensors responded to density of ice.

The Type 2/Type 1 sensor ratios are shown in **Figure 29** for rime, mixed and glaze ice cases. This ratio was not identical for the various ice cases. Thus, while both Type 1 and Type 2 sensors did respond to changes in ice properties, this effect could not be factored out completely. For the 5°F icing case, because of the strange behavior of the Type 2 sensor, the ratio was flat.

An investigation into the anomalous behavior of the Type 2 sensor at 5°F was conducted. **Figure 30** shows the temperature calibration of the Type 1 and Type 2 elastic sensors performed in the lab freezer. As the temperature changed from 0°F to 32°F, the Type 1 sensor capacitance increased by 3 pF but the increase in the Type 2 sensor capacitance was 32 pF. In the tunnel, when icing was started at 5°F, the temperature of the sensor jumped from 5°F to near 32°F due to latent heat of fusion. The Type 2 sensor capacitance jumped during this period not because it was responding to ice but because it was reacting to the sudden temperature gradient. This response to temperature seemed to drown the initial sensor response to ice. After this jump, as icing continued, the temperature started dropping until it reached 5°F. Now the sensor started reacting to ice thickness and not to temperature. Thus towards the end of the icing test, the final values of the ratio were indicative of ice thickness. This effect was not observed at 15°F and 25°F because the temperature gradient was a lot smaller, making the temperature effect less dominant. Thus, temperature compensation will be required in future tests to cancel the change in capacitance of sensor due to temperature effects.

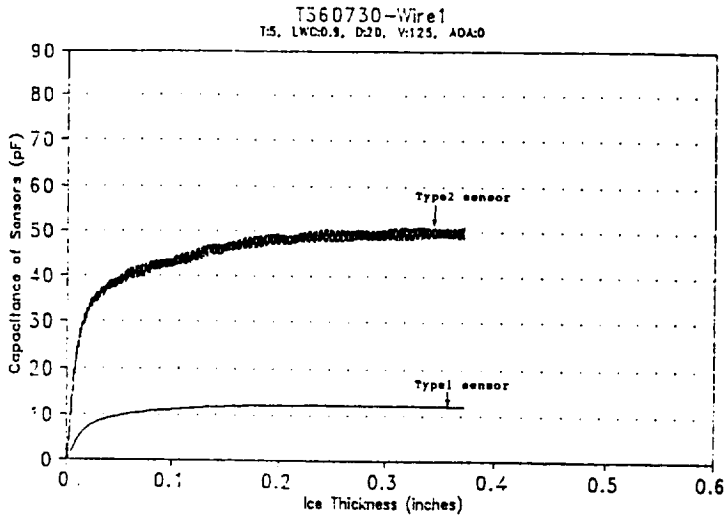

(a)

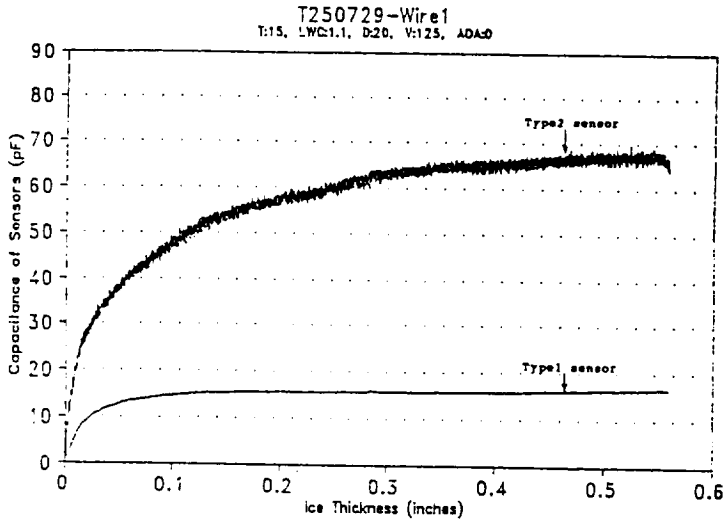

(b)

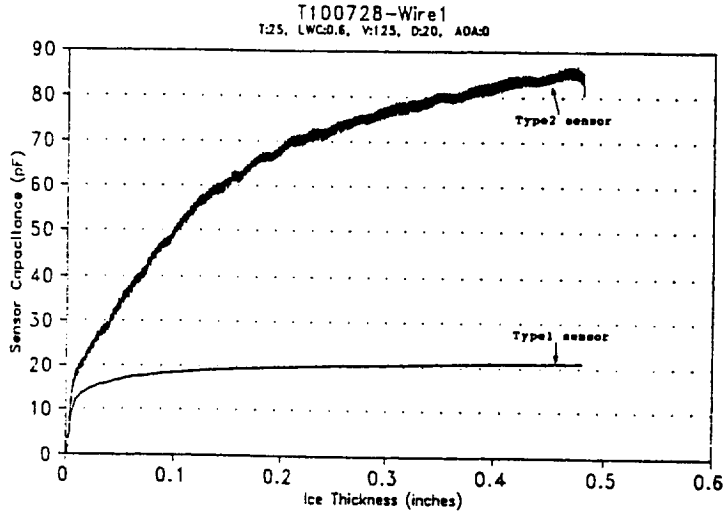

(c)

Figure 28. Elastic Type 1 and Type 2 wire sensor response to a) rime, b) mixed and c) glaze ice at IRT.

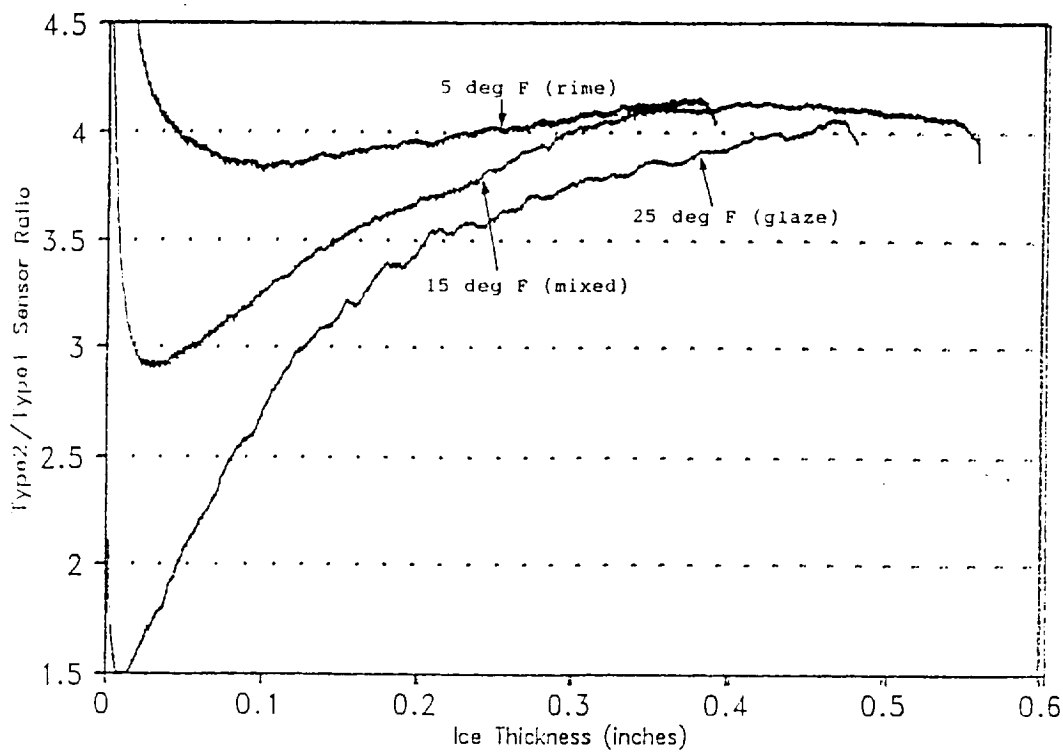

Figure 29. Elastic Type2/Type1 sensor ratio for different ice types at IRT.

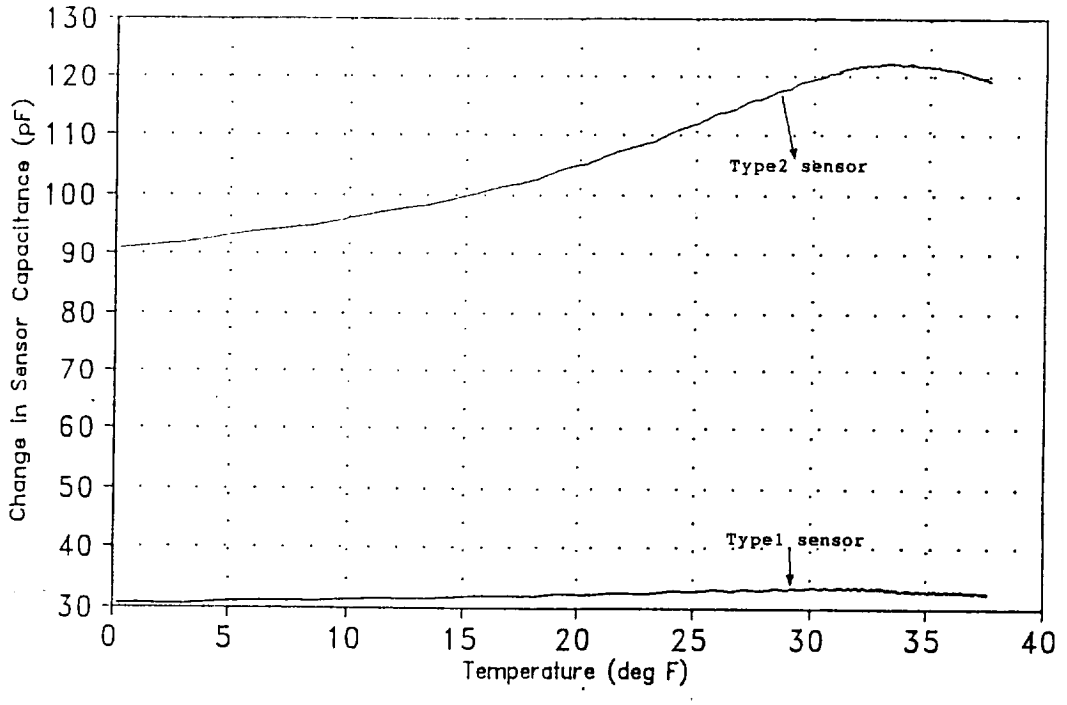

Figure 30. Effect of temperature on Type 1 and Type 2 elastic sensor capacitance's in the lab freezer.

Wind Tunnel Tests at BFGoodrich De-Icing Division

Wind tunnel tests were performed at the BFGoodrich Icing Wind Tunnel, IWT, from October 26 through October 28 1992. The objectives of this test were 1) to evaluate the performance of a fabric sensor that could stretch in both the chord and spanwise directions, 2) evaluate the performance of a rigid sensor that would be mounted under the de-icing boot, 3) determine the benefits of operating the sensors in guard mode, and 4) obtain data that could be used to calibrate the sensors used in the NASA Otter flight tests. During the tests data collection proceeded very smoothly, but as the data were post-processed at IDI it became apparent that much of the data were contaminated with noise. Due to this noise the first three of the stated objectives were only partially achieved and the fourth objective was not accomplished. The following sections detail the development work performed at IDI to optimize the sensors used in these tests, the data acquisition hardware used, and the results obtained.

Sensor Development

We continued refining the elastic wire and rigid underboot sensors that were tested in the second NASA IRT test. Tests were conducted to determine an optimal sensor width that would give good sensitivity to ice accretions up to 0.5" thick while still being narrow enough to fit within the stitch lines of a standard pneumatic de-icing boot. For the underboot sensor the influence of Type 1 width was looked at. During this period BFGoodrich requested that we investigate sensors that could work with boots using inflation tubes running in the chordwise direction as well as the spanwise direction. To accomplish this we investigated making sensors out of a lycra material that was chemically treated to be electrically conductive. We had investigated this material previously and found that it performed well, but due to its limited availability had not pursued it further. Because of its ability to stretch in both directions and thus work with either orientation of boot inflation tubes we decided to resume our efforts to develop a bi-directionally elastic fabric sensor. In addition to improving sensor performance through sensor design modifications we also investigated using an electronic guard circuit technique. By controlling the electrical potentials of the sensor elements we were able to further improve sensor performance and eliminate some of the drawbacks intrinsic to our design such as temperature sensitivity and low signal resolution.

Wire Sensor Development

Work was performed on optimizing the sensor geometry to improve the output sensitivity throughout the operating range from 0" to 0.5" of ice thickness. Testing was focused on the overall sensor width of the Type 2 wire sensor. Tests were conducted with the sensor attached to the nose of a graphite MD-91 tail section (identical to that used in the BFGoodrich IWT tests) to include the effects of sensor curvature. Paper, which has a dielectric constant similar to that of rime ice, was used to simulate ice growth in all of the tests.

The width of the Type 2 sensor can not be increased indefinitely for two reasons. The first reason is that from an installation perspective it is easier to bond the sensor between two of the spanwise stitch lines in the boot which eliminates the chance that the bond will fail in the steep

valley formed at the stitch line when the boot is inflated. This stipulation limits the overall width of the Type 1 and Type 2 sensor to roughly 1.25".

The second reason is associated with the fact that our sensors generate an output proportional to the volume of ice within the field lines above the sensor. To correlate that volumetric measurement to a thickness measurement we need to make some assumptions about the length and width of the measurement volume. If we assume that the field lines are uniformly covered in the spanwise direction (which is a good assumption for the sensor/wing combinations tested to date) then the thickness value interpreted from the sensor readings is an integrated average over the chordwise extent of the field lines. If the sensor is relatively narrow and located beneath the center of the ice pack then the integrated ice thickness will be representative of the peak thickness. A number of these spanwise sensors distributed along the chord can give a rough estimate of the chordwise extent and shape of the ice pack. If the sensor is too wide the integrated thickness will be a function of not only the average thickness, but also of the chordwise extent of the ice pack. A very wide sensor would have trouble distinguishing between a thick, narrow ice pack and a thin, wide ice pack.

Tests were conducted on three different width Type 2 wire sensors all made with .010" Monel wire using .040" gaps between wires, 0.010" thick neoprene insulator, and RTV silicone adhesive. The results from these tests are shown below in **Figure 31**. The initial sensitivity to thin layers of ice is best for the 0.85" wide sensor and roughly the same for the 0.65" and 0.75" wide sensors. As the simulated ice thickness was increased the sensitivity of the two wider sensors became more similar while that of the 0.65" sensor fell below the others. Because the performance of the 0.85" sensor was no better than that of the 0.75" wide sensor in the critical thick ice regime it was decided to use a 0.75" wide Type 2 sensor in the subsequent BFGoodrich wind tunnel tests.

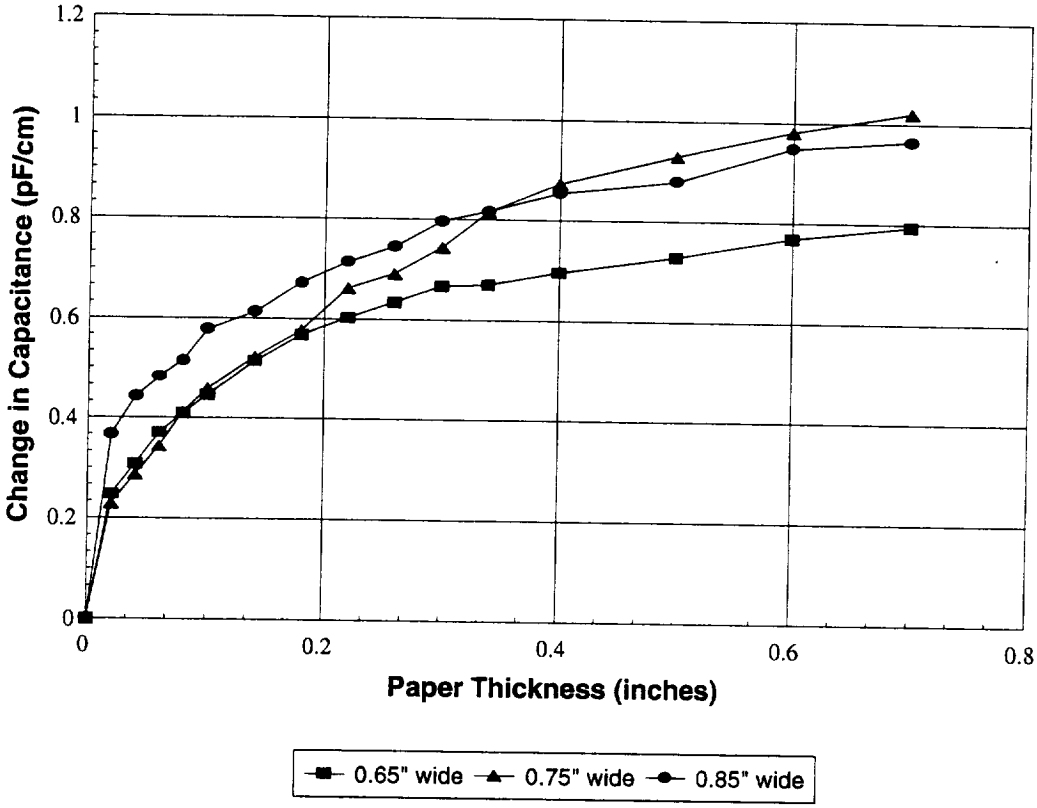

Figure 31. The influence of Type 2 sensor width on performance. All sensors were fabricated with 0.010" Monel wire on 0.040" gaps, a 0.010" neoprene insulating layer, and RTV silicone adhesive.

Fabric Sensor Development

In order to develop a fully compatible pneumatic boot elastic sensor, at BFGoodrich's request, that could stretch both in the chordwise and spanwise directions we resumed the development of a sensor based on an electrically conductive lycra fabric[1]. The fabric investigated, a standard lycra material treated with polypyrrole, is sold by Milliken Research Corporation under the trade name of Contex Fabric.

The resulting sensor was configured very similarly to the wire sensor. The Type 2 sensor was fabricated from two identical pieces of lycra, 0.75" wide by 11" long, co-located and glued to the top and bottom of a .010" neoprene insulator. The Type 1 sensor was similarly formed by attaching one 11" length of .010" Monel wire to the top of the same neoprene sheet and a second length of wire to the bottom of the neoprene directly below. The Type 1 sensor ran parallel to the Type 2 with a 0.4" separation gap between them. Use of a metal wire for the Type 1 sensor would preclude the bi-directional elasticity that would eventually be needed, but was temporarily used to allow the evaluation of the fabric Type 2 sensor in actual icing conditions.

Laboratory tests of the fabric sensor were performed on the MD-91 wing section using paper to simulate rime ice. The results indicate that the fabric sensor performs qualitatively the same as the wire Type 2 sensor but has greater sensitivity to thin layers of ice, as shown in **Figure 32**. It was later discovered that due to the low conductivity of the fabric the sensitivity of the sensor decreased with increasing distance from the electrical connections. This means that the change in capacitance values (pF/cm) shown in the below figure are lower than would be reported for a shorter sensor of similar construction. The scientists at Milliken feel that they can improve the conductivity of the fabric which should increase the overall output for sensors of the length being investigated here. The graph shown below is for the actual sensor used in the BFGoodrich wind tunnel tests as tested at IDI before it was embedded into a boot by BFG.

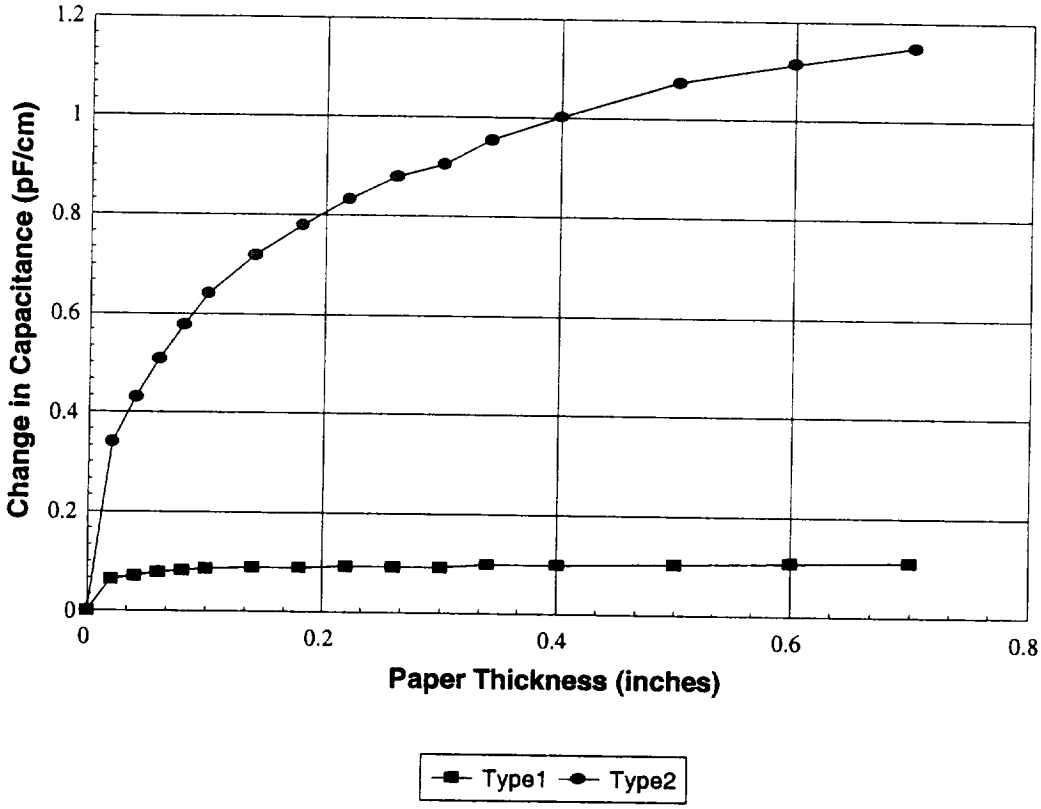

Figure 32. Change in capacitance versus simulated ice thickness for a 0.75" wide conductive fabric Type 2 sensor and a single wire Type 1 sensor. Both fabricated with 0.010" Monel wire, 0.010" neoprene insulating layer, and RTV silicone adhesive.

Guard Circuit

Experiments were performed to see if a guard circuit technique could be used to improve the performance of our system. This technique involves using additional electronics to generate a guard signal that is at the exact voltage and phase as the measurement signal going to the positive electrode in our sensor. Since there are no electric field lines between two equipotential surfaces a third guard electrode can be placed between the positive electrode and the ground plane to

block the field lines. In our design a guard electrode was placed below the positive electrode to block the primary field lines going directly to ground. Because the electronics are designed to disregard any capacitance between the guard and ground and measure only the capacitance between the positive electrode and ground virtually all of the initial baseline capacitance of the sensor was eliminated. Additionally the shield of the coaxial cable used to connect the capacitance meter to the sensor is also connected to the guard which eliminates the baseline capacitance of the cable. Using the guard circuit with a typical Type 2 sensor and coaxial cable can reduce the initial baseline capacitance from something in the range of 1500 pF to roughly 5 pF. Because the capacitance of the coaxial cable is almost completely canceled the cables can be any length for any aircraft and the range of the capacitance meter does not have to be customized. This dramatic reduction in baseline capacitance also allows for the redesign of the capacitance meters so that the roughly 100 pF change in capacitance associated with icing can consume a majority of the meters range allowing for better accuracy and resolution than previously achievable.

A second benefit of the guarded sensor is that the effect of temperature on baseline capacitance is virtually eliminated. As mentioned above, with unguarded sensors most of the baseline capacitance comes from the primary field lines going directly from the positive electrode, through the neoprene insulator, to the ground. As the temperature of the sensor changes the neoprene will expand and contract which creates a linearly proportional change in the sensor's baseline capacitance. Even though the change in neoprene thickness may be less than 1% this creates a change in baseline capacitance which is roughly of the same order of magnitude as that created by the ice build-up. By eliminating the primary field lines and thus the large baseline capacitance the guarded sensor exhibits virtually no change in output with temperature.

This idea was verified in a test performed in the cold chamber at IDI. A wire Type 2 sensor instrumented with a T type thermocouple was attached to the MD-91 wing section and placed into the cold chamber. Once the temperature stabilized the wing section was removed from the chamber and the temperature and capacitance were simultaneously recorded with a computerized data acquisition system. Data were collected with the sensor operating in unguarded and guarded mode and are presented below in **Figure 33**. The results are clear. Use of the guard circuit alleviates the problem of having to temperature compensate the output of the sensor making the system that much more accurate and reliable.

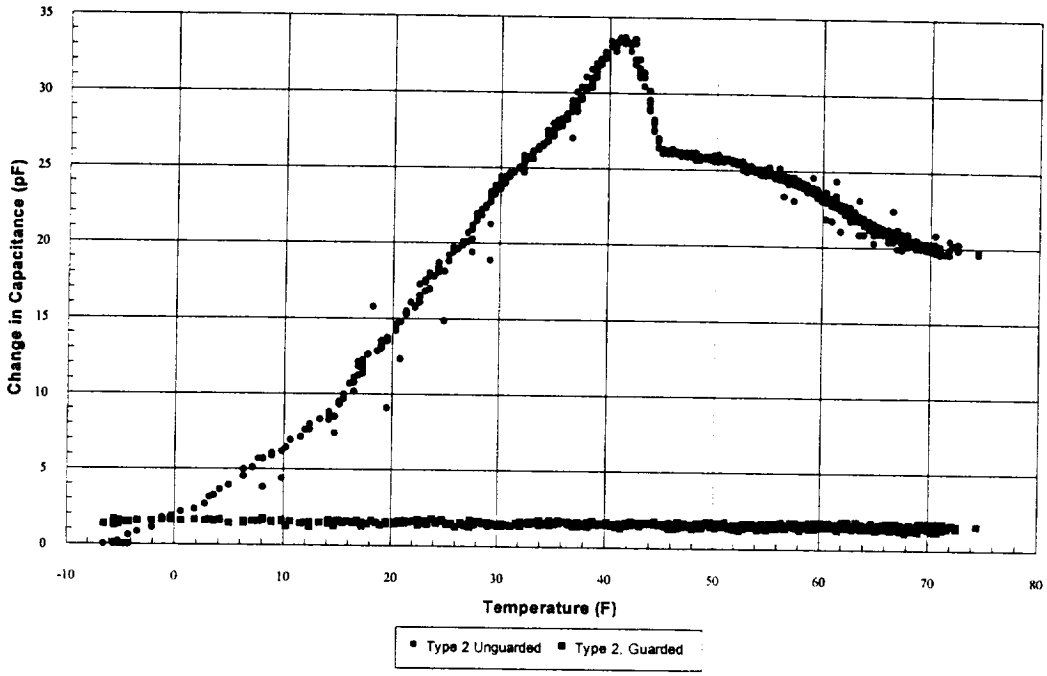

Figure 33. Change in capacitance versus sensor temperature for a wire Type 2 sensor operating in guarded and unguarded modes.

A report in *NASA Tech Briefs* indicated that using a very wide guard electrode could increase both the range of the capacitive sensor and its sensitivity[2]. These claims were investigated through tests on a wire sensor mounted to an MD-91 wing section. Tests using paper to simulate rime ice were performed with various width guard electrodes placed between the top positive electrode and the ground plane. The results shown below in **Figure 34** indicate that as the guard width was increased the sensitivity to thin ice decreased rapidly while the sensitivity to thicker ice and thus the range was relatively unchanged. These trends are also seen in the BFGoodrich wind tunnel data discussed below.

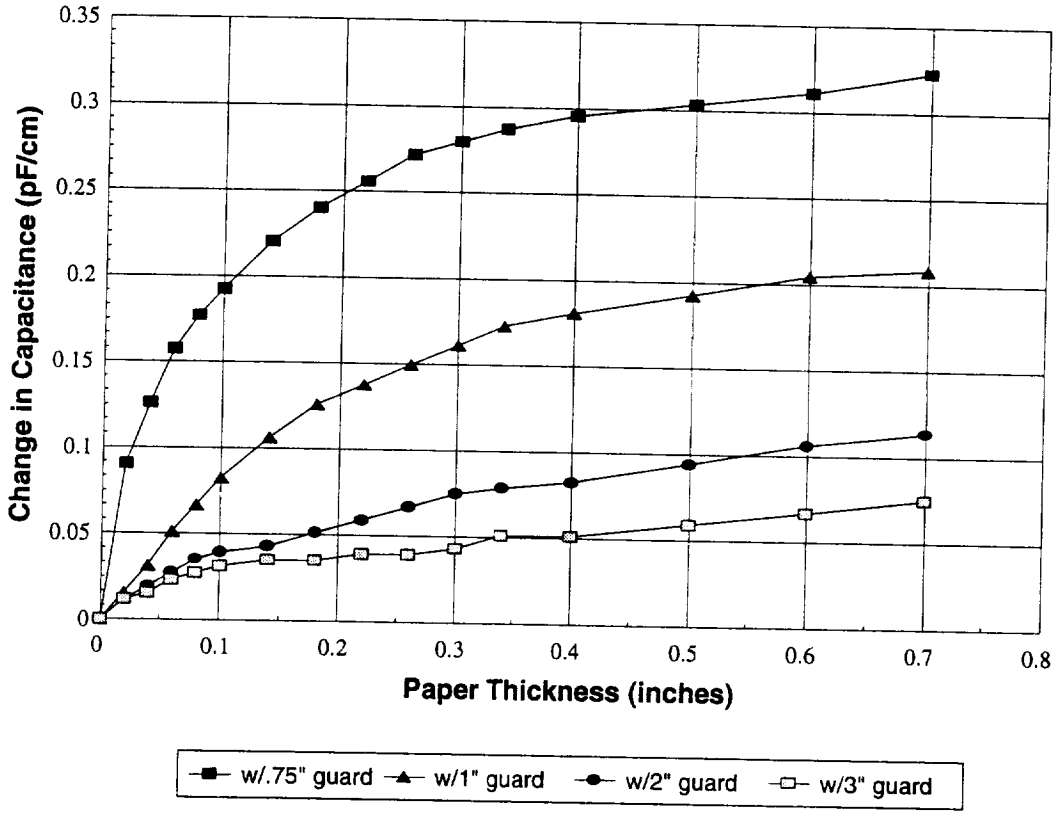

Figure 34. Change in capacitance versus paper thickness for a wire Type 2 sensor operating with different width guard electrodes.

It appears that the claim of increased range and sensitivity is based on the belief that the electric field lines normally present in the gap between the positive electrode and ground are "squeezed" out of this gap when the guard electrode is used resulting in a larger charge distribution on the upper surface. The greater charge density would generate a greater number of field lines on the upper surface of the positive electrode which would conceivably increase the sensitivity and range of the sensor. They seem to indicate in their argument that the number of charges on the sensor have remained the same (with the addition of the guard) while the sensor baseline capacitance has dropped dramatically. According to capacitance theory to maintain the same number of charges, Q, the voltage applied to the sensor, V, would have to be increased inversely proportional to the drop in capacitance, C, according to the equation[3] V=Q/C. If this is the case, then for this new higher voltage system a given change in capacitance will lead to a larger change in output voltage which may be increasing their signal to noise ratio. With a better signal to noise ratio the system would be able to detect smaller changes in the weaker distant field lines and thus improve their observed range and sensitivity. It is our assumption that it was a better signal to noise ratio and not an increase in the number of field lines that accounts for the results discussed in the Tech Brief. We have not discussed these ideas with the author of the Tech Brief and therefore they must be considered conjecture at this time. It should be noted that a better signal to noise ratio can also be achieved by using better electronics and a narrower guard and thus get good sensitivity over both short and long ranges.

At the time that the sensors were fabricated for the BFGoodrich wind tunnel tests and the NASA Otter flight tests the contradiction between the NASA Tech Brief and our results was not very obvious. Thus, a moderate width of 1.25" was used for the guard electrodes. This compromise delivered the benefits of reduced baseline capacitance and greatly enhanced temperature stability, but in hind sight reduced the sensors sensitivity to thin ice accretions. Subsequent sensors will be fabricated with the guard electrode being the same width as the positive electrode.

Wind Tunnel Experimental Apparatus

Sensors

Three sensors were fabricated for testing in the BFGoodrich Icing Wind Tunnel, a wire sensor, a fabric sensor, and an underboot sensor. All three used 0.75" wide Type 2 electrodes and 0.4" gaps between the edges of the Type 1 and Type 2 electrodes. The fabric and wire sensors used a 0.010" thick neoprene insulator, a single 0.010" Monel wire for the Type 1 electrode, and RTV silicone adhesive. Two Type 1 sensors, 0.150" and 0.175" in width, were tested with the rigid underboot sensor as shown in **Figure 35**. All three of the sensors were designed so that the Type 2 sensor could be tested in guarded and unguarded modes. In all of the tests where the sensor was in unguarded mode the guard electrode was connected to ground.

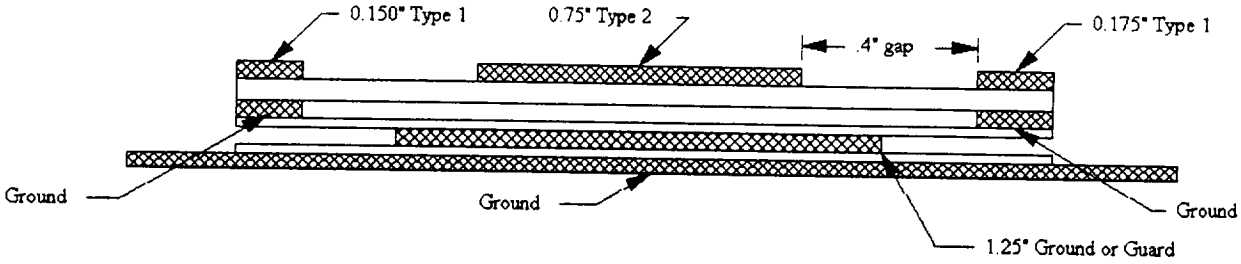

Figure 35. Cross-sectional view of the rigid underboot sensor showing the Type 1, Type 2, and Guard electrodes. All crosshatched regions are either copper or aluminum and the white regions are dielectric material.

The fabric and wire sensors were embedded into functional non-conductive pneumatic de-icing boots by the engineers at BFGoodrich which were then attached to MD-91 wing sections modified to mount into the IWT. The underboot sensor was affixed to a third MD-91 wing section and then covered with a functional non-conductive de-icing boot. All three sensors were instrumented with T type thermocouples before being installed on the wing sections.

Data Acquisition Hardware

The data acquisition hardware used for the BFGoodrich IWT test was typical of that used in the previous NASA IRT wind tunnel tests (shown in **Figure 15**). Type 1 and Type 2 capacitance data were collected using TBE 214 capacitance meters whose analog output was amplified and fed into a Metrabyte DAS-20 data acquisition card. Temperature information from the T type thermocouple attached to each sensor was processed by an Analog Devices 5B47-T-06 signal

conditioning module and fed into the same DAS-20 card residing in an IBM compatible computer. Data logging was controlled using the Labtech Notebook software package.

Experimental Results

Anomalies in Measured Capacitance

The three sensors, wire, fabric, and underboot, were tested in both guarded and unguarded modes in glaze, mixed, and rime icing conditions. Icing parameters used for the three icing conditions are listed in **Table 4**. Results for the three sensors under glaze icing conditions in general looked good, but for some of the glaze tests and for all of mixed and rime icing tests there were anomalies in the capacitance readings. For all of these cases the capacitance values to some degree or another tracked the temperature readings, a typical example is shown in **Figure 36**. It was initially thought that the observed fluctuations were due to the temperature sensitivity of the capacitance sensors and that the fluctuations could be compensated for during post-processing. Subsequent tests performed at IDI concluded that magnitude of the fluctuations were too large to be attributed to sensor temperature sensitivity. A second possible explanation was that the capacitance sensors were picking up some form of EMI noise from the tunnel that was some how associated with changes in the tunnel temperature, i.e. from the refrigeration system. After discussing this with the engineers at BFGoodrich it was concluded that there was nothing in the tunnel that would create EMI noise of the kind observed in the data. It was suggested that there was a problem with electrical "crosstalk" between the thermocouple and capacitance channels in our data acquisition system. While this is definitely conceivable from the data shown in **Figure 36** it is not supported in **Figure 37** which shows anomalies in both the temperature and capacitance data which are not coincident in time. Further more testing at IDI to determine the influence of temperature on the baseline capacitance of the sensors (with no ice on the surface), which were done with the same data acquisition system used at BFG, showed no evidence of "crosstalk".

Ice Type	Liquid Water Content (g/m^3)	Droplet Size (microns)	Airspeed (MPH)	Temperature (deg F)
Rime	0.4	17	125	-5
Mixed	0.6	20	125	10
Glaze	0.8	20	125`	25

Table 4. Summary of test conditions used at the BFGoodrich IWT test.

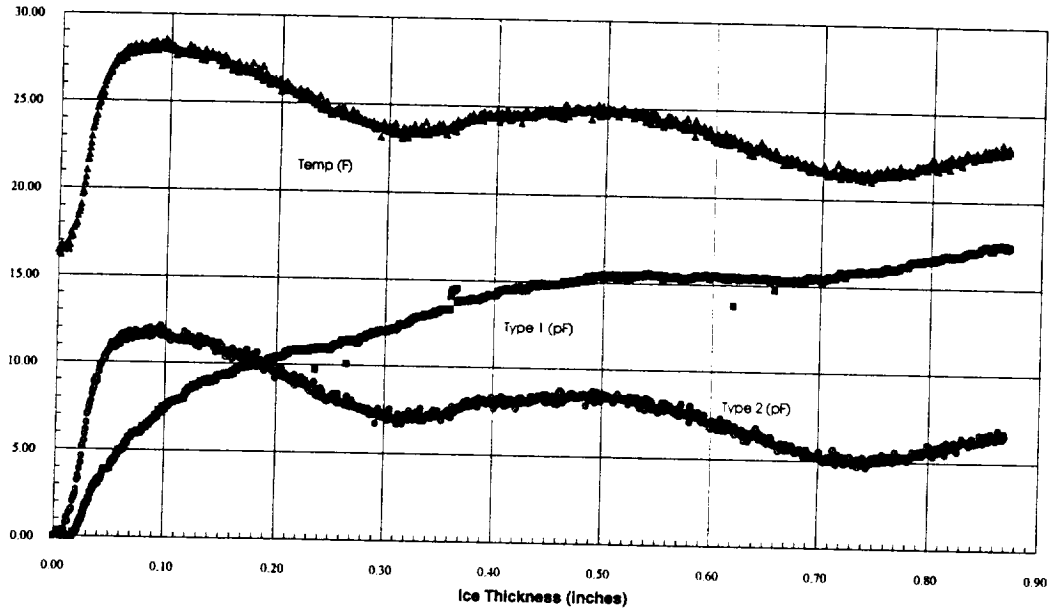

Figure 36. Typical example showing influence of temperature on capacitance data for the underboot sensor in guarded mode for mixed ice conditions using the 0.175" wide Type 1 sensor.

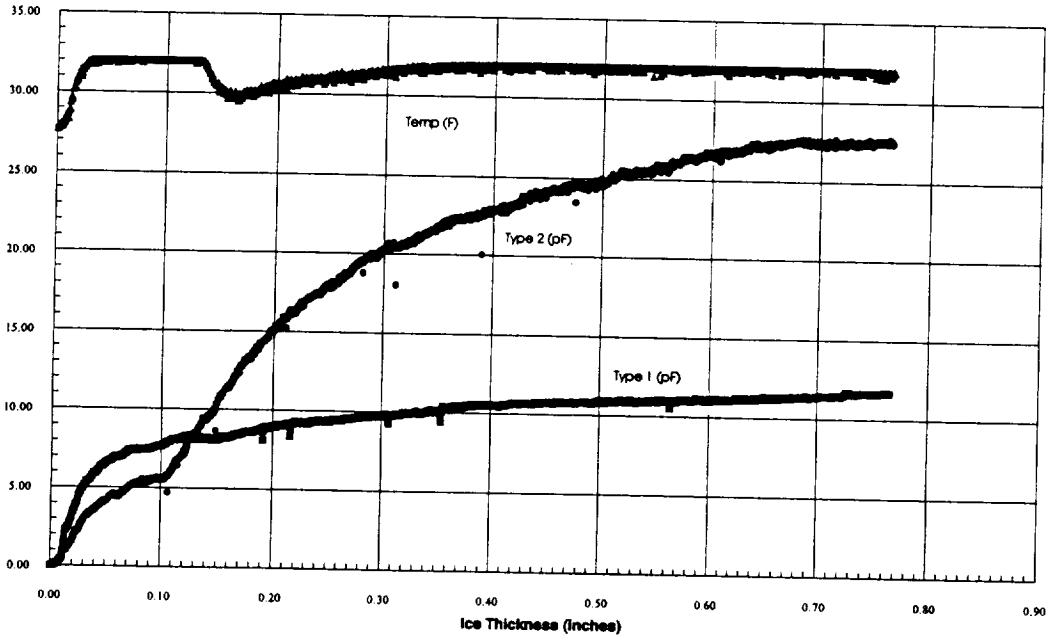

Figure 37. Capacitance and temperature data for the underboot sensor in guarded mode for glaze ice using the 0.15" wide Type 1 sensor.

At this time it appears that the problem is associated with small amounts of water that accumulate in the ice pack during the accretion process. From this and previous tests it appears that for all icing conditions, wet glaze through dry rime, water is present in the outer layers of the ice pack. As the tunnel temperature and thus the net heat transfer balance for the ice pack varies the amount of liquid water present will vary. Because water has such a high dielectric constant (roughly 80 as compared 20 for glaze ice and 3 for rime ice) small changes in the amount of water can result in relatively large changes in the measured capacitance values. This effect was first investigated during the April IRT test. It was observed that the measured capacitance dropped off sharply when the icing spray was turned off due to the freezing of the water in the ice pack (see **Figure 20**). Subsequently when the icing spray was turned back on to the previous values the measured capacitance initially increased at a higher than expected rate as water was re-accumulated in the outer surface of the ice pack.

It is believed that a similar phenomenon was occurring during the BFGoodrich tests. While it is true that the spray conditions were held constant during each run, there were large changes in the ambient tunnel temperature for many of the runs. When the tunnel temperature goes up sharply heat transfer from the ice pack is lowered allowing more water to accumulate in the ice pack resulting in a higher measured capacitance. Similarly as the tunnel temperature drops sharply some of the water present in the ice pack will freeze lowering the measured capacitance. A plot of tunnel spray conditions collected by BFGoodrich on their data acquisition system is shown in **Figure 38** for the same run shown in **Figure 37**. As can be seen there is a sharp drop of 15 ^{o}F in ambient tunnel temperature just before 0.1" of ice was accumulated. This increases the heat loss from the ice surface allowing some of the water present in the ice pack to freeze resulting in a step in the Type 2 capacitance output. A short time later the reduction in ambient tunnel temperature is detected by the thermocouple mounted beneath the de-icing boot. The thermal insulating properties of the ice and boot over the thermocouple account for the lag in the response. The change in water content appears to be primarily a surface effect for this run because the output of the Type 1 sensor is not affected. The correlation between changes in tunnel temperature and fluctuations in capacitance output is consistent for other runs investigated. It is assumed that this problem was not observed in the IRT during runs where the spray was on continuously because the ambient tunnel temperature was held fairly steady. Because both ambient temperature and accretion rate vary during natural icing encounters similar fluctuations or "dips" in the capacitance output were observed for much of the data collected during the subsequent Otter flight tests.

At this time ways of mitigating the influence of water on the capacitance measurements are being investigated, but these methods can not be applied to the data already collected. For now we are limited to analyzing only the glaze ice data from the BFGoodrich tunnel tests as these were the least influenced by changing water content.

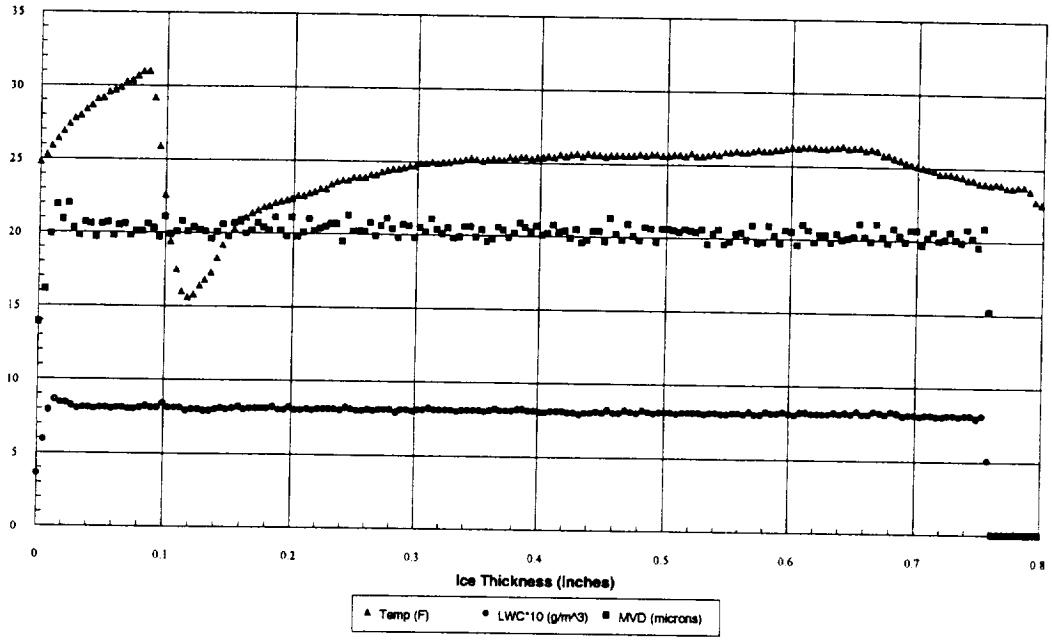

Figure 38. Tunnel temperature, MVD, and LWC data collected by BFGoodrich for the same run shown in **Figure 37** above.

Glaze Ice Data

Despite the limited scope of the available data some observations can still be made. A comparison between **Figures 39** and **40** indicates that the Type 2 underboot sensor operating in guarded and unguarded modes has similar sensitivities for thick ice in the range of 0.3" to 0.5". This confirms the laboratory results which indicated that the guard electrode does not significantly increase the thick ice sensitivity. It can also be seen that the 1.25" wide guard electrode does reduce the thin ice sensitivity in the range from 0" to .2", again confirming the laboratory tests. These observations were also made for the wire and fabric sensors operating in guarded and unguarded modes.

The influence of the guard circuit on the Type 1 sensor is not clear. Laboratory experiments at IDI indicated that the guard would not interfere with proper operation of the Type 1, but as can be seen in **Figures 37** and **40** for the underboot 0.15" wide Type 1 in guarded and unguarded modes respectively there are some differences. When operated in unguarded mode the Type 1 sensor output goes up quickly and maintains a relatively constant value as ice thickness increases. When the same sensor is operated in guarded mode the output does not flatten out as well as it does when the guard electrode is not present. It should be noted that the behavior of the Type 1 sensor in guarded mode may be due to the fact that the tunnel temperature is going up gradually for most of the test. The 0.175" wide Type 1 sensor was only tested in guarded mode, but as can be seen in **Figure 39** the output did more or less flatten to the same degree as for the 0.15" wide sensor in unguarded mode.

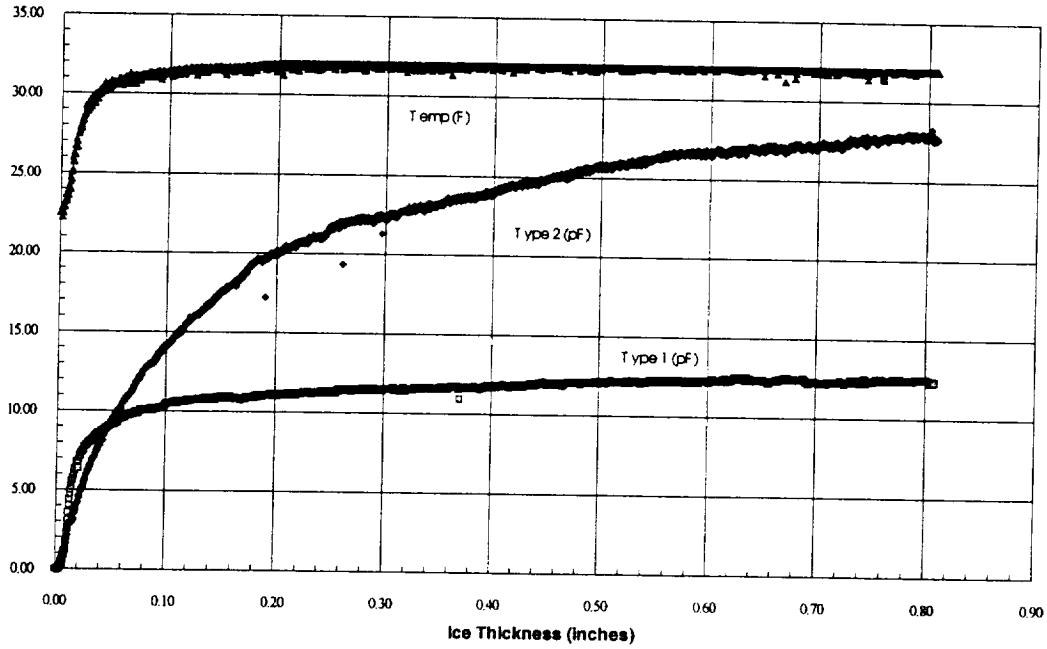

Figure 39. Typical example showing temperature behavior for a glaze icing test (underboot sensor operating in guarded mode using the 0.175" wide Type 1 sensor).

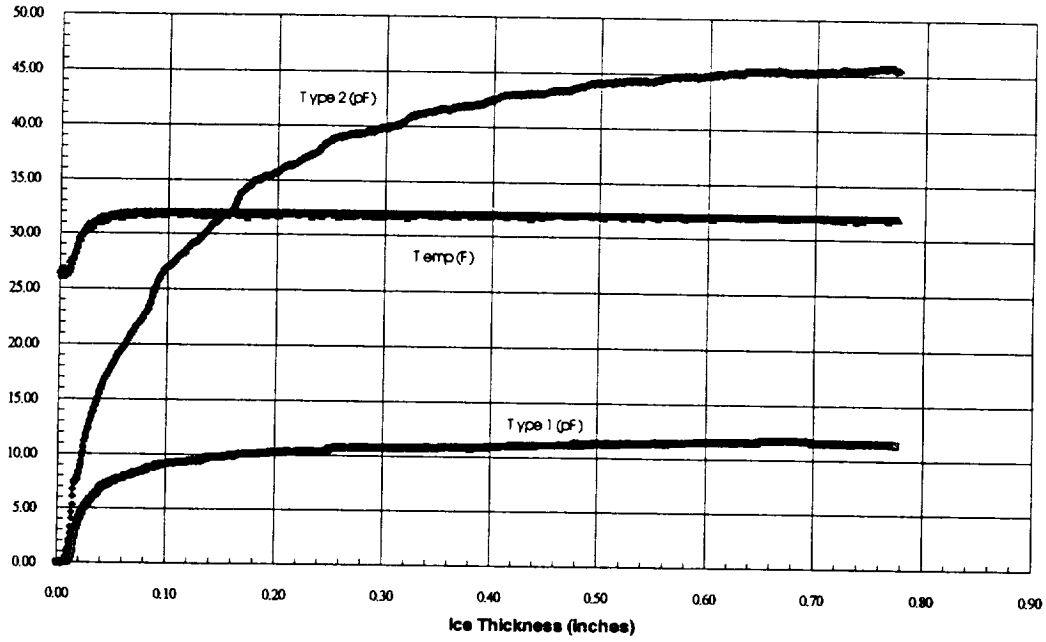

Figure 40. Change in capacitance versus ice thickness for the underboot sensor operating in unguarded mode in glaze icing conditions using the 0.15" wide Type 1 sensor.

While the output from both of the Type 1 underboot sensors did become reasonably flat as discussed above, they never completely flattened out as well as the wire sensor Type 1 as shown in **Figure 41**. Future underboot Type 1 sensors were made narrower to prevent the slow increase in output with increasing ice thickness.

Output from the fabric sensor operating in guard mode under glaze icing conditions, shown in **Figure 42**, indicates that the Type 2 sensor has very similar characteristics to both the underboot and wire Type 2's. The Type 1 output is substantially different from that generated by the Type 1 element used in the wire sensor which is unexpected since the two Type 1's consisted of a single run of 0.010" Monel wire placed 0.4" away from the edge of the Type 2 sensor. The reason for these differences in output are not known at this time.

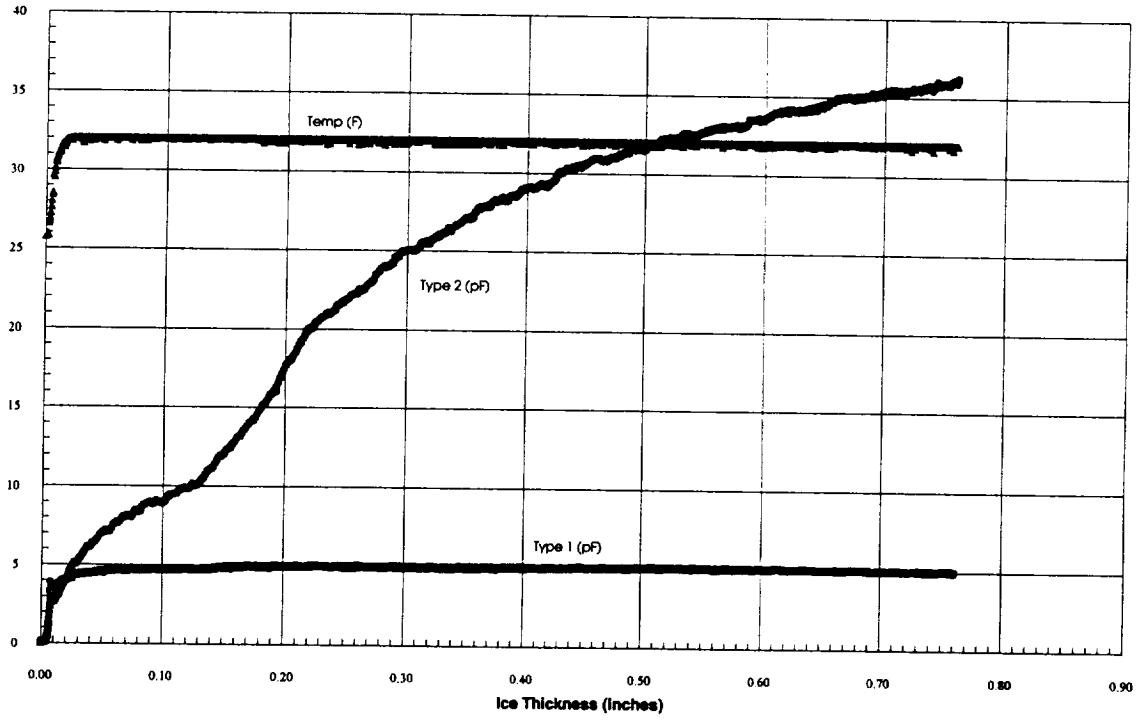

Figure 41. Sensor temperature and change in capacitance versus ice thickness for the wire sensor operating in guarded mode in glaze icing conditions using a 0.010" wire Type 1 sensor.

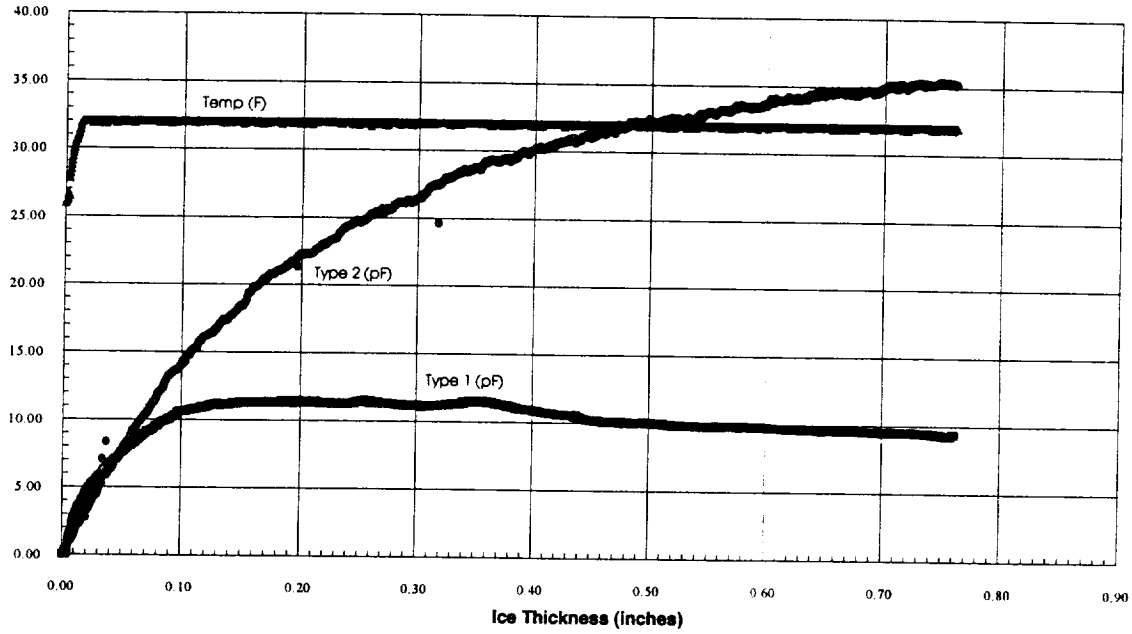

Figure 42. Sensor temperature and change in capacitance versus ice thickness for the fabric sensor operating in guarded mode in glaze icing conditions using a 0.010" wire Type 1 sensor.

Conclusions

The primary result obtained from testing in the BFGoodrich Icing Wind Tunnel is that our system as tested is very sensitive to water in the ice pack and changes in the amount present. The quantity of water in the ice pack is a function of the ambient temperature and the accretion rate which in turn is dependent on factors such as the liquid water content, mean volume diameter, airspeed, etc. Variations in any of these icing conditions can lead to changes in the amount of water present resulting in fluctuations in the sensor output which are not accounted for in the NASA patent.

Application of the guard circuit to our system appears to be beneficial in both reducing the initial baseline capacitance of the sensor and cables and virtually eliminating the temperature sensitivity of the sensor. The guard circuit did not appreciably increase the sensitivity of the sensor to thick ice, but the guard electrode used in these tests did reduce the sensitivity to thin ice.

Improvements in the design of the Type 2 sensors appear to be beneficial in increasing the sensor sensitivity to thick ice over what was observed for earlier designs in the previous wind tunnel tests. The Type 1 sensor used with the wire design seemed to flatten out as predicted in the original NASA patent, but the underboot and fabric Type 1 sensors need to be refined further.

References

[1]Gregory, R.V., W.C. Kimbrell, and H.H. Kuhn, *Electrically Conductive Non-Metallic Textile Coatings*, Journal of Coated Fabrics, Volume 20, January 1991.

[2]*Capacitive Proximity Sensor Has Longer Range,* NASA Tech Briefs, pp. 22-23, August 1992.

[3]Hayt, William H. Jr., Engineering Electromagnetics, Third Ed., Ch. 5, McGraw-Hill Book Co., New York, 1974.

NASA Otter Flight Test

Shortly after completion of the BFG Icing Wind Tunnel tests the ice detection system was installed and flight tested on the NASA DHC-6 Twin Otter Icing Research Aircraft. These tests were designed to evaluate system performance under natural icing conditions and determine its ability to detect the onset of an icing encounter and estimate ice thickness. Additional tests were performed to ascertain if the system could evaluate the success of a boot de-icing cycle and monitor for boot failure such as auto-inflation and frozen tubes. Throughout the test program system susceptibility to noise from structural vibration was monitored as well as interference from and with communication and navigation equipment. Installation of the system began on November 16, 1992 with test flights extending from November 30 to December 8.

For these tests two sensors were mounted end to end along a 50" span wing cuff (the same cuff that was used during the two IRT tests) attached to the starboard wing of the Otter. A non-elastic underboot sensor and an elastic wire sensor were integrated with a functional non-conductive BFGoodrich pneumatic de-icing boot. A fabric sensor was embedded into the outer layers of the boot, but problems during the installation process rendered this sensor inoperable and the wire sensor tested was attached to the outer surface of the boot immediately above the non-functioning fabric sensor. The addition of the wire sensor over the fabric sensor did not create any problems for data collection, but the presence of two elastic sensors over each other did impede the inflation of the boot requiring some extracurricular flight maneuvers to remove the ice immediately over these sensors. The non-elastic sensor, mounted under the boot, did not interfere with the de-icing of that side of the boot.

During the 8 icing flights we encountered a wide envelope of icing conditions ranging from very dry rime to heavy glaze, but never reached high enough accretion rates to generate large ice horns. The sensors were capable of detecting the onset of icing for all of the conditions encountered, but under certain conditions ran into problems in determining if the ice pack was still growing and in evaluating ice thickness. Both of these problems were created by the same phenomenon observed in the BFG tests, namely a changing quantity of water in the ice pack.

The system could detect the inflation and deflation of the boot and could thus diagnose an inoperable boot. For most de-icing episodes the system could evaluate if the ice was removed, but in the rare case where the ice adhesion to the boot was broken but the ice was only displaced slightly and not removed the system did return an ambiguous evaluation. There was only a slight indication that the system was sensitive to vibration noise and no indication of interference with or from the communications or navigation equipment. The problems discovered during the flight tests are currently being addressed and it is felt that solutions are available that will allow AIMS to achieve its goal of successfully operating a pneumatic de-icing system in a closed loop autonomous manner without pilot intervention.

Data Acquisition Hardware

The data acquisition hardware consisted of; a wing cuff attached to the starboard wing, a functional non-conductive BFGoodrich de-icing boot, a non-elastic sensor mounted under the boot, a wire sensor attached to the outer surface of the boot, one T type thermocouple mounted

on each sensor, two capacitance meters, two thermocouple signal conditioning modules, and a computer.

The sensors were very similar in design to those used at the BFG tests, but were roughly 18" long. The underboot sensor was fabricated from Bend/Flex material using a 0.75" wide Type 2 element, a 1.25" wide guard electrode, and a 0.125" wide Type 1 element, **Figure 43**. The sensor was attached to the surface of the aluminum wing cuff, which acted as the ground electrode for the Type 2, and was covered with the non-conductive de-icing boot.

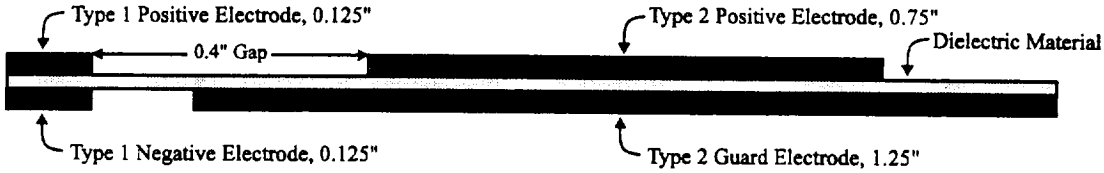

Figure 43. Cross-sectional view of the underboot sensor.

The elastic wire sensor was constructed with a 0.75" wide Type 2 element fabricated from 0.01" diameter Monel wire adhered to a 0.01" thick neoprene dielectric with RTV silicone adhesive. The guard electrode was a 1.25" wide length of conductive Contex fabric similar to that tested in the BFG tests, and the Type 1 element consisted of two lengths of 0.01" dia. Monel wire, as shown in **Figure 44**. There was a 0.4" gap between the edge of the Type 2 wires and the Type 1 wire. This sensor was attached to the outside surface of the de-icing boot and smoothened using RTV silicone adhesive. Again the grounded wing cuff was used as the ground electrode for the Type 2 element. For all of the tests conducted both Type 2 elements were operated in guard mode and both Type 1 elements were unguarded.

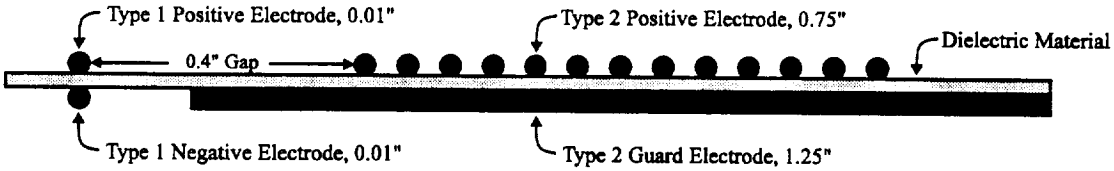

Figure 44. Cross-sectional view of the elastic wire sensor.

The four sensor elements were all connected to coaxial cables which were routed through the wing into the cabin of the airplane. The shields on all of the cables were connected to guard circuits to eliminate the large baseline capacitance that would have resulted if they were grounded. For both Type 1 sensors the outboard end of the shield was left unattached and the Type 1 ground wires were secured to the cuff. A separate wire was attached to the cuff and grounded at the instrumentation in the airplane to ensure that all grounds were at the same potential.

The coaxial cables were connected to the capacitance meters in the instrumentation rack and the analog outputs from the meters were recorded and displayed by the rack mounted computer. Because only two capacitance meters were available data were collected for one sensor group at a time. Signals from the two thermocouples were conditioned, amplified and sent to the computer for storage and display. Two thermocouple signal conditioning modules were available so

temperature data were always collected from both sensors regardless of which capacitance sensors were currently being used. All data sent to the computer was digitized with a Metrabyte DAS-20 data acquisition card and recorded using the Labtech Notebook software package. Capacitance and temperature data were displayed in real time on the computer monitor and stored to hard disk for later retrieval and analysis.

Once data were collected for one sensor the airplane was flown out of the icing cloud, the boot was de-iced, and the second sensor was attached to the capacitance meters. The de-icing boot on the cuff was operated off a pneumatic system completely isolated from the primary Otter system to avoid any problems should the cuff fail in any form. The pneumatic system for the cuff de-icer employed a bottle of compressed nitrogen mounted to the floor of the Otter (regulated down to a maximum pressure of 25 PSI), a vacuum pump attached to the side of the instrumentation rack, and a three way solenoid valve to control the flow to the boot. A pneumatic hose was routed through the Otter wing for connection to the cuff.

Test Procedure

Tests were conducted to determine the response of both sensors to natural icing conditions and to measure the influence of temperature on sensor output. Typical procedures for the collection of icing data were to begin acquisition and storage as soon as the engines were started and research power was available. Data were collected during takeoff and during the flight through clear air to the icing cloud. Once icing conditions were found the plane was trimmed to a predetermined angle of attack that centered the stagnation line on the sensor and ice was accumulated. Data from the wire capacitance sensors and from both temperature channels were collected until the pilots indicated that roughly 0.5" of ice was present over the sensor. At this time the plane ascended over the cloud and stereo pictures of the ice pack were taken. The boot on the cuff was then de-iced, the underboot sensor connected to the meters, and the plane flown back into the icing cloud to repeat the data collection process. If time and weather conditions permitted a third and fourth set of data were collected. During the test period a wide variety of icing conditions were experienced with substantial enough accretion rates to allow the accumulation of 0.5" or more of ice during each encounter.

When there were no icing clouds in the vicinity data were collected on the change in measured capacitance with temperature as the plane was flown through clear air to high altitudes. These data were subsequently used to compensate the icing capacitance data for temperature effects.

At the conclusion of each flight all data stored to disk on the computer was backed up to floppy disk and then transferred to desktop computer for subsequent post processing. The film was removed from the stereo camera and sent out for developing. The data acquisition hardware and the sensors were examined for any indications of wear and if needed the nitrogen bottle for inflating the boot was refilled.

Experimental Results

Data collection during the course of the flight tests went very well. Reportedly the icing conditions encountered were some of the best seen in a number of years with high accretion rates

of a wide variety of ice types. Everything from very dry rime to wet glaze was encountered with the only notable exception being that the glaze icing conditions never produced large ice horns. During the course of the 8 icing flights 9 data sets were collected with the wire sensor and 14 data sets were collected with the underboot sensor.

Both ice sensors worked very well in determining the onset of all types of ice and for the most part could detect the successful de-icing of the boot. Neither sensor appeared to be susceptible to or interfere with navigation or communication equipment.

The goal of evaluating the sensors ability to measure ice thickness was not achieved. It was observed that during icing conditions when the liquid water content, LWC, changed rapidly there was a similar change in the output of the sensors. This would often result in a drop in the capacitance output when the LWC went from a large value to a lesser value and a subsequent rise as either the ice thickness increased or the LWC went up. This substantial effect of LWC on the measured capacitance made the correlation of capacitance to ice thickness for these cases impossible. This effect was observed previously in the NASA Icing Research Tunnel but to a much lesser degree and more recently in the BFGoodrich Icing Wind Tunnel to a larger extent but was not diagnosed until after the Otter flight tests.

As will be shown in the figures below most of the objectives of these tests were accomplished very successfully. The sensors and the data acquisition hardware performed without any problems and data were collected over virtually the entire icing envelope. The problems associated with the "dips" in the data are currently being investigated and it appears that there may be a relatively simple solution to this. Work is progressing on optimizing the system with the goal of commercialization in the near future.

Temperature Calibration

The influence of temperature on the baseline capacitance of the sensors was determined by conducting flights in clean air while measuring both the capacitance and temperature of the sensors. Data were collected during three flights from ground level up to the operational ceiling of the Otter to cover as wide a range of temperatures as possible.

The effect of temperature on the baseline capacitance results from the electric field lines that pass from the top, positive electrode through the boot and sensor materials to the grounded wing. As the temperature of the boot and sensor change their dimensions change due to thermal expansion. This change in dimension although small can create a noticeable change in capacitance if the baseline capacitance value is relatively large. For the wire Type 1 sensor the baseline capacitance is small and the influence of temperature is negligible as shown in **Figure 45** where change in baseline capacitance is plotted against sensor temperature for three data sets.

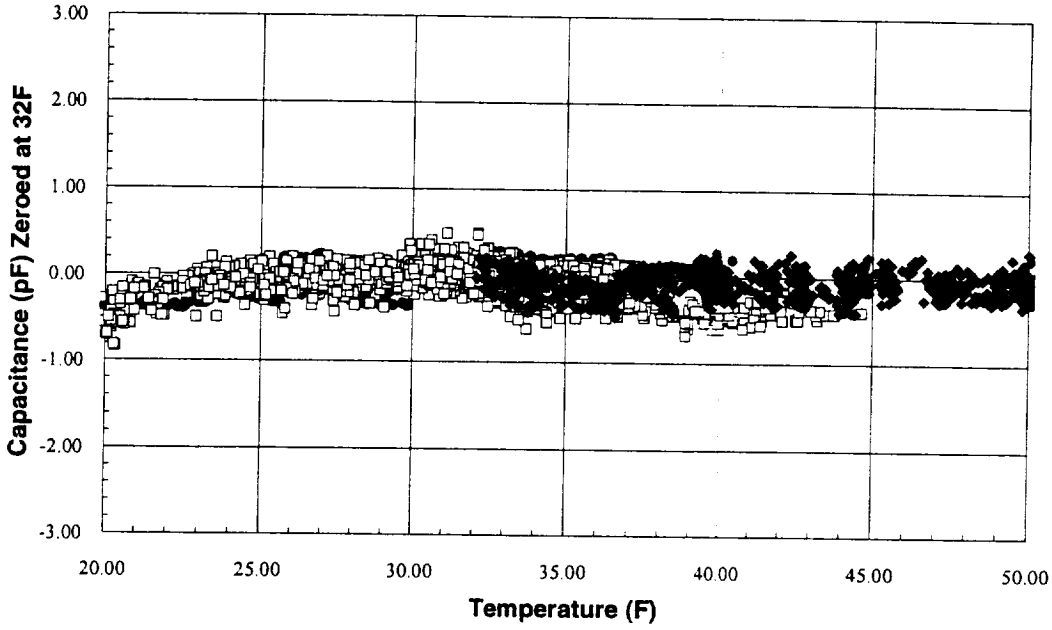

Figure 45. Change in baseline capacitance versus temperature for the Type 1 wire sensor.

The Type 1 underboot sensor does have a relatively large baseline capacitance due to its geometry and construction materials and as can be seen in **Figure 46** is sensitive to temperature. For this sensor a linear relationship between temperature and baseline capacitance was determined by a best fit to the curve and was used to correct all of the icing capacitance data for temperature effects.

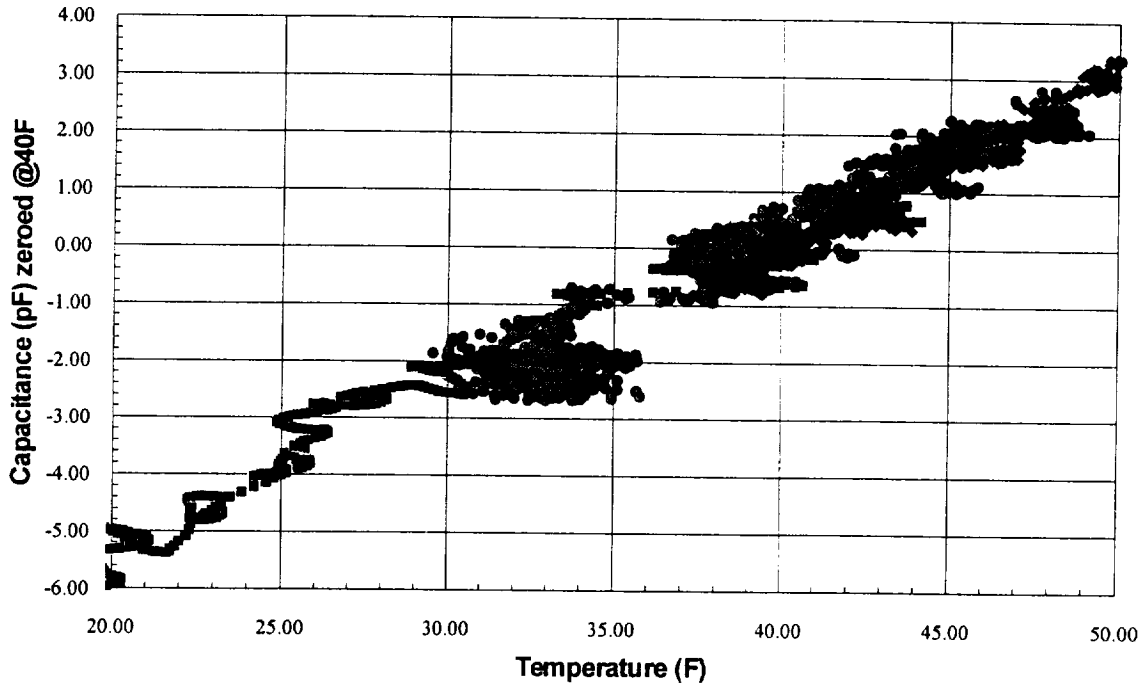

Figure 46. Change in baseline capacitance versus temperature for the Type 1 underboot sensor.

It was anticipated that both of the Type 2 sensors would be insensitive to temperature because of their guard electrodes which should have virtually eliminated the baseline capacitance. This was the case for the underboot sensor which used a solid copper guard electrode as can be seen in **Figure 47**. The wire sensor used a conductive fabric guard electrode which, as was determined later, did not fully guard the positive wire electrode out to its full 18" length. It appears that due to the low conductivity of the conductive fabric there is a limit to the length of material that can be used. Because the wire sensor was not fully guarded out to its tip it did display some temperature sensitivity as is shown in **Figure 48**. Again a straight line was fit to these data and used to compensate the icing capacitance data.

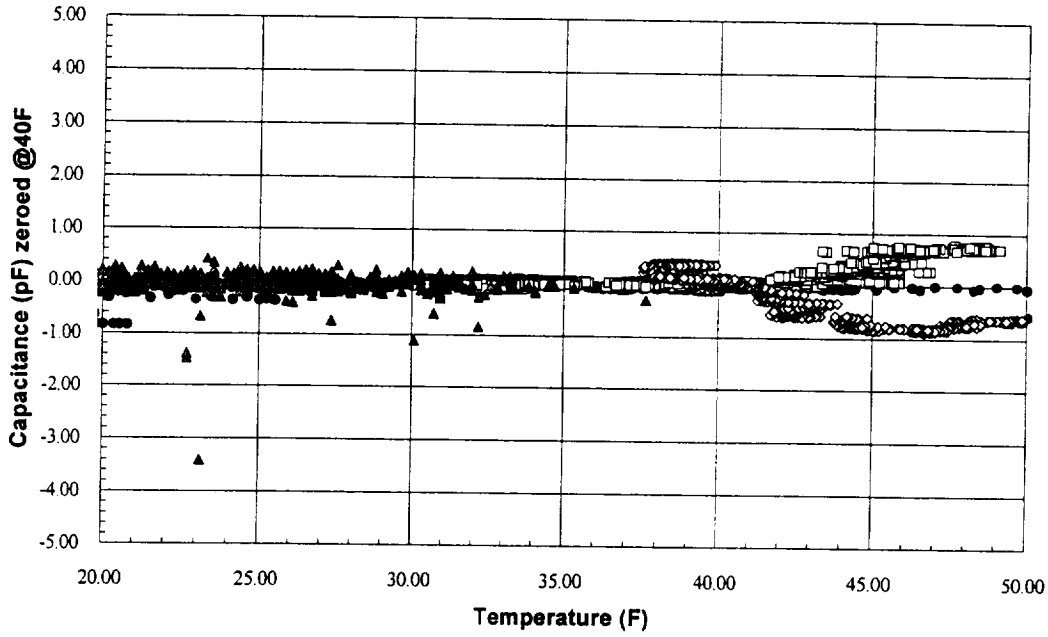

Figure 47. Change in baseline capacitance versus temperature for the Type 2 underboot sensor.

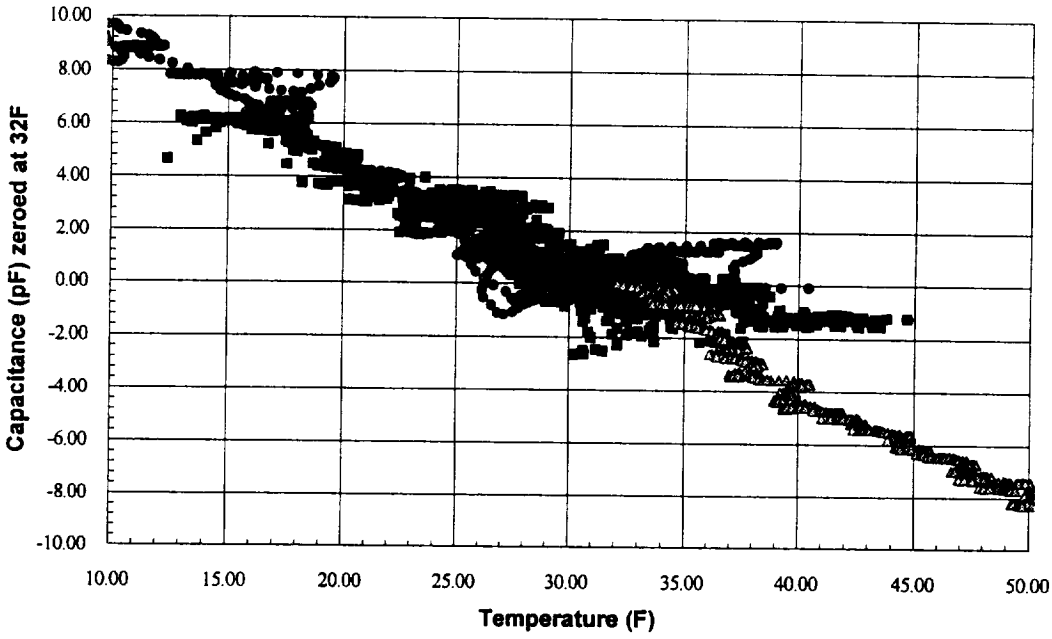

Figure 48. Change in baseline capacitance versus temperature for the Type 2 wire sensor.

In general the temperature compensation worked well. The use of small, low mass thermocouples placed directly on the sensors measured the appropriate temperatures as best as possible but the procedure was not perfect. As can be seen in **Figure 49** during the fast temperature transients associated with the onset of aerodynamic heating on takeoff there was some difference in the measured temperature and the true sensor temperature. It appears that the temperature measured by the thermocouple is correctly detecting the aerodynamic heating, but there is little change in the uncompensated baseline capacitance. Thus when the temperature compensation is applied an artificial jump is imposed on the capacitance data.

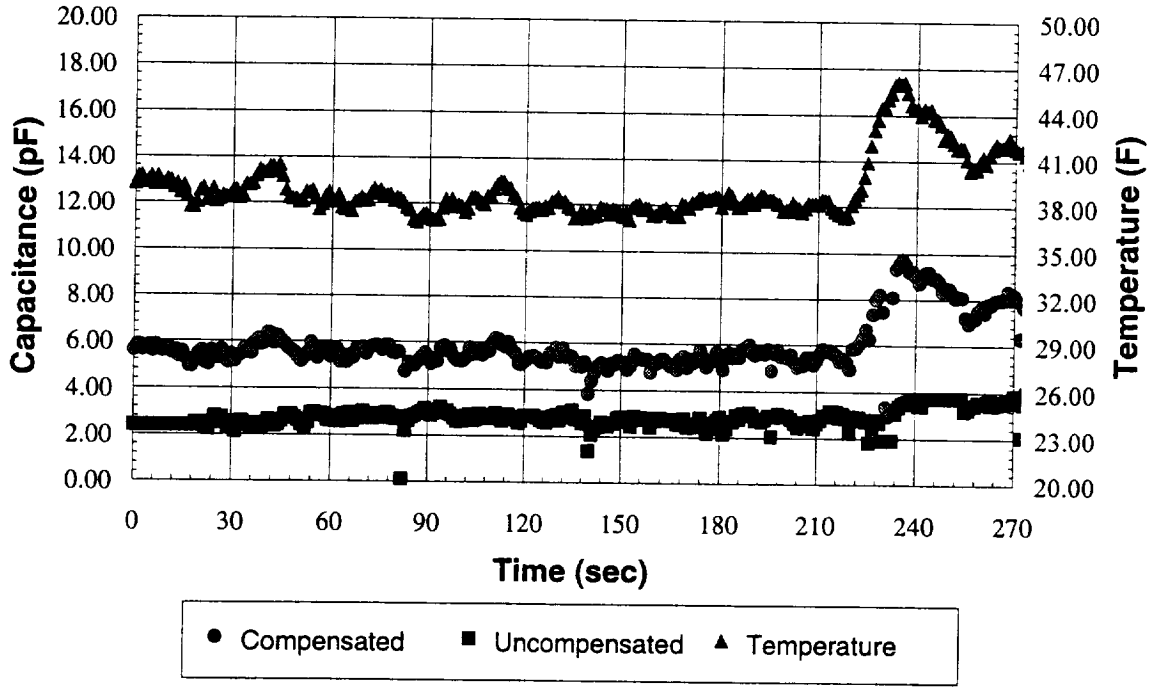

Figure 49. Example of poor temperature compensation during takeoff for the wire Type 2 sensor. December 2, Flight 93-4, Run #1.

An example showing proper application of temperature compensation is shown in **Figure 50** for the underboot Type 1 sensor in a light mixed icing encounter. Initially the LWC is less than 0.05 gms/m^3 while the ambient temperature is dropping. The drop in sensor temperature is lowering the baseline capacitance faster than the rise associated with the ice accumulation and the uncompensated capacitance is actually going down. Once the temperature effects are compensated for the capacitance data show the correct behavior and start going up as soon as ice starts to form over the sensor.

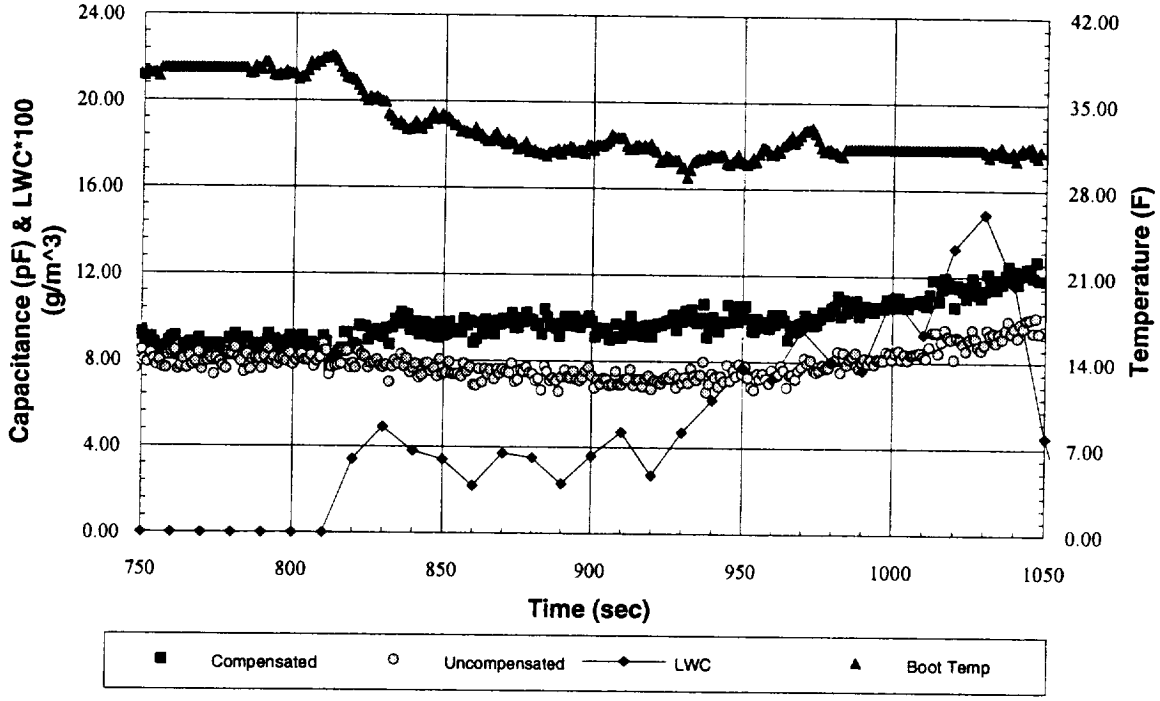

Figure 50. Example of proper temperature compensation during the initial phase of a light icing encounter with dropping ambient temperature for the underboot Type 1. December 4, Flight 93-7, Run #5.

All of the Otter flight test data presented in this report have been compensated for temperature. Future work will focus on improving the ability to compensate for fast transients in temperature and on developing sensors that do not require any compensation.

Noise Immunity

Throughout the course of the flight tests there were no indications that the ice sensors were picking up noise from either the communications or navigation equipment. Similarly there were no reports from the pilots indicating that the sensors or data acquisition equipment were in any way interfering with their use of the communications and navigation equipment. Occasionally the data would become noisy, but would usually stabilize within a few seconds. The source of this noise is most likely due to vibration of the coaxial cables. The outer shield of the cables were used to carry the signal for the guard electrode which was 500 mVAC. Although the guard signal level should be relatively stable it is possible that as its capacitive coupling to the aircraft ground changed due to vibration its effectiveness in guarding the positive electrode was altered. This fluctuation in guard signal would show up as noise in the measured capacitance data. To prevent this problem in future tests triaxial cable will be used with the center conductor connected to the positive electrode, the inner shield layer connected to the guard electrode, and the outer shield layer connected to ground.

A typical example of immunity to noise from communication and navigation equipment can be seen in **Figure 49** which shows data that were collected during taxi from the NASA hangar to the runway, through the takeoff procedure, and into the first icing encounter. Long term stability of the wire sensor in clear air is shown in **Figure 51** where data were collected for roughly 20 minutes before the onset of icing. The initial drift in the Type 2 sensor is due to deficiencies in the temperature compensation which will be addressed in future work.

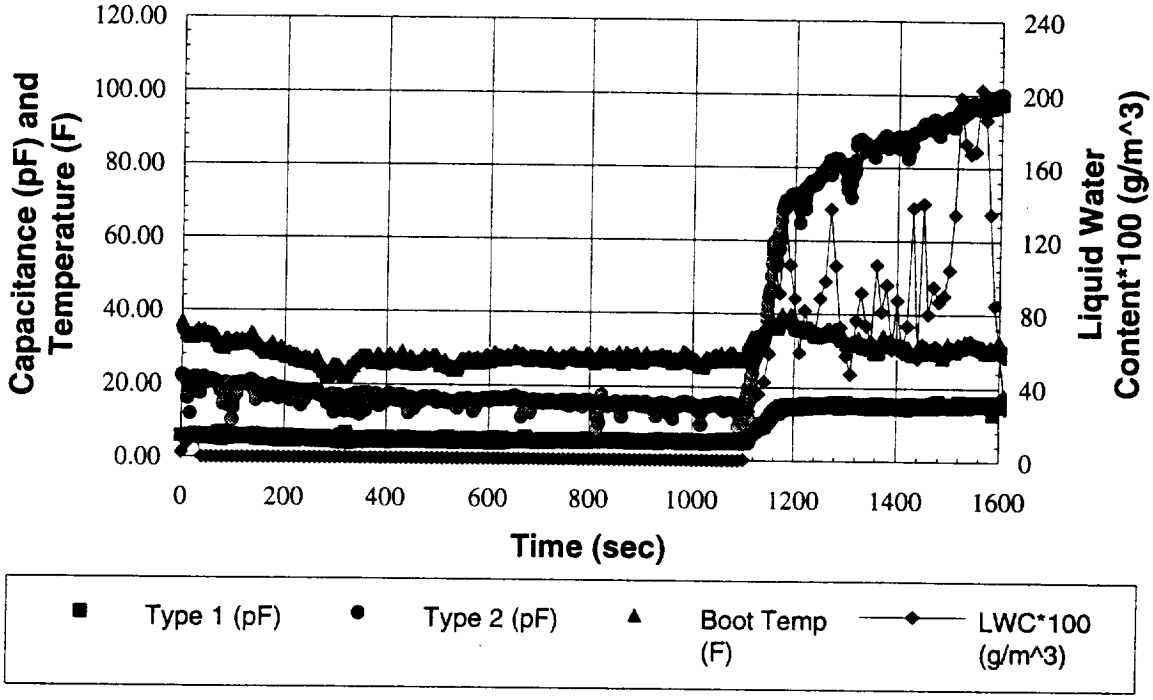

Figure 51. Example of long term signal stability during flight in clean air for the wire sensor. The initial drift in the Type 2 sensor output is due to overcorrection by the temperature compensation algorithm. December 1, Flight 93-3, Run #1.

Initial Ice Warning

One of the primary functions of the ice detection system is to give an early indication of the onset of icing. It is important to quickly and accurately warn the pilots of ice formation on wings and tailplane surfaces which in many cases are not visually accessible from the cockpit. In the current system an initial indication of icing is inferred when the output from one or both of the sensors rises above the noise floor. Examples of this can be seen in **Figure 51** for the wire sensor and **Figure 52** underboot sensor for similar mixed/glaze icing encounters with high LWC. As can be seen outputs from both the Type 1 and Type 2 sensors increase quickly with the onset of icing (which is indicated by the non zero LWC measurement). These examples are probably best case scenarios because the ice is a dense formation which has a relatively high dielectric constant and the LWC increases quickly to a very high value.

A photograph taken at the end of the underboot sensor icing encounter is presented in **Figure 53** showing the clear glaze ice along the stagnation line with mixed ice near the upper and lower impingement limits. The faint white spanwise line along the center of the ice pack indicates the center line of the sensors.

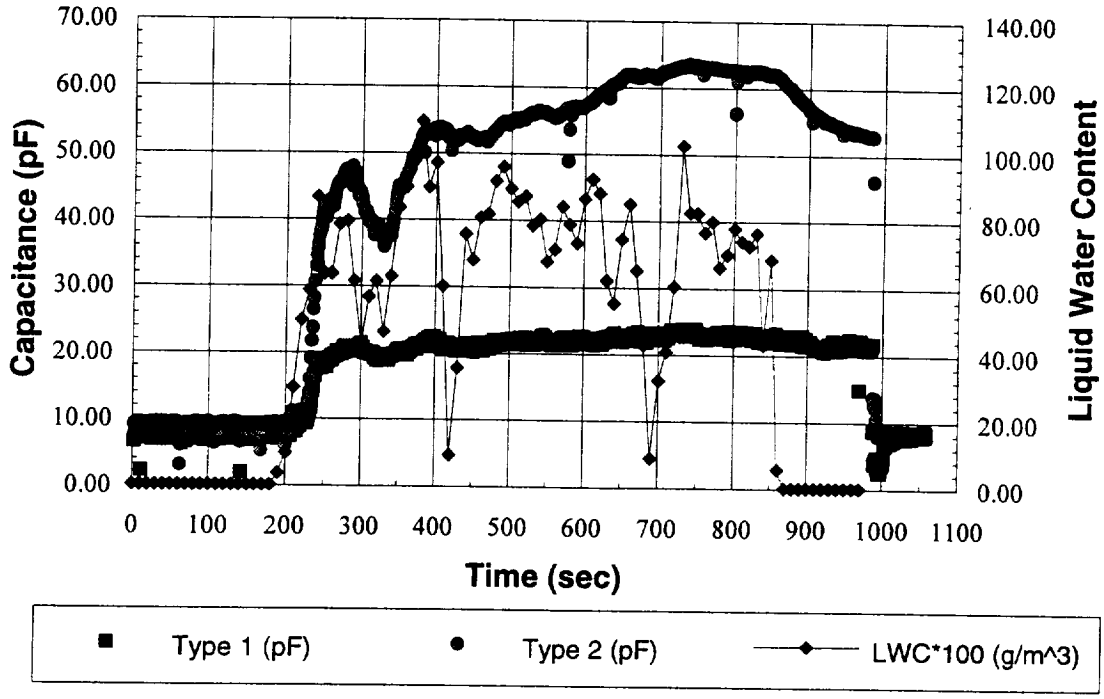

Figure 52. Data from the underboot sensor showing the detection of icing onset in mixed/glaze icing conditions. December 1, Flight 93-3, Run #2.

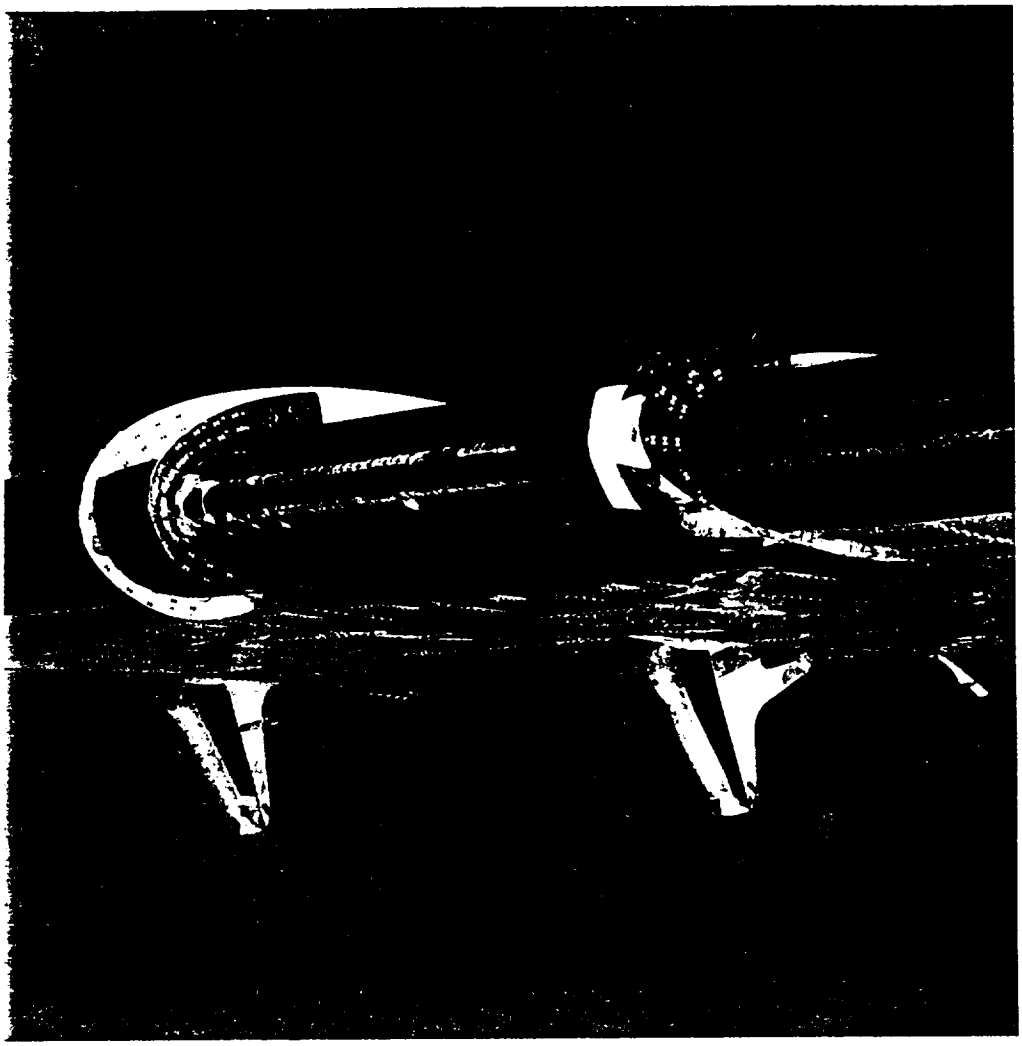

Figure 53. Photograph of a mixed/glaze ice formation on the IDI wing cuff. The faint white spanwise line centered along the ice pack designates the center of the sensors. December 1, Flight 93-3, Run #2.

Detecting the onset of icing becomes increasingly difficult if the ice pack has more of a rime content due to the greater porosity and resulting lower dielectric constant of the ice. A thicker initial layer of ice is needed to raise the capacitance signals out of their respective noise levels. Typical examples of initial ice detection for mixed/rime conditions with the wire and underboot sensors are shown in **Figures 54** and **55** respectively. A picture of the ice pack taken after the wire sensor test is shown in **Figure 56**. From the picture it appears that some of the rime feathers have broken off during the icing encounter. Both the wire and underboot Type 1 and Type 2 sensors react to the ice slower than that observed for the mixed/glaze cases due to the reduced ice dielectric constant and the lower LWC readings. It is interesting to note that output from both of the Type 1 sensors exhibit brief periods of excessive noise during these sequential icing encounters.

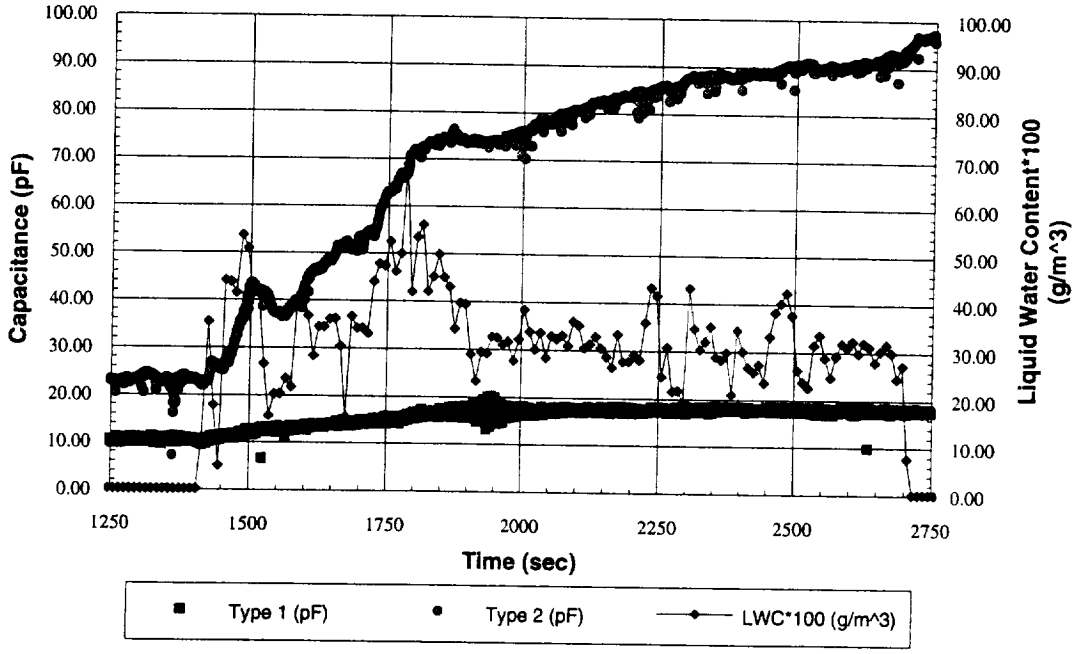

Figure 54. Data from the wire sensor showing the detection of icing in mixed/rime conditions. December 3, Flight 93-5, Run #1.

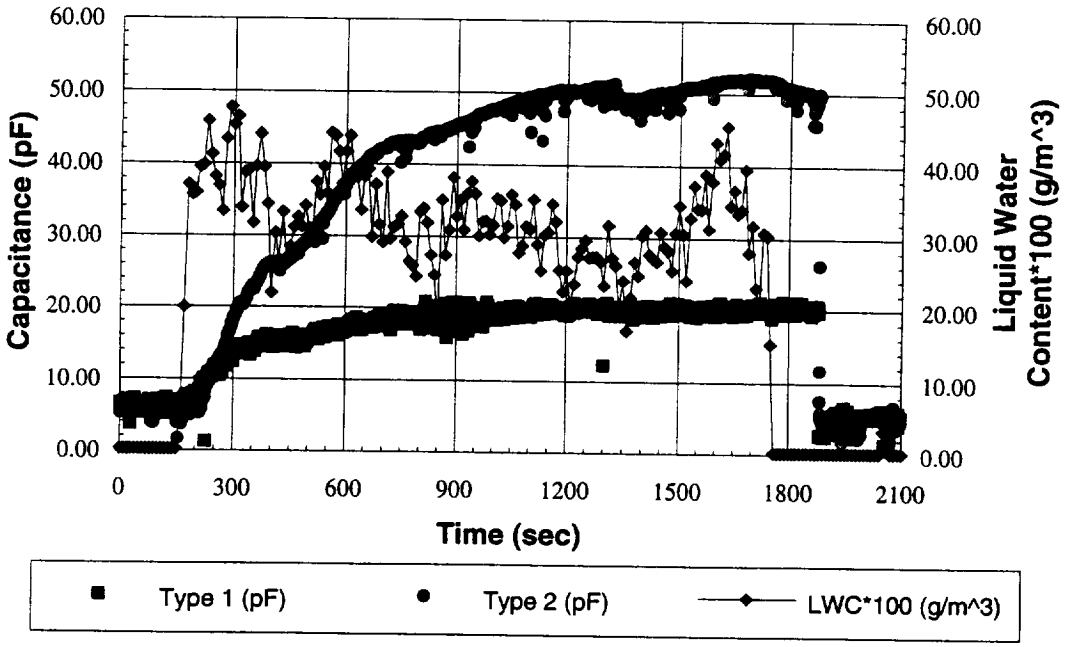

Figure 55. Data from the underboot sensor showing the onset and growth of ice in mixed/rime conditions. December 3, Flight 93-5, Run #2.

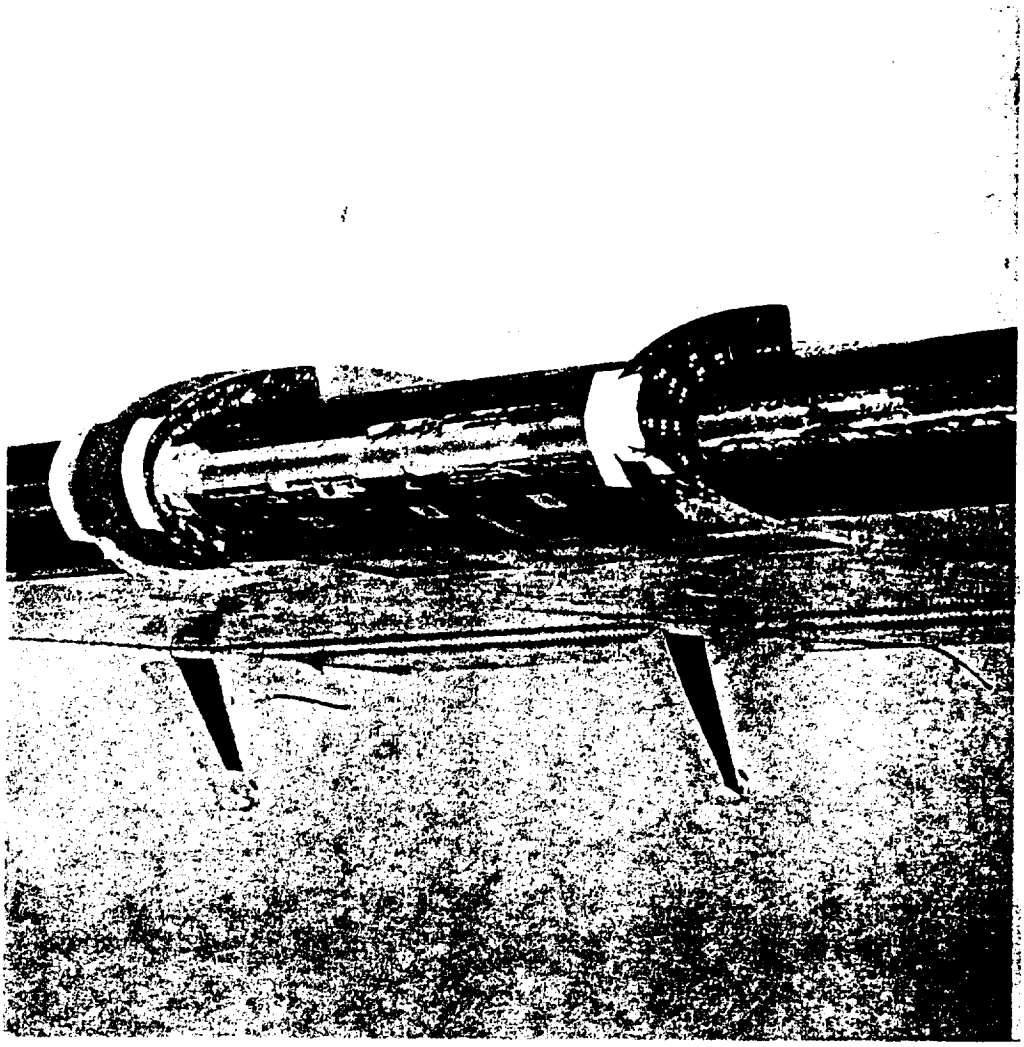

Figure 56. Photograph of a mixed/rime ice formation on the IDI wing cuff. December 3, Flight 93-5, Run #2.

Very dry rime ice is the most difficult to detect because of its low dielectric constant. Two examples of rime ice formation on the wire and underboot sensors are shown respectively in **Figures 57** and **58**. A picture of the ice pack taken after the underboot sensor test is shown in **Figure 59**. Two interesting phenomena that can be seen in the graphs are the influence of temperature on the wire Type 2 capacitance data at the end of the icing encounter, and the relative sensitivities of the Type 2 sensors as compared to their respective Type 1 sensors. Both of these observations will be discussed later.

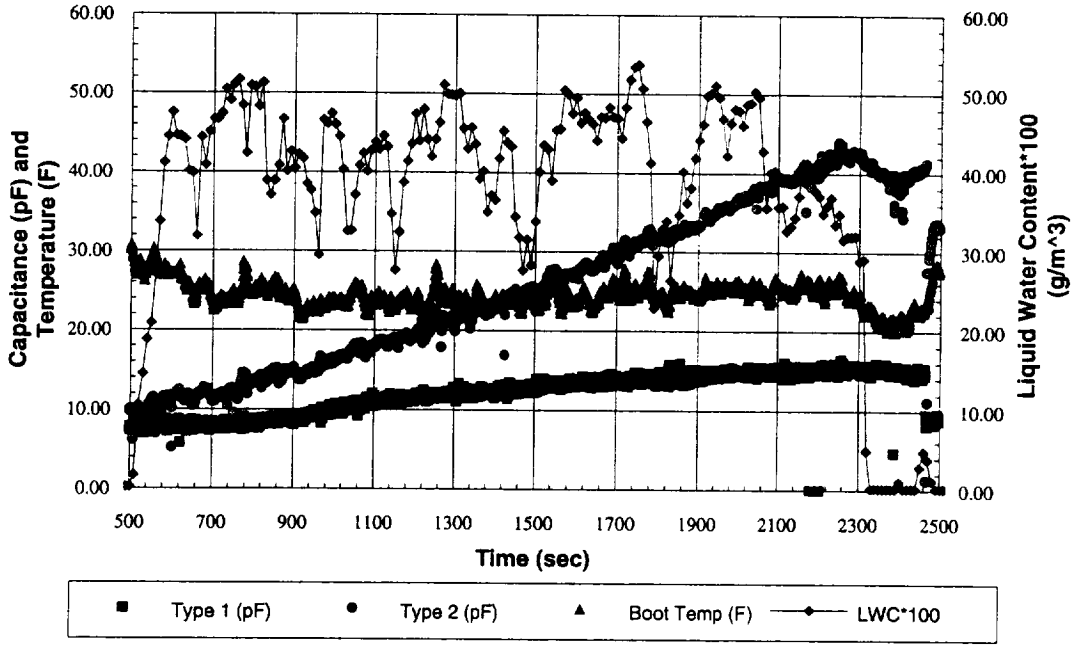

Figure 57. Data from the wire sensor showing the detection of icing in dry rime conditions. December 8, Flight 93-10, Run #1.

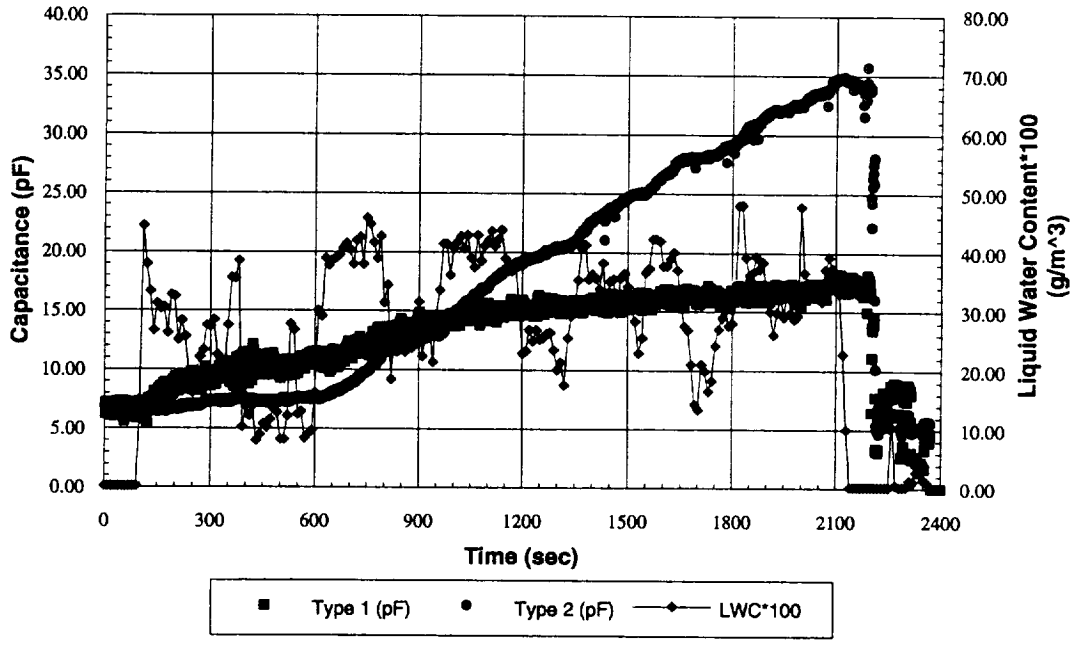

Figure 58. Data from the underboot sensor showing the onset and growth of dry rime ice. December 8, Flight 93-10, Run #2.

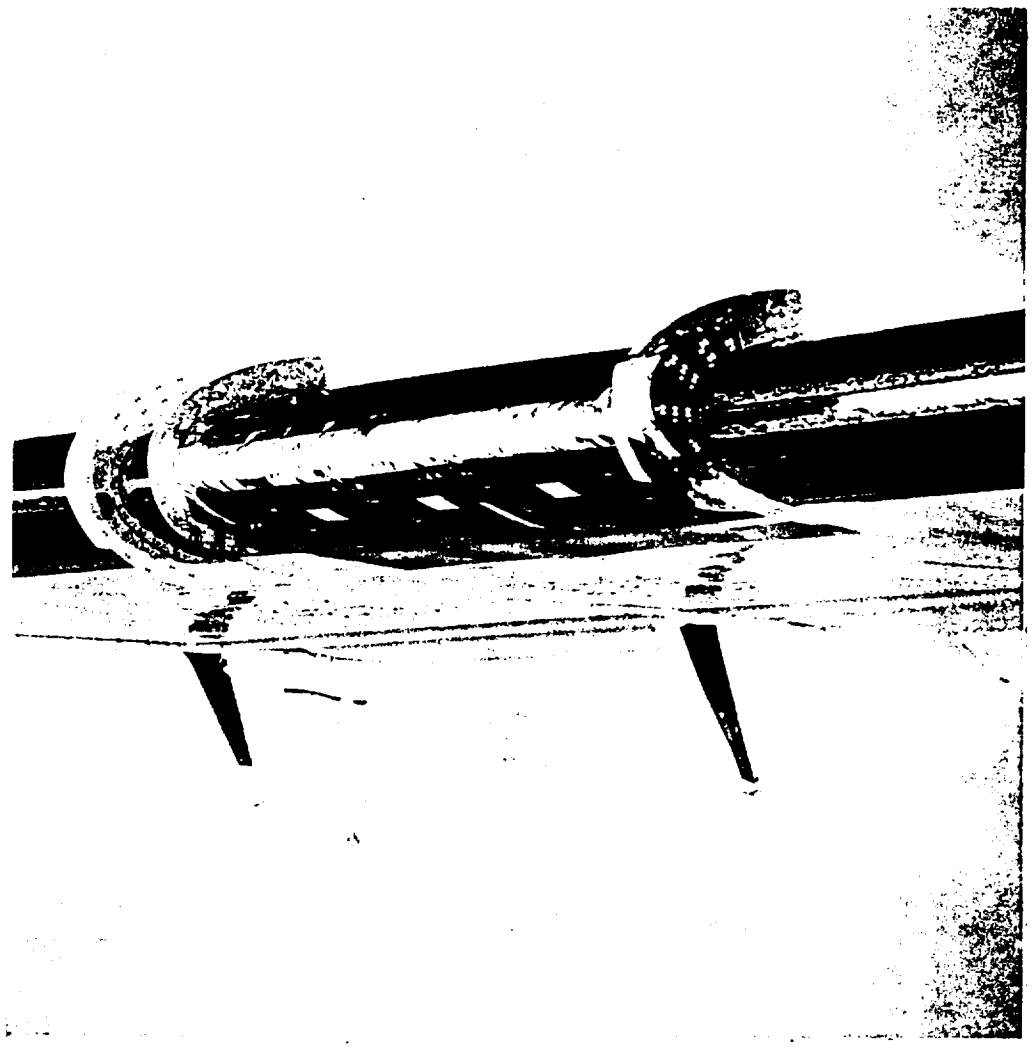

Figure 59. Photograph of a dry rime ice formation on the IDI wing cuff. December 8, Flight 93-10, Run #2.

At this time the sensors have not been independently calibrated and there is no convenient way to infer the corresponding ice thickness levels for the above graphs. A limited number of data sets were collected on approach to Cleveland-Hopkins Airport when icing clouds were present at low levels near the airport. For these cases the plane was landed without de-icing the wing cuff and final ice thickness measurements were made by hand. A linear growth rate was assumed and the capacitance data for these tests were plotted as a function of ice thickness. Graphs of capacitance versus ice thickness are shown for the underboot sensor in mixed/glaze, mixed/rime, and rime icing in **Figures 60, 61,** and **62** respectively. It is realistic to assume that noise levels for both the Type 1 and 2 sensors can be reduced to roughly ± 2 pF with better electronics and cabling. With these noise levels the minimum detectable thickness for each of the three ice types encountered in the graphed runs are approximately .015", .020", and .040" respectively.

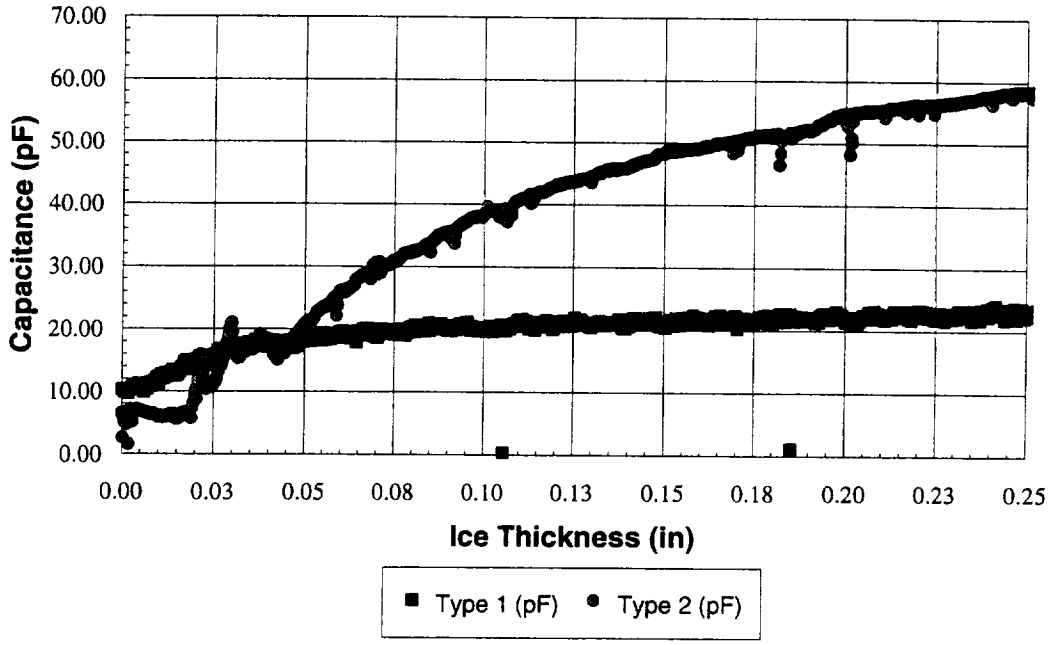

Figure 60. Plot of measured capacitance versus approximate ice thickness for the underboot sensor in mixed/glaze ice. December 7, Flight 93-8, Run #4.

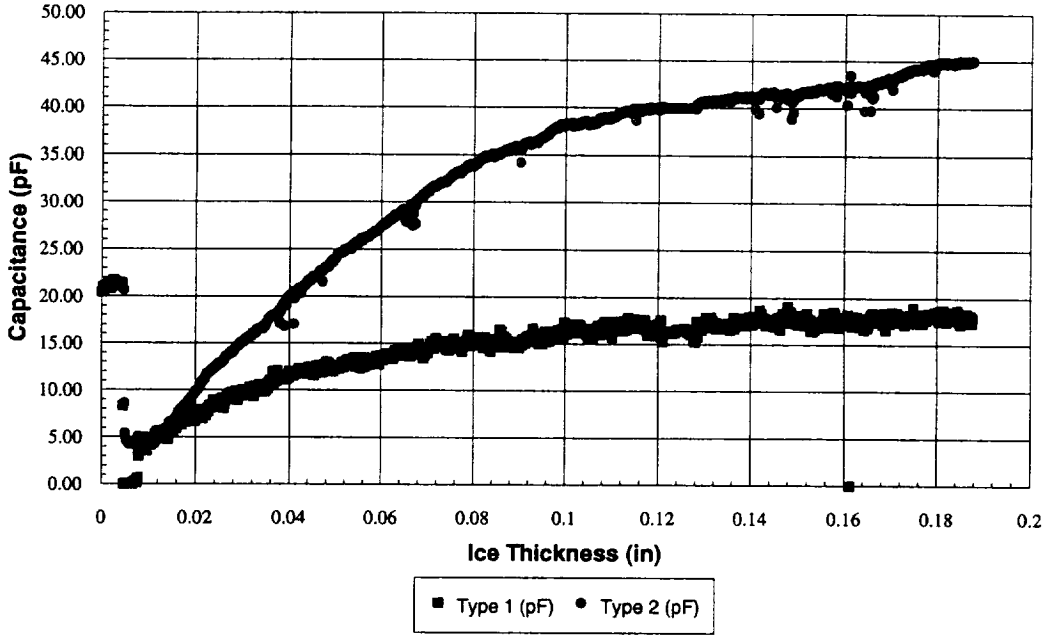

Figure 61. Plot of measured capacitance versus approximate ice thickness for the underboot sensor in mixed/rime ice. December 7, Flight 93-9, Run #8.

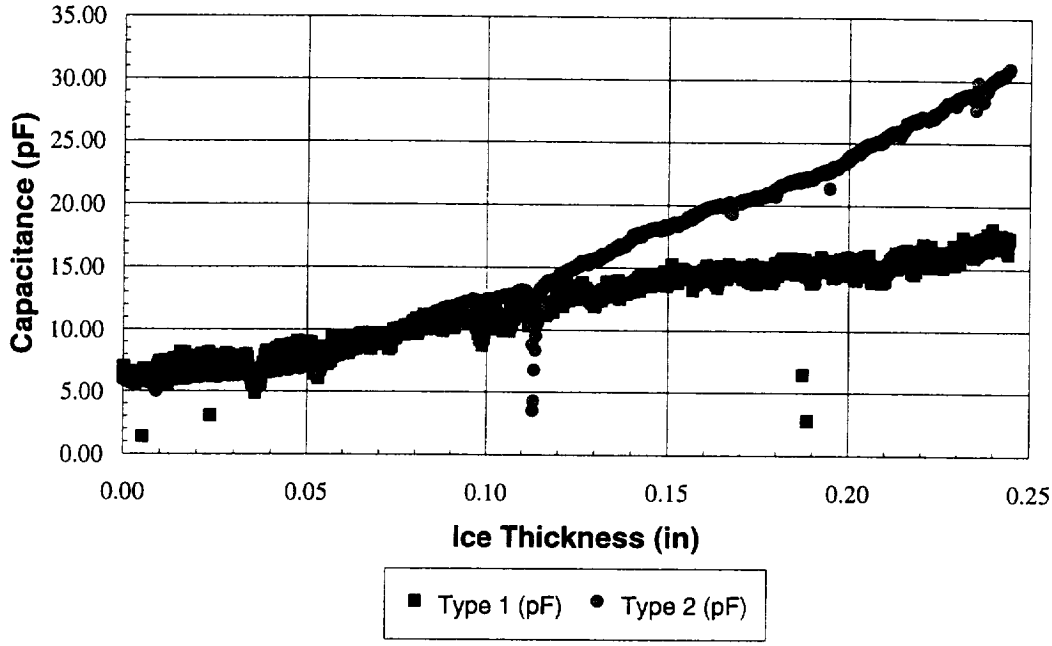

Figure 62. Plot of measured capacitance versus approximate ice thickness for the underboot sensor in rime ice. December 8, Flight 93-10, Run #3.

These minimum detectable thickness values can be improved by lowering noise levels, by reducing drift in the meters, and/or by increasing the sensitivity of the actual sensor. Future designs will reduce system noise levels by using triaxial cable instead of coaxial cable and by tailoring the range of the capacitance meters to match the output of the sensors. Drift in the meters will be eliminated by incorporating a computer controlled autozeroing feature that has recently been developed at IDI.

Techniques to improve the sensitivity of the sensors are currently being investigated. One way to do this is to increase the overall length of the sensor. The edges of the sensor give the greatest contribution to thin ice sensitivity. A sensor designed specifically for the detection of the onset of icing would take advantage of this and be fabricated from a series of long, very narrow electrodes closely spaced and connected in parallel. Data from these flight tests and previous wind tunnel tests have indicated that the use of a guard electrode wider than the positive electrode does not improve the range of the sensor and counter productively eliminates many of the strong edge field lines that are useful in the detection of thin ice. This latter phenomenon is evidenced by the observation that the wire Type 2 sensor is more sensitive to thin ice than the underboot Type 2 as compared to their respective Type 1's. This is most likely due to the fact that the fabric guard electrode used with the wire Type 2 sensor was not fully effective (as mentioned above in the section on temperature compensation) and did not eliminate all of the edge field lines as did the copper guard electrode used with the underboot sensor. Future Type 2 style sensors will incorporate a guard electrode that is the same width as the positive electrode.

Future ice detector systems developed at IDI for commercial applications will incorporate the improvements just discussed. It is conceivable that these systems will be able to give the first indication of ice formation when accretions are on the order of .010" or less for all types of icing conditions.

Ice Thickness Measurements

The use of a single capacitance sensor to measure ice thickness is not readily feasible because the sensor output is a function of both the dielectric constant of the ice as well as the thickness. To overcome this the present sensor employs both Type 1 and Type 2 style sensors to measure ice thickness based on the NASA patent by Dr. L. Weinstein (see section on patent sensor design). The patent proposes that the final saturated output from the Type 1 sensor is a good indicator of the average dielectric constant of the ice pack. Thus dividing the output of the Type 2 sensor by that from the Type 1 should give a capacitance value that can be correlated to ice thickness independent of the type and dielectric constant of the ice.

This method is quite applicable if the ice is homogeneous in composition all the way through. Problems arise if the dielectric constant changes after enough ice has formed to saturate the Type 1 sensor. If this happens the output from the Type 2 sensor is then being compensated based on an incorrect dielectric constant and the inferred ice thickness can be either greater or less than what is actually present.

Variations in dielectric constant can result from at least three sources: The type of ice forming on the leading edge will change if the ambient icing conditions vary with time. The effective dielectric constant of the outer layers of ice will change if the amount of liquid water near the surface of the ice changes with changing temperature or impingement rate. The dielectric constant of the ice will change as the temperature of the ice pack changes.

Contrary to what is encountered in a wind tunnel, natural icing conditions rarely stay constant even when experienced NASA pilots try their best to orbit in a good icing cloud. Conditions are even more transient for general aviation aircraft that usually encounter icing as they ascend or descend through clouds encountering variable LWC, temperature, etc. Thus the while assumption of uniform ambient icing conditions is fine for wind tunnels, and acceptable for icing test flights, it is not applicable to general aviation aircraft. The level of error incurred in measuring ice thickness due to changing ambient conditions has yet to be fully evaluated.

The effects of water in the ice pack and changing ice temperature on the measured dielectric were dramatically observed during the flight tests. An extreme example of the measured capacitance changing due to varied dielectric constant while the ice thickness remained relatively constant is shown in **Figure 63**. At the onset of icing both the wire Type 1 and Type 2 sensors react quickly to the mixed type ice and the capacitance goes up indicating an increasing thickness of ice. When the LWC suddenly drops and the icing stops two effects occur; 1) any liquid water present in the ice pack will freeze, and 2) the temperature of the ice pack will drop as the amount of latent heat released due to the transformation of water to ice goes to zero.

At the measurement frequency of the existing capacitance meters, 10 kHz, the dielectric constant of water is 80 as compared to roughly 33 for solid ice at 32°F. Additionally at this frequency the dielectric of pure ice drops with temperature to roughly 3 at -25°F. These two effects combine to create the sharp decrease in the measured capacitance of the Type 2 sensor as seen in **Figure 63**. Because these effects are predominantly felt at the surface of the ice pack they are more noticeable in the Type 2 output and usually are only observable in the Type 1 output if the ice pack is very thin or the change in temperature and liquid water are relatively severe.

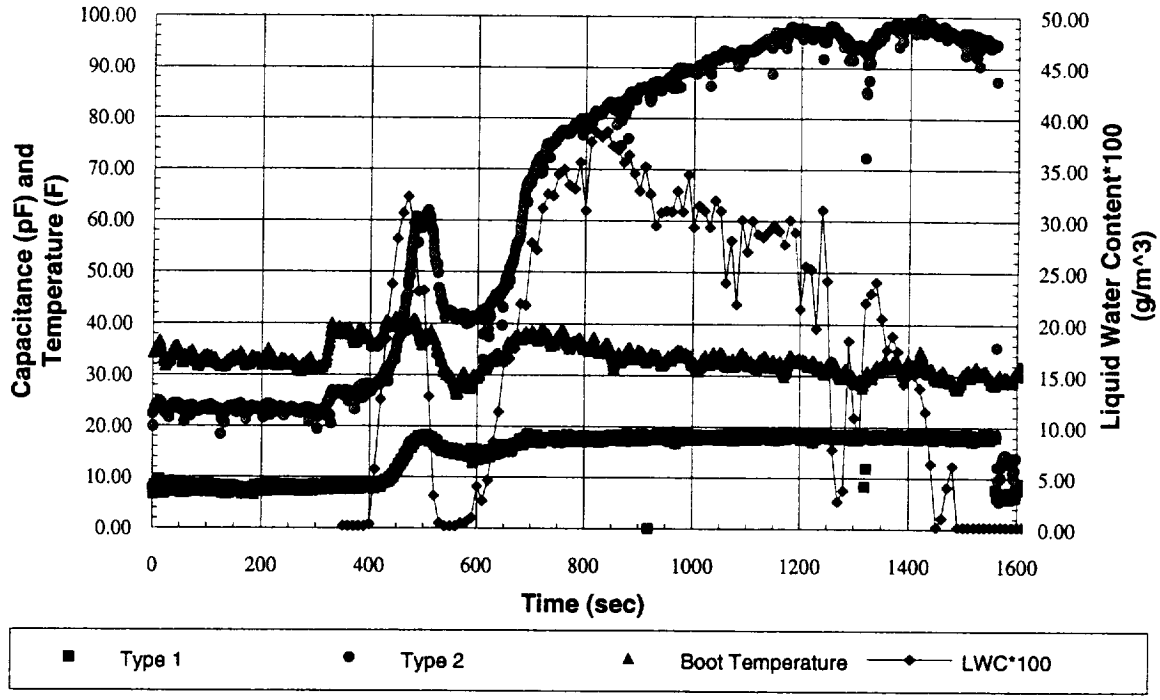

Figure 63. "Dip" in the measured capacitance of the Type 2 and to some degree Type 1 wire sensors due to a drop in the LWC. December 7, Flight 93-8, Run #1.

This change in dielectric constant would have little affect on the Type 2 divided by the Type 1 algorithm if the dielectric changed in a uniform and homogeneous fashion. Unfortunately these effects bias the Type 2 sensor output more than the Type 1 and the result on the algorithm is clearly shown in **Figure 64**. A correlation between the divided capacitance outputs and ice thickness is not possible because, for example, there are three distinct ice thickness levels that all correlate to a ratio value of three.

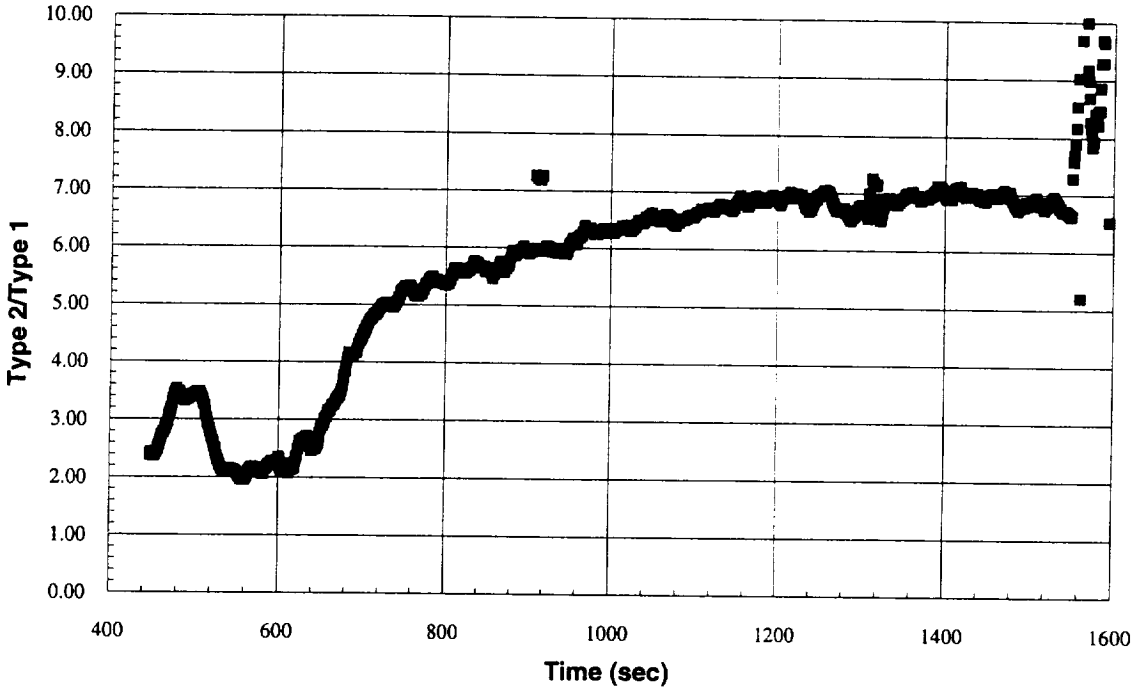

Figure 64. Impact of the "dip" on the Type 2 divided by the Type 1 algorithm for correlating sensor output to ice thickness. December 7, Flight 93-8, Run #1.

Dips in the capacitance output of the Type 2 sensor were observed in a good percentage of the icing tests for both the wire and underboot sensors typical of that shown in **Figures 52** and **54** above. A good example of the influence of temperature on the dielectric constant of the ice pack can be seen in the wire Type 2 capacitance data shown in **Figure 65**. Near the end of this test run, after the plane left the icing cloud, the boot temperature and presumably the ice pack temperature briefly dropped and then rose resulting in a similar change in the output of the Type 2 sensor. The dip in the capacitance output occurs in both the raw and compensated data and thus is not an artifact of improper temperature compensation. It is conceivable that this dip is the result of water in the ice pack freezing as the temperature initially drops and then melting as the ice pack warms, but this seems unlikely for dry rime ice such as this.

Work is currently being done at IDI to investigate ways to minimize the influence of temperature and water content on the measured capacitance. It appears from the literature that using a lower signal frequency for the capacitance meters will help substantially. At frequencies closer to 100 Hz the dielectric constant of pure ice is roughly 80 which is similar to that for water and additionally the dielectric constant is relatively stable with respect to temperature in the range between 32°F and -25°F[1-2]. Currently capacitance is being measured at 10 kHz where the dielectric constant for pure ice varies between 33 at 32°F and 3 at -25°F.

Future wind tunnel tests have been planned to verify these predictions. If these anticipated benefits are realized not only will the dip problem be minimized, but the output of the sensors will increase for thin ice (due to the higher dielectric constant) improving the systems initial ice warning capability.

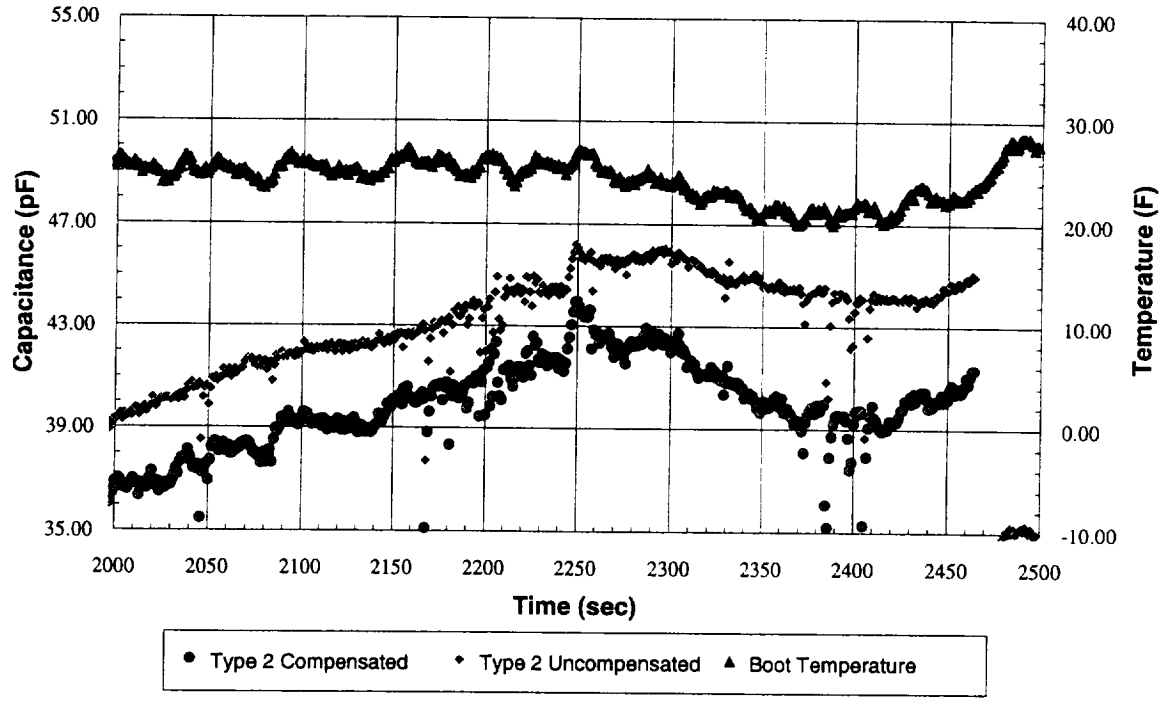

Figure 65. Wire Type 2 capacitance data showing the influence of changing ice pack temperature on measured capacitance for a dry rime accretion. December 8, Flight 93-10, Run #1.

Boot Diagnostic Capabilities

One of the primary advantages of an ice detector integrated into the de-icing boot as opposed to a remote sensor such as the Rosemount unit is that the integrated system can directly determine the success of a boot inflation. The IDI system can determine if the ice pack has been removed from the boot and estimate the amount of residual ice. If required the system can automatically initiate subsequent boot inflations until the boot is clear or it is determined that the remaining ice can not be removed.

Both the underboot and wire sensors change baseline capacitance when the boot is inflated allowing the IDI system to be used in diagnosing boot failures. As a standard procedure the pilot would initiate a boot inflation when the wing was clean and below the freezing point. If the boot failed to inflate, the sensors would detect this and the system would interrogate the pressure sensors currently built into BFGoodrich de-icing systems. If the pressure sensors indicated no

pressure at the boot the problem would be pneumatic, but if the boot was pressurized and still failed to open the system would deduce that the tubes were frozen closed.

Typically output from the underboot sensors would return cleanly back to their baseline values once the wing cuff boot was de-iced as can be seen in **Figures 52** and **55** above. As mentioned previously the wire sensor usually did not de-ice cleanly because of the inoperable fabric sensor embedded into the boot directly below it. For this reason good wire de-icing data are not available. A detailed graph of the de-icing sequence at the end of the mixed/rime icing encounter shown graphically in **Figure 55** and pictorially in **Figure 56** is shown in **Figure 66**. The roughly 0.5" of ice was removed with the first inflation and the latter two inflations depict the output typical of a clear air boot diagnostic test. In one test the boot inflation only removed some of the ice covering the sensor, while the remaining ice appeared to be debonded from the boot but held in place by air pressure. For this case the sensors dropped to a value only slightly elevated from their baselines. To be able to detect a situation like this the baseline capacitance values will have to be very stable and the system will have to have relatively low noise levels. These issues are currently being addressed by IDI.

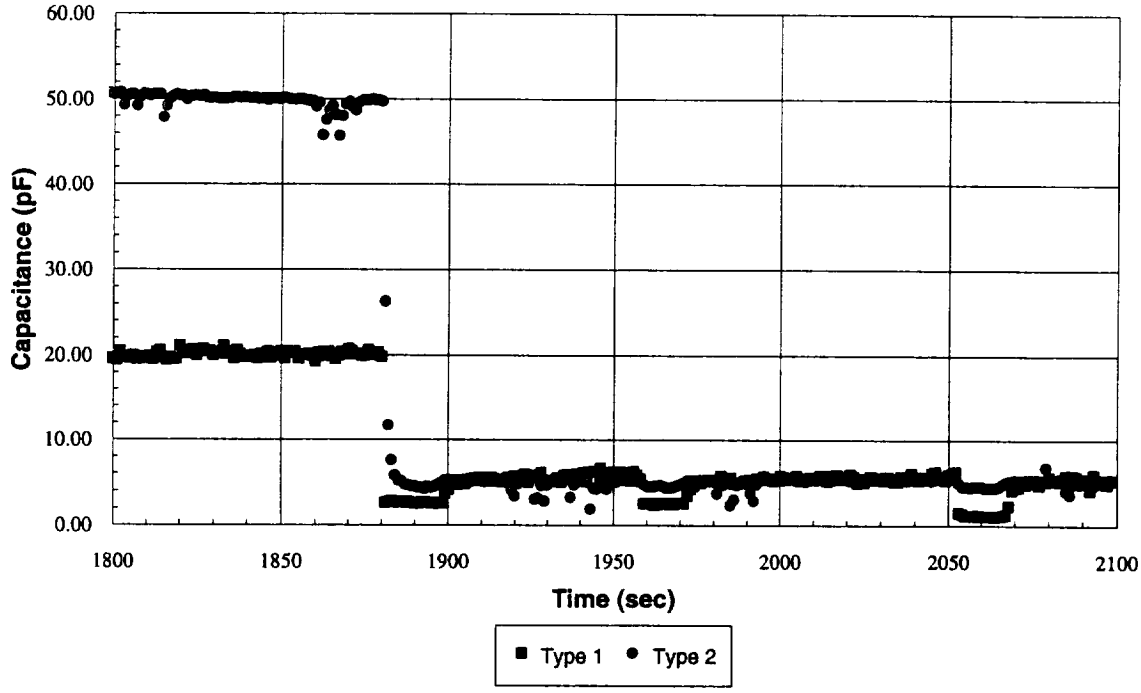

Figure 66. Underboot sensor showing boot inflation cycles removing roughly 0.5" of mixed/rime ice. December 3, Flight 93-5, Run #2.

Conclusions

The flight test program for IDI's ice detection system was very successful. The sensors proved capable of operating successfully in the harsh flight environment without any malfunctions or the need for repairs or modifications. The electronics appear to be immune to electro-magnetic interference from the Otter's navigation and communications equipment and did not disrupt the flight crews use of this equipment. The system is well suited for detecting the initial accumulations of different types of leading edge ice with minimum detectable thicknesses of roughly .015", .020", and .040" for mixed/glaze, mixed/rime, and dry rime ice respectively. The measurement of precise ice thickness was hampered by the effects of changing temperature and the presence of water in the ice pack. The applicability of the Type 2 divided by Type 1 algorithm for use with general aviation aircraft could not be fairly assessed with the current data. The underboot sensor worked very well in evaluating the proper inflation of the pneumatic boot and in determining the success of a de-icing operation.

Work is currently being performed at IDI to reduce the system noise levels and to improve the sensitivity of the sensors. These efforts should reduce the minimum detectable ice thickness to roughly .01" or less for all types of ice. Experiments are being performed in IDI's icing chamber and are planned for BFGoodrich's Icing Wind Tunnel to investigate ways of minimizing the influence of temperature and water content on the dielectric of the ice pack. The use of capacitance meters operating at close to 100 Hz may result in at least a partial solution to this problem. These efforts will improve the signal to noise ratio of the system allowing better quantification of the residual ice left after a boot inflation.

The collection of icing data in true atmospheric conditions has been invaluable in the refinement of IDI's ice detection system for commercial applications. The conditions encountered in flight are not easily duplicated in wind tunnels and have provided both answers and questions.

Acknowledgments

IDI would like to expressly thank Tom Ratvasky, Andrew Reehorst, Jon Yencho, and Chris Hegedus for their help in setting up and conducting these flight tests. The NASA pilots, engineers, and aircraft technicians were extremely accommodating and helpful with all of our requests. Discussions with and input from the NASA and Sverdrup scientists were also very helpful and insightful. Finally we must thank whoever it was at NASA who arranged with Mother Nature for the great icing conditions. IDI would also like to thank the BFGoodrich De-Icing Systems Division in Uniontown, Ohio for use of their Icing Wind Tunnel facility and for supplying custom de-icing boots without which some of this research may not have been possible.

Commercial Applications

IDI is developing a Phase III working agreement with BFGoodrich De-Icing Systems to continue the development of the AIMS ice detection system. The ice sensors will be incorporated into the pneumatic boot during the manufacturing stages and sold as an integrated unit. The primary market will be tailplane ice protection for turboprop commuter aircraft. A cooperative work

schedule is being formulated which includes joint and independent development efforts by BFGoodrich and IDI. A series of wind tunnel tests are planned as well as a flight test program on IDI's Piper Malibu. The initial phase of the plan culminates with the FAA certification of an ice protection system for the Malibu. This will pave the way for certification of systems on larger more complex aircraft.

IDI is investigating methods for employing capacitive ice measurement techniques for other aerospace applications. Leading edge ice detector systems are being developed for the special requirements of unmanned air vehicles and rotorcraft. Research is also underway on the development of a capacitive ice sensor for detecting the adherence of ice to aircraft top wing surfaces.

References

[1]Auty, Robert P. and Robert H. Cole, *Dielectric Properties of Ice and Solid D_2O*, The Journal of Chemical Physics, Volume 20, Number 8, August, 1952.

[2]Evans, S., *Dielectric Properties of Ice and Snow - A Review*, J. of Glaciology, 5, pp. 773-792, 1965.

;